JUSTUS-LIEBIG-
UNIVERSITÄT
GIESSEN

Contributions to understanding adenylate kinase and myristoylation reactions in the malaria parasite *Plasmodium falciparum*

A thesis submitted to the faculty of Biology and Chemistry (FB 08) in fulfilment of the requirements of the Doctor of Science Degree of Justus Liebig University Giessen, Germany

By

Jipeng Ma

From
Shaanxi, China

September 2012

Declaration

I declare that this thesis is my original work and other sources of information have been properly quoted. This work has not been previously presented to obtain any other degree from any other university.

Ich erkläre: Ich habe die vorgelegte Dissertation selbständig und ohne unerlaubte fremde Hilfe und nur mit den Hilfen angefertigt, die ich in der Dissertation angegeben habe. Alle Textstellen, die wörtlich oder sinngemäß aus veröffentlichten Schriften entnommen sind, und alle Angaben, die auf mündlichen Auskünften beruhen, sind als solche kenntlich gemacht. Bei den von mir durchgeführten und in der Dissertation erwähnten Untersuchungen habe ich die Grundsätze guter wissenschaftlicher Praxis, wie sie in der „Satzung der Justus-Liebig-Universität Gießen zur Sicherung guter wissenschaftlicher Praxis“ niedergelegt sind, eingehalten.

Giessen, 4th , September 2012 …….

Dedication

To my family

The thesis was presented for examination on the 10th September 2012 to the faculty of Biology and Chemistry of the Justus Liebig University Giessen, Germany. This thesis was supervised by Prof. Dr. Katja Becker and Prof. Dr. Peter Friedhoff.

The thesis defense examination committee was composed of:

Prof. Dr. Katja Becker

Biochemistry and Molecular Biology

Interdisciplinary Research Centre (IFZ)

Justus-Liebig-University Giessen

Heinrich-Buff-Ring 26-32, 35392 Giessen

Germany

Prof. Dr. Peter Friedhoff

Institute of Biochemistry

Justus Liebig University Giessen

Heinrich-Buff-Ring 58, 35392 Giessen

Germany

Prof. Dr. Eveline Baumgart-Vogt

Institute of Anatomy and Cell Biology

Justus Liebig University Giessen

Aulweg 123, 35385 Giessen

Germany

Prof. Dr. Adriaan Dorresteijn

Institute of Zoology and Developmental Biology

Justus Liebig University Giessen

Stephanstr. 24, 35390 Giessen

Germany

Acknowledgements

In this part, I would like to thank many people. It is clear that without all of you, this work would have become much more difficult.

First of all, I would like to sincerely thank Prof. Katja Becker for giving me the opportunity to study in her laboratory and for supervising my PhD project. Her exceptional ideas, profound knowledge, and continuous guidance and encouragement supported me during the whole time of my PhD project. I also wish to thank Prof. Dr. Peter Friedhoff for being my second supervisor and giving me valuable discussions and advice.

Many thanks go to all outstanding members of Prof. Becker's group. To Dr. Stefan Rahlfs, I would say I owe my deepest gratitude to you for your professional supervision and assistance. You not only taught me a lot in the scientific field but also supported me to live a happy life in Germany. I also would like to thank Elisabeth Fisher for her excellent cell culture work. I wish to thank Marina Fisher for teaching me a lot in enzyme kinetics. Special thanks go to Michaela Stumpf for her professional assistance during crystallization experiments. I would also like to say thank you to Timothy D. Bostick for the efficient correction of my thesis. And I also thank Dr. Esther Jortzik for her valuable work of my paper revision. Many thanks go to Sebastian Kehr for his help with my experiments and especially for picking me up from the airport on my first day. Besides, I would like to thanks all other group members, including Rimma Iozef, Beate Hecker, Ulrike Burkhard-Zahrt, Jochen Bathke, Jette Pretzel, Janina Preuss, Franziska Mohring, Anne Röseler, and Kathleen Zocher for all the help you provided.

Special thanks go to my best friends and colleagues, Dennis Matovu Kasozi, Lihui Wang, and Tao Zhang for your great ideas and discussions. I would like to give many thanks to my friends in Giessen. They are Puyan Zhao, Dilin Liu, Liang Li, Qing Zhao, Qianhui Dai, Wenyu Chen and Jiuce Sun. I cannot imagine my life without all of you. I appreciate all the encouragements from you in every difficult time.

I would like to thank the China Scholarship Council for giving me this opportunity to study in Germany and their generous financial support throughout my PhD study.

Finally, I would like to thank all my family members for their support. I am greatly indebted to my mother, father, and younger brother. They inspire me to pursue my dream no matter when or where I am. I feel grateful to my family with their sacrifices and encouragements.

List of Publications

1. **Ma J**, Rahlfs S, Jortzik E, Heiner Schirmer R, Przyborski JM, Becker K. (2012). Subcellular localization of adenylate kinases in *Plasmodium falciparum*. FEBS Lett. Online 17 July 2012 [ahead of print.]

2. Jortzik E, Wang L, **Ma J**, Becker K (2012). Flavins and flavoproteins – applications in medicine. In: Meth Mol Biol, Humana Press USA, in press.

Conferences and Scientific Meetings

1. **Ma J**, Rahlfs S, Przyborski JM, Schirmer RH, Becker K (**2012**). Characterization and localization of adenylate kinases in *Plasmodium*. *Tropical Medicine and Parasitology, 25th Annual Meeting German Society for Parasitology*, Heidelberg, March 14th-17th, 2012.

2. **Ma J**, Rahlfs S, Przyborski JM, Schirmer RH, Becker K (**2011**). Characterization and localization of adenylate kinases in *Plasmodium*. *4th Annual Conference of the International Giessen Graduate School for the Life Sciences (GGL)*, Giessen, September 21st-22nd, 2011.

3. **Ma J**, Rahlfs S, Przyborski JM, Schirmer RH, Becker K (**2010**). Characterization and localization of adenylate kinases in *Plasmodium*. *3th Annual Conference of the International Giessen Graduate School for the Life Sciences (GGL)*, Giessen, September 29th-30th, 2010.

4. **Ma J**, Rahlfs S, Przyborski JM, Schirmer RH, Becker K (**2010**). A new adenylate kinase in *Plasmodium* - biochemical characterization and localization. *Joint Meeting of the German Societies of Parasitology and Protozoology*, Düsseldorf, March 17th-20th, 2010.

5. **Ma J**, Rahlfs S, Przyborski JM, Schirmer RH, Becker K (**2009**). A new adenylate kinase in *Plasmodium*-biochemical characterization and localization. *"New Trends in Infectious Disease Research" 5th Joint Ph.D Students Meeting of the Collaborative Research Centers SFB 544 Heidelberg, SFB 630 Würzburg and SFB 766 Tübingen*, Heidelberg, November 19th-21st, 2009.

Table of Contents

Declaration ..... **I**
Dedication ..... **II**
Acknowledgements ..... **IV**
List of Publications ..... **V**
Conferences and Scientific Meetings ..... **V**
Table of Contents ..... **VI**
List of Figures ..... **IX**
List of Tables ..... **XI**
List of Abbreviations ..... **XII**
Summary ..... **XIV**
Zusammenfassung ..... **XVI**
1. Introduction **1**
1.1 Malaria **1**
1.1.1 Malaria: Past and present 1
1.1.2 Life cycle of *Plasmodium falciparum* 2
1.1.3 Antimalarial drugs and malaria vaccine for malaria control 4
1.2 Adenylate kinase **7**
1.2.1 Molecular and biochemical properties of adenylate kinase 7
1.2.2 Structure and catalysis of adenylate kinase 8
1.2.3 Energy metabolism and signal pathway 11
1.2.4 Adenylate kinase in *Plasmodium* 15
1.3 Myristoylation and N-myristoyltransferase **17**
1.3.1 Protein lipidation 17
1.3.2 Protein myristoylation event 18
1.3.3 Click reaction in myristoylation research 20
1.3.4 N-myristoyltransferase 22
1.3.5 N-myristoyltransferase as a drug target 24
1.4 Objective of study **26**
1.4.1 Adenylate kinase networks 26
1.4.2 Myristoylation 26
1.4.3 N-myristoyltransferase 26
2. Materials **27**
2.1 Antibiotics **27**
2.2 Antibodies **27**
2.3 Buffers and solutions **27**
2.3.1 Buffer for DNA electrophoresis 27
2.3.2 Buffer for extraction of *P. falciparum* parasites 27
2.3.3 Buffer for AK assay 28
2.3.4 Buffer for protein purification 28

2.3.5 Buffer for SDS-PAGE electrophoresis 28
2.3.6 Western blot buffer 29
2.3.7 Stock solutions 29
2.4 Biological materials 29
2.4.1 Plasmids 29
2.4.2 *E. coli* strains 30
2.4.3 *Plasmodium falciparum* strain 30
2.5 Chemicals 30
2.6 Enzymes 32
2.6.1 Restriction Enzymes 32
2.6.2 DNA Polymerase 32
2.6.3 Other enzymes 33
2.7 Instruments 33
2.8 Kits 34
2.9 Materials of affinity chromatography 34
2.10 Media for *E. coli* culture 34
2.11 Protease inhibitors 35
3. Methods 36
3.1 General methods 36
3.1.1 Agarose gel electrophoresis 36
3.1.2 Cleavage of double strand DNA by restriction endonuclease 36
3.1.3 Determination of DNA concentration 36
3.1.4 Preparation of competent cells 36
3.1.5 Ligation and transformation 37
3.1.6 SDS-polyacrylamide gel electrophoresis 37
3.1.7 Western blot 38
3.1.8 Determination of protein concentration 39
3.1.9 Cell culture of *P. falciparum* 39
3.1.10 Magnetic purification of *P. falciparum* in trophozoite stage 40
3.2 Adenylate kinase 40
3.2.1 Cloning of *Pfaklp1* and *Pfaklp2* 40
3.2.2 Overexpression and purification of *Pf*AKLP1 and *Pf*AKLP2 42
3.2.3 Gel filtration of *Pf*AKLP1 and *Pf*AKLP2 42
3.2.4 His-tag cleavage of recombinant proteins by thrombin enzyme 43
3.2.5 Enzyme assay 43
3.2.6 GFP constructs of all wild type AKs 44
3.2.7 GFP construction of a mutant *Pf*AK2 at the myristoylation site 46
3.2.8 Parasite transfection 46
3.2.9 Immunofluorescence imaging 46
3.2.10 Western blot analysis 47
3.3 N-myristoylation in *P. falciparum* 47

3.3.1 Metabolic labeling of *P. falciparum* in cell culture with azido myristic acid 47
3.3.2 Preparation of parasite cell lysate and click reaction 48
3.3.3 Visualization of myristoylated proteins by streptavidin-HRP blot.....49
3.3.4 Pull-down assay of myristoylated proteins with avidin beads from *P. falciparum* 49
3.3.5 Prediction of myristoylation in *P. falciparum*.....49
3.4 Crystal screening of N-myristoyltransferase 50
3.4.1 Overexpression and purification of N-myristoyltransferase from *P. falciparum* ...50
3.4.2 *Pf*NMT crystal screening 51
3.4.3 Homology modeling of *Pf*NMT.....52
3.4.4 Crystal screening of *Pf*NMT and the *Pf*AK2 complex.....52
4. Results 55
4.1 *Pf*AKLP1 and *Pf*AKLP2.....55
4.1.1 Sequence alignment and phylogenetic tree 55
4.1.2 Cloning of *Pfaklp1* and *Pfaklp2*.....57
4.1.3 Overexpression and purification of recombinant *Pf*AKLP1 and *Pf*AKLP2.....58
4.1.4 Cleavage of His-tag of recombinant *Pf*AKLP1 and *Pf*AKLP2 by thrombin.....59
4.1.5 Enzyme assay.....59
4.2 Localization of *Pf*AK1, *Pf*AK2, *Pf*GAK, *Pf*AKLP1, and *Pf*AKLP2 61
4.2.1 Localization of AKs and GAK in *Plasmodium*.....61
4.2.2 Localization and N-myristoylation of *Pf*AK2.....61
4.3 N-myristoyltransferase from *P. falciparum* 63
4.3.1 Sequence alignment 63
4.3.2 Overexpression and purification of recombinant *Pf*NMT.....65
4.3.3 Complex of *Pf*NMT/AK2 67
4.3.4 Crystallization of *Pf*NMT 68
4.3.4.1 Crystallization screening of *Pf*NMT in complex with myristoyl-CoA 68
4.3.4.2 Crystallization screening of the complex comprising *Pf*NMT with its natural substrate *Pf*AK2 69
4.3.5 Homology modeling of *Pf*NMT.....70
4.4 Myristoylation in *P. falciparum* 72
4.4.1 Metabolic labeling of myristoylated proteins in *P. falciparum* 72
4.4.2 Pull-down assay 72
4.4.3 Prediction of myristoylated proteins in *P. falciparum*.....73
5 Discussion.....81
5.1 AK networks and energy metabolism.....81
5.2 N-myristoyltransferase structure analysis for the potency of an antimalarial drug target 84
5.3 Myristoylation in *P. falciparum* 87
6 References.....90

List of Figures

Figure 1.1 Worldwide distribution of countries at risk of malaria in 2010 2

Figure 1.2 Life cycle of malaria 4

Figure 1.3 Parasite targets in different stages of the malaria life cycle used for vaccine development 7

Figure 1.4 3D structure of adenylate kinase with closed and open conformations 9

Figure 1.5 Schematic diagram of hydrogen bonds between Ap_5A and the polypeptide of AK 9

Figure 1.6 Structures of AK during the extreme stages of catalysis 10

Figure 1.7 Proposed mechanism for AK catalysis 11

Figure 1.8 Energy transfer shuttle catalyzed by AK from production to utilization 12

Figure 1.9 AK-mediated AMP signal pathways and monitor system 13

Figure 1.10 Effects of activation of AMPK on cellular metabolism 14

Figure 1.11 Adenylate kinase isoforms network and intracellular localizations 15

Figure 1.12 Metabolic and energetic pathways in *P. falciparum* 16

Figure 1.13 Process of protein myristoylation on the nascent polypeptide 18

Figure 1.14 Post-translational myristoylation of proteins during apoptosis 19

Figure 1.15 Three bio-orthogonal ligation reactions in use 21

Figure 1.16 The complete procedure of identifying myristoylated proteins by bio-orthogonal analogs of myristic acid 22

Figure 1.17 NMT catalytic mechanism 23

Figure 1.18 Crystal structure of NMT 24

Figure 3.1 Transfer stack in semi-dry Western blot. 39

Figure 3.2 Overall reaction in an adenylate kinase-coupled assay 43

Figure 3.3 AK protein-fused GFP for sublocalization 45

Figure 3.4 Schematic diagram of Hanging drop (A) and Sitting drop (B) for protein crystallization. 51

Figure 3.5 Flow chart of Protein 3D structure modeling. 54

Figure 4.1 Multiple sequence alignment of AK family members 56

Figure 4.2 Radial phylogenetic tree generated by using the neighbour-joining method based on the results of multiple sequence alignments of AKs from various species 57

Figure 4.3 12% SDS-PAGE gel after affinity chromatography purification 58

Figure 4.4 SDS-PAGE and Western blot of recombinant *Pf*AKLP1 and *Pf*AKLP2 58

Figure 4.5 12% SDS-PAGE gel and Western blot after His-tag cleavage by thrombin 60

Figure 4.6 Localization of *P. falciparum* AKs fused to GFP 61

Figure 4.7 Localization of PfAK2 62

Figure 4.8 Subcellular localizations of *Pf*AK2 and *Pf*AK2G2A in *P. falciparum* 63

Figure 4.9 Multiple sequence alignment of NMT from various species 64

Figure 4.10 10% SDS-PAGE gel of *Pf*NMT after Protino Ni-TED purification 66

Figure 4.11 10% SDS-PAGE gel of *Pf*NMT after gel filtration purification 67

Figure 4.12 Gel filtration and SDS-PAGE gel analysis 68

Figure 4.13 Secondary structure prediction of *Pf*NMT 70

Figure 4.14 The *Pf*NMT model and details of substrate binding sites 71

Figure 4.15 Streptavidin-HRP blot of myristoylated proteins in *P. falciparum* by metabolic labeling 72

Figure 4.16 Pull-down assay of myristoylated proteins from *P. falciparum* 73

Figure. 5.1 Scheme of the subcellular localization of known adenylate kinases in *P. falciparum* 82

Figure 5.2 Integrated communications between cellular sites of ATP utilization and ATP generation 84

Figure 5.3 Comparison of human NMT type I (brown) (amino acids 115 to 496) and a model of *Pf*NMT (teal) (amino acids 27 to 410) 86

Figure 5.4 Biotin tags for the chemical reporter method 88

List of Tables

Table 1.1 Principle available antimalarial drugs……5

Table 1.2 Properties of AK isozymes from *Plasmodium falciparum* 17

Table 3.1 Composition of SDS-PAGE gels. 38

Table 3.2 Primers for AK-GFP constructs 44

Table 3.3 Compositions of CuAAC click reaction 48

Table 4.1 Optimization of the heterologous overexpression of *Pf*NMT 66

Table 4.2 Promising conditions for crystallization screening 69

Table 4.3 Crystallization conditions for NMT from other organisms 69

Table 4.4 Myristoylated protein prediction of the whole proteome of *P. falciparum* via the MYR Predictor tool 78

Table 4.5 Myristoylated protein prediction of the whole proteome of *P. falciparum* by the Myristoylator tool 80

List of Abbreviations

ACTs	Artemisinin-based combination therapies
AK	Adenylate kinase
AKLP	Adenylate kinase like protein
AMP	Adenosine monophosphate
AMPK	AMP-activated protein kinase
ATP	Adenosine triphosphate
APS	Ammonium persulfate
BSA	Bovine serum albumin
CQ	Chloroquine
dNTP	Deoxynucleotide triphosphate
DMSO	Dimethyl sulfoxide
DNA	Deoxyribonucleic acid
DNase	Deoxyribonuclease
DTT	1, 4-Dithiothreitol
E. coli	*Escherichia coli*
EDTA	Ethylenediaminetetraacetic acid
FPLC	Fast protein liquid chromatography
H_2O_{dd}	Double distilled water
IPTG	Isopropyl-β-D-thiogalactopyranoside
kDa	Kilodalton
LB	Lysogeny Broth Medium
NADH	β-Nicotinamide adenine dinucleotide, reduced disodium salt
Ni-NTA	Nickel nitrilotriacetic acid
NMT	N-myristoyltransferase
OD	Optical density
PBS	Phosphate buffered saline
PCR	Polymerase chain reaction

PEG	Polyethylene glycol
Pf	*Plasmodium falciparum*
PMSF	Phenylmethylsulfonylfluoride
PVDF	Polyvinyl difluoride
RBC	Red blood cells
RBM	Roll Back Malaria
SDS	Sodium dodecyl sulphate
SDS-PAGE	Sodium dodecyl sulphate – polyacrylamide gel electrophoresis
TB	Terrific Broth medium
TEMED	N,N,N',N'-Tetramethylethylenediamine
WHO	World Health Organisation
µg	Microgram
µl	Microliter

Summary

Malaria remains a fatal tropical disease caused by a protozoan known as *Plasmodium* and is threatening almost half the world's population. Due to the absence of effective malaria vaccines and remarkable increase of drug resistance, the deep understanding of parasite biology and identification of new drug targets are desperately required. In this thesis, three aspects have been studied to better understand the energy metabolism of *Plasmodium falciparum* and to support the search for new potential drug targets.

First, two new adenylate kinase-like proteins have been successfully overexpressed in *E. coli* cells and purified via affinity chromatography. Different substrates of nucleoside triphosphate and monophosphate were used for determining the enzyme activity. However, *Pf*AKLP1 (*Plasmodium falciparum* adenylate kinase-like protein 1) only exhibited low activity with ATP and AMP as substrates in the enzymic assay *in vitro* while there was no detectable activity for recombinant *Pf*AKLP2 (*Plasmodium falciparum* adenylate kinase-like protein 2). Besides, we also investigated the subcellular localization of all five adenylate kinases characterized from *Plasmodium falciparum* systematically by fusing GFP to the respective adenylate kinase. *Pf*AK1, *Pf*AKLP1, and *Pf*AKLP2 were all shown to be localized in the cytosol of the parasites while *Pf*GAK which only showed high activity with GTP as substrate was found to be in the mitochondrion. Interestingly, *Pf*AK2, a unique myristoylated adenylate kinase, was demonstrated to be targeted to the PVM (parasitophorous vacuole membrane). A mutation in the myristoylation site of *Pf*AK2 could entirely change the subcellular localization from PVM to cytosol, showing that myristoylation is responsible for such localization. Results from Western blots using the transfected parasite lysate could confirm the membrane associated localization of *Pf*AK2. Unlike adenylate kinase in other species, no adenylate kinase which utilized ATP as substrate was localized in the mitochondrion. This might indicate that the mitochondrion is not the main source of ATP in *Plasmodium*, also taking into account that a novel branched tricarboxylic acid pathway was demonstrated. These findings enhance our knowledge on adenylate kinase isoforms and energy metabolism mediated by adenylate kinase in *Plasmodium falciparum*.

Secondly, an overexpression and purification method for recombinant *Pf*NMT with relatively high yield and purity was established. More than 500 crystallization solutions were tested to obtain the promising conditions for *Pf*NMT crystallization. At least two conditions were further studied to crystallize *Pf*NMT. Although no high quality crystals have been obtained so far, the screening seems to be worth of further optimization. To gain first structural insights, a model of *Pf*NMT was acquired based on the structure of NMT from *Plasmodium vivax* which showed 80% identity in the amino acid sequence. By comparison the model of *Pf*NMT with the structure of human NMT1, differences in two regions related to the peptide substrate binding were observed, which may

provide the basis for selective inhibition of NMT.

Thirdly, a metabolic labeling method was applied to study protein myristoylation in *P. falciparum*. The myristoylated proteins were metabolically labeled by a myristic acid analogue and further biotinylated via the so-called click reaction. The myristoylated proteins could then be detected by a streptavidin-HRP blot. The avidin beads were used to enrich the target proteins so as to identify these targets by mass spectrometry. Furthermore, two bioinformatic tools for myristoylation prediction based on the conserved myristoylation motif were used to predict the potential targets in the whole proteome. As a result, 42 proteins were assumed to be myristoylated by the MYR Predictor tool and 64 proteins were discovered by the Myristoylator tool. Although it was possible to predict the myristoylated proteins from their amino acid sequences, the results from the two bioinformatic tools compared with the experimentally identified targets implied that some real targets might be easily overlooked by the bioinformatic approaches. Therefore, the metabolic labeling study is a beneficial method not only to understand the biological pathways involved in myristoylation but also to discover novel myristoylated proteins from *P. falciparum*.

Zusammenfassung

Die tropische Erkrankung Malaria wird durch ein Protozoon namens *Plasmodium* verursacht und bedroht nahezu die Hälfte der Weltbevölkerung. Da es keine wirksame Malariavakzine gibt und die Resistenz des Erregers gegen vorhandene Medikamente ständig steigt, ist es wichtig, die Biologie des Parasiten besser zu verstehen und neue Ziele für die Medikamentenentwicklung zu entdecken. In dieser Dissertation wurden drei Aspekte untersucht, um den Energiestoffwechsel des Parasiten besser zu verstehen und nach neuen möglichen Medikamentenzielen zu suchen.

Erstens wurden zwei neue Adenylatkinase-ähnliche Proteine erfolgreich in *E. coli*-Zellen überexprimiert und mittels Affinitätschromatographie gereinigt. Verschiedene Nukleosidtri- und monophosphate wurden als Substrate eingesetzt, um die Enzymaktivitäten zu untersuchen. *Pf*AKLP1 (*Plasmodium falciparum* Adenylatekinase-ähnliches Protein 1) zeigte in den *in vitro* enzymatischen Assays geringe Aktivität mit ATP und AMP als Substrat, während für ebenso rekombinant hergestelltes *Pf*AKLP2 (*Plasmodium falciparum* Adenylatekinase-ähnliches Protein 2) keine Aktivität zu messen war. Weiterhin untersuchte ich die subzelluläre Lokalisation von allen 5 bisher bekannten Adenylatkinasen aus *Plasmodium falciparum* systematisch durch den Einsatz von GFP-gekoppelten Adenylatkinase-Konstrukten. *Pf*AK1, *Pf*AKLP1 und *Pf*AKLP2 ließen sich alle im Zytosol des Parasiten entdecken, während *Pf*GAK, das nur mit GTP als Substrat hohe Aktivitäten zeigte, im Mitochondrium lokalisiert werden konnte. Interessanterweise wurde von *Pf*AK2, die eine einzigartige myristoylierte Adenylatkinase darstellt, gezeigt, dass sie in der PVM (*parasitophorous vacuole membrane*) gefunden werden konnte. Eine in die Myristoylierungsstelle von *Pf*AK2 eingefügte Mutation konnte die subzelluläre Lokalisation komplett von der PVM in das Zytosol verschieben und zeigte somit, dass die Myristyolierung für diese Lokalisation verantwortlich ist. Western Blot-Untersuchungen mit Lysat von infizierten Parasiten konnten die Membran-Assoziation bestätigen. Im Gegensatz zu Adenylatkinasen aus anderen Organismen konnte keine Adenylatkinase, die ATP als Substrat nutzt, im Mitochondrium gefunden werden. Dies mag darauf hinweisen, dass das Mitochondrium im Parasiten nicht die Hauptquelle für die ATP-Gewinnung darstellt, besonders, wenn man die neue Entdeckung eines verzweigten Trikarbonsäurezyklusses mit berücksichtigt. Diese Ergebnisse erweitern unsere Kenntnisse von verschiedenen Adenylatkinase-Isoformen und den durch sie vermittelten Energiefluss in *Plasmodium falciparum*.

Zweitens konnte ein Überexpressions- und Reinigungsprotokoll für die Herstellung von rekombinanter *Plasmodium falciparum* N-Myristoyl-Transferase (*Pf*NMT) mit relativ hoher Ausbeute und hohem Reinheitsgrad etabliert werden. Mehr als 500 Kristallisationslösungen wurden getestet, um die besten Bedingungen für die Kristallisation von *Pf*NMT zu finden. Unter wenigstens zwei Bedingungen konnten erste Anzeichen einer Kristallisation beobachtet werden, weshalb diese weiter optimiert wurden. Obwohl noch keine Kristalle erhalten werden konnten, sind diese Bedingungen vielversprechend und sollten weiter verfolgt werden. Anhand der bekannten *Plasmodium vivax* NMT-Struktur konnte ein Strukturmodell der *Pf*NMT erstellt werden, da die Aminosäuresequenzähnlichkeit mit 80% hoch genug für ein solches *Modeling* ist. Beim Vergleich des erstellten *Pf*NMT Strukturmodells mit der bekannten Struktur der humanen NMT konnten zwei

Regionen gefunden werden, die Unterschiede im Bereich der Substratbindung aufweisen und somit als Basis für die Entwicklung von Inhibitoren dienen könnten, die selektiv das Malariaenzym und nicht das humane hemmen.

Drittens wurde eine metabolische Markierungsmethode angewendet, um die Myristoylierung in *P. falciparum* zu untersuchen. Die myristoylierten Proteine in *P. falciparum* wurden mit einem Myristinsäureanalog metabolisch markiert und konnten dann durch eine sogenannte Klickreaktion biotinyliert werden. Somit konnten myristoylierte Proteine durch einen Streptavidin-HRP Blot detektiert werden. Avidin-Kügelchen wurden benutzt, um die biotinylierten Zielproteine anzureichern und für weitere Untersuchungen (Massenspektrometrie) in ausreichender Menge zur Verfügung zu haben.

Weiterhin wurden zwei bioinformatische Programme benutzt, um basierend auf dem konservierten Myristoylierungsmotiv und der bekannten Struktur von NMTs mögliche Zielproteine des gesamten Proteoms zu finden, die myristoyliert werden können (das Myristyolom). Das Ergebnis waren bei dem MYR-Predictor Programm 42 vorhergesagte mögliche myristoylierte Proteine, beim Myristoylator Programm waren es 64 Proteine. Obwohl es also möglich ist, myristoylierte Proteine anhand ihrer Aminosäuresequenz mit bioinformatischen Methoden vorherzusagen, zeigen die Vergleiche mit experimentell erhaltenen Daten, dass dabei immer noch einige wirkliche Zielproteine übersehen werden können. Deshalb stellen metabolische Markierungsstudien eine wirkungsvolle Methode dar, um nicht nur den biologischen Weg der Myristoylierung aufzuzeigen, sondern auch, um neue myristoylierte Proteine aus *P. falciparum* zu entdecken.

1. Introduction

1.1 Malaria

1.1.1 Malaria: Past and present

Malaria is the most serious tropical disease caused by protozoan parasites of the genus *Plasmodium*, which is transmitted to humans by the bite of infected mosquitoes. The word "mal' aria," which means "bad air" in Italian, was first used in English when H. Walpole described the disease in 1740. "*Plasmodium*" is believed to have been a human pathogen for the entire history of the species (CDC website 2012). Up to now, 1,277 plant species from 160 families have been used as herbal medicines to treat malaria, some having even been used thousands of years ago (Willcox *et al.*, 2004). The *qing hao* plant was first used to treat acute intermittent fever, a malaria-like disease in the 4th century, from which artemisinins are isolated as a potent and effective drug today (CDC website 2012). The cinchona bark containing quinine was also introduced to cure malaria in the 16th century in Western countries (CDC website 2012). These traditional medicines still can be exploited for novel antimalarial drugs as affordable and effective treatment in poor, rural areas with malaria epidemics (Willcox *et al.*, 2004).

Historically, malaria had been epidemic in most countries of the northern hemisphere as far as the Arctic Circle until the mid-19th century, threatening an estimated 90% of the world's population (Mendis *et al.*, 2009). There are several key events that occurred at the end of 19th century in malaria history. First, the parasites in patient's blood were identified in 1880 for the first time by Charles Louis Alphonse Laveran, who was awarded the Noble Prize in 1907 (CDC website 2012). Around the same time, Ronald Ross (honored with Nobel Prize in 1902) and Giovanni Battista Grassi both demonstrated that female *Anopheles* mosquitoes could transmit malaria (CDC website 2012). Although people have combated malaria for a long time, the first incomplete, successful Global Malaria Eradication Program was initiated by the WHO in 1955 (WHO, 1999), relying on chloroquine for treatment and prevention as well as DDT for vector control. This campaign succeeded in eliminating malaria from North America, the Caribbean, South-Central America, Europe, and parts of Asia (Carter *et al.*, 2002). With the emergence of *Plasmodium* parasites resistant to chloroquine (CQ) and DDT-resistant *Anopheles* mosquitoes (Brito, 2001), global eradication was abandoned in 1972. Starting from post-global eradication, the malaria situation has slowly and progressively deteriorated (Trape, 2001). In order to combat this worsening situation and disaster, several programs have been launched to control or eliminate malaria as a public health problem. For example, the Roll Back Malaria (RBM) program is a global initiative for the effective control of malaria by establishing a global partnership and was started in 1998 by the World Health Organization, the United Nations Development Program, the United Nations Children's Fund, and the World Bank (WHO website 2012). The publicized aim of this program was to halve the global malaria burden of risk, morbidity, and mortality by 2010 (Hay *et al.*, 2004). The program has applied multiple tools for malaria control including expanding effective treatment and providing insecticide-treated mosquito nets for vector control, encouraging the development of new drugs and vaccines against malaria, and setting up an emergency response for malaria epidemics. Remarkably, RBM intends to improve local health systems when realized that malaria was becoming a health and socioeconomic problem in epidemic areas, especially sub-Saharan

Africa (WHO website 2012). Despite eminent progress reported, an estimated 3.3 billion people are at risk of malaria (WHO, 2011), which and was responsible for approximately 655,000 to 1.24 million deaths (Murray *et al.*, 2012) and 216 million infections in 2010 (WHO, 2011) leads to a great socioeconomic and health burden. Up to 81% of the cases and 91% of the deaths occurred in Africa, predominantly among pregnant women and children under five (WHO, 2011; Murray *et al.*, 2012).

As reported by the WHO in 2011, malaria is prevalent in 106 countries of the tropical and subtropical world as shown in Figure 1.1, among which 35 countries in central Africa bore the burden of the most cases and deaths (WHO, 2011). Compared to one century ago, the worldwide area at risk of malaria has shrunk from 53% to 27%, and the number of countries exposed to malaria has decreased from 140 to 106 (Hay *et al.*, 2004; WHO, 2011). Malaria mortality rates have fallen by more than 25% globally since 2000, and by 33% in the WHO African Region (WHO, 2011). Coverage of insecticide-treated nets (ITN) and indoor residual spraying (IRS) has increased, and more pregnant women are receiving chemoprevention (WHO, 2011). The supply of rapid diagnostic tests (RDTs) and artemisinin combination therapies (ACTs) has risen globally, the latter of which was 32% more than that in 2010 (WHO, 2011). However, there were malaria cases with suspected artemisinin resistance identified in three additional border areas between Thailand and Cambodia and the rapidly growing threat of resistance to the insecticide, pyrethroid (WHO, 2011).

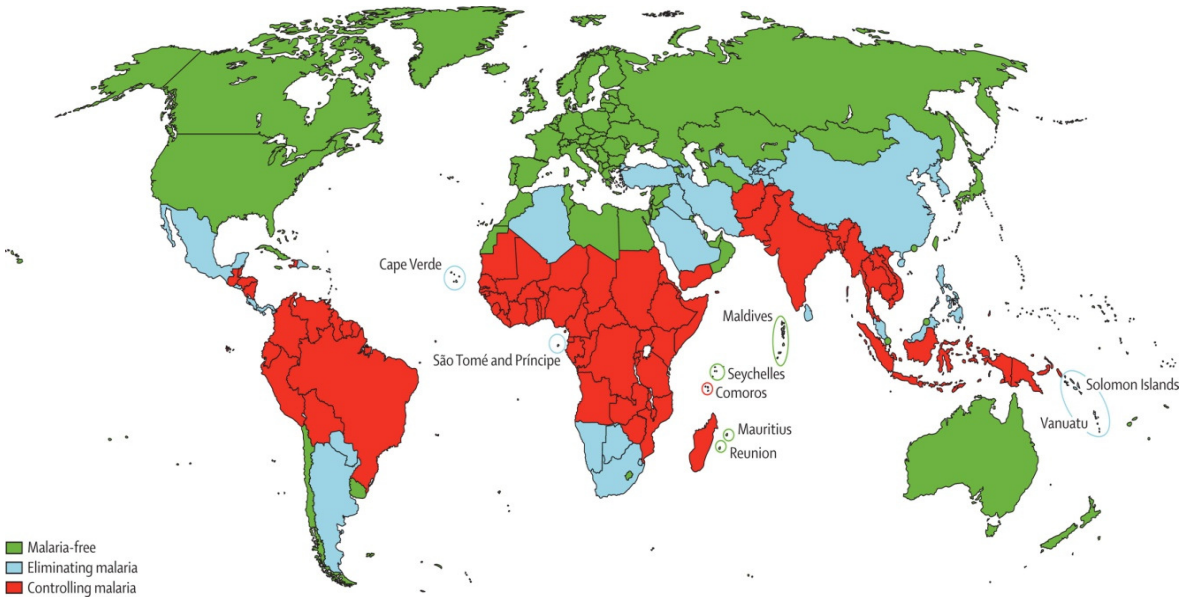

Figure 1.1 Worldwide distribution of countries at risk of malaria in 2010 (Feachem *et al.*, 2010)

1.1.2 Life cycle of *Plasmodium falciparum*

Caused by five species of *Plasmodium* from the phylum *Apicomplexa* that infect humans, including *P. falciparum*, *P. knowlesii* (Singh *et al.*, 2004; Collins, 2012), *P. malariae*, *P. ovale*, and *P. vivax*, *P. falciparum* and *P. vivax* are the predominant species responsible for most malarial infection (WHO, 2011). *P. falciparum* is the most severely lethal in Africa for most malarial deaths while *P. vivax* is more frequent and more widely distributed outside Africa with less virulence compared to *P. falciparum* (WHO, 2011). *Plasmodium malariae*, also called quartan malaria, causes a fever with a

periodicity of four days, while the other malarial parasites have only the two-day intervals. *P. vivax* and *P. ovale* are difficult to eradicate because they can evolve into a hypnozoite, a small structure that can hide dormant in the liver for a long period of time. *P. knowlesii*, a malaria parasite of the long-tailed macaque, also naturally infects humans (Singh *et al.*, 2004).

Malaria parasites display a complex life cycle with different stages and multiple forms occurring in the vertebrate (human) and invertebrate (*Anopheles* mosquito) hosts (Figure 1.2). All five species exhibit a similar life cycle with slight variations.

Sporozoites from the saliva of an *Anopheles* female mosquito are transmitted to humans by a bite as an initial step of infection (Step 1 in Figure 1.2). Normally more than 25 sporozoites are likely to be injected into the subcutaneous tissue from where they can migrate into the blood stream. Through the circulatory system, sporozoites are carried to the liver where they invade hepatocytes. The intracellular parasite undergoes asexual replication known as exoerythrocytic schizogony (Step 2 – 4 in Figure 1.2), which last roughly 5.5 days. Notably unlike the others, *P. vivax* and *P. ovale* are capable of undergoing a dormant period instead of asexual replication within hepatocytes. After this liver stage, thousands of mature merozoites are released from the hepatocytes and invade the erythrocytes upon entering the bloodstream. The invasion process is mediated by an apical complex, pellicle, and surface coat. Upon entering the erythrocytes, the parasites lose their invasion organelles, the apical complex and surface coat, and form trophozoites. Parasites as immature trophozoites stay within a parasitophorous vacuole in the erythrocyte cytosol. The young trophozoites, in a form called the ring stage due to its morphology, develop into mature trophozoites within 24 hours after merozoite invasion. Multiple rounds of nuclear division without cellular segmentation manifest the advent of the schizont stage. Later these schizonts develop and form approximately 16-18 merozoite cells in the erythrocyte. Red blood cells are ruptured and the merozoites burst from infected erythrocyte after 48 hours of invasion (72 hours for *P. malariae*). Invasion of new erythrocyte reinitiates another erythrocytic life cycle (Step 5 in Figure 1.2). The blood stage is responsible for the pathology associated with malaria and various symptoms in malaria patients.

During the erythrocytic stage, a few of the blood-stage merozoites differentiate into macrogametocytes (female) and microgametocytes (male) instead of developing into schizonts (Step 6 in Figure 1.2). When a female mosquito bites an infected human, the gametocytes with both types are ingested into mosquito gut (Step 7 in Figure 1.2). Macrogametocytes (female) and microgametocytes (male) develop into gametes in mosquitos (Step 8 in Figure 1.2). There are several factors to induce this gametogenesis: a sudden drop in temperature, a rise in pH, an increase in carbon dioxide, and metabolites within the mosquito. Then female gametes are fertilized by male gametes to form zygotes (Step 9 in Figure 1.2). The zygotes later elongate and develop into ookinetes (Step 10 in Figure 1.2). The zygote and ookinete are the only diploid stages of *Plasmodium*. Once traversing the peritrophic membrane and epithelium of the mosquito midgut and going into basal lamina, ookinetes develop into oocysts there (Step 11 in Figure 1.2). Numerous haploid sporozoites are formed after oocyst maturation and ruptured from the oocysts, releasing them into the haemolymph (Step 12 in Figure 1.2). The sporozoites migrate into the salivary glands for the next round infection (Step 13 in Figure 1.2). Once such mosquitos bite other health humans, they can be infected and a new life cycle of *Plasmodium* starts. Two weeks could be a time frame when the mosquito becomes infectious after ingesting gametocytes from an infectious

human bloodmeal.

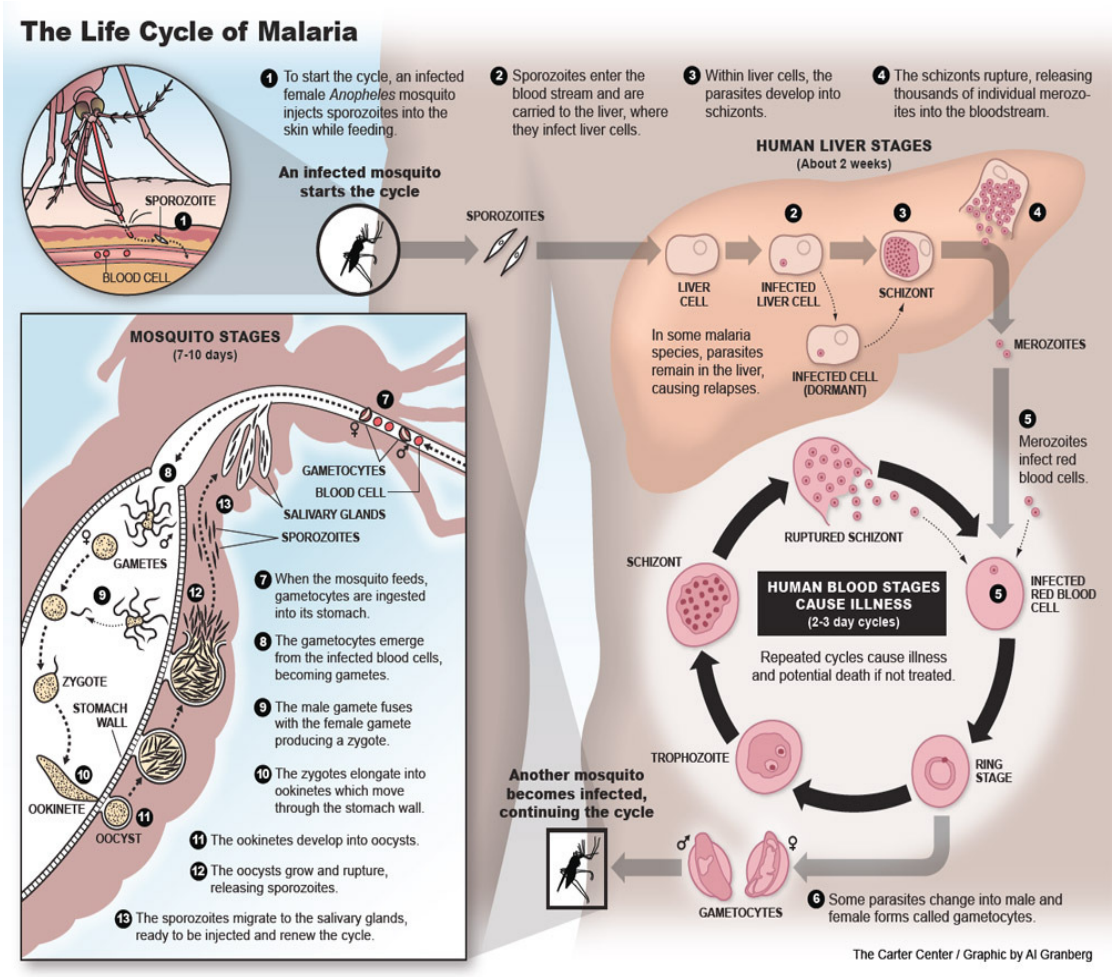

Figure 1.2 Life cycle of malaria (http://www.cartercenter.org/health/malaria_control/index.html).

1.1.3 Antimalarial drugs and malaria vaccine for malaria control

The unicellular *Plasmodium* must combat the diverse environments and barriers it encounters during its complicated life cycle by employing more than 5,000 genes (Gardner *et al.*, 2002). Thus, each developmental stage of *Plasmodium* provides a potential drug target for disrupting the parasitic life cycle. Among numerous potential lead compounds and drugs, the most widely used drugs currently are limited to a few categories: quinine, chloroquine, pyrimethamine, atovaquone, artemisinin, and their derivatives (Table 1.1).

Before the introduction of combination therapies, quinoline as an antimalarial drug is the lead member in antimalarial therapy. This family comprises chloroquine, quinine, amodiaquine, piperaquine, primaquine, and mefloquine, which function by binding to heme and inhibiting its detoxification in the food vacuole (Fitch, 2004). Sulfadoxine-pyrimethamine, a co-formulation of two different medicines, is widely used to treat chloroquine-resistant malaria (WHO, 2010). Remarkably, infants and pregnant women are treated with this drug because of its long half-life, low cost, and safety (WHO, 2010). Studies on treatment failure revealed a much higher rate in Africa than in other regions and a fast development of resistance once nation-wide intensive usage of this medicine occurred (WHO, 2010).

The combination of atovaquone with proguanil is an antimalarial medication used in both the treatment and prevention of malaria (WHO, 2010). Malarone as a trade name for this combination has been commercially available from GlaxoSmithKline since 2000. It is suitable for travelers as a prophylaxis because the drug is taken starting 1-2 days before traveling with good tolerance. Compared to most previous antimalarial drugs, artemisinin and its derivatives have more beneficial properties such as rapid elimination and targeting all the blood stages of the malaria life cycle including early ring forms, which are especially profitable for the treatment of severe malaria.

Chemical family	Drugs
4-Aminoquinolines	Chloroquine, amodiaquine, piperaquine
Amino-alcohols	Quinine, quinidine, mefloquine, halofantrine, lumefantrine
Sulfonamides and sulfones	Sulfadoxine, sulfalene, dapsone
Biguanides	Proguanil, chlorproguanil
Diaminopyrimidine	Pyrimethamine
8-Aminoquinoline	Primaquine
Sesquiterpene lactones	Artemisinin, arteether, artemether, artesunate, dihydroartemisinin
Naphthoquinone	Atovaquone
Antibiotics	Azythromycin, clindamycin, doxycycline, tetracycline

Table 1.1 Principle available antimalarial drugs (WHO, 2010).

Today, combination therapy is applied to the treatment of malaria cases because of its multiple advantages such as a reduced possibility of resistance development, an enhanced efficacy of treatment, and fewer side effects. Thus artemisinin-based combination therapies (ACTs) are the pillars of first-line treatment of malaria cases. There are currently five recommended combinations: artemether-lumefantrine, artesunate-amodiaquine, artesunate-mefloquine, artesunate-sulfadoxine-pyrimethamine, and dihydroartemisinin-piperaquine (WHO, 2010). In spite of the emergence of *P. falciparum* strains resistant to artemisinins in Southeast Asia (Dondorp *et al.*, 2009; Anderson *et al.*, 2010), ACTs globally achieve more than 90% clinical efficacy (WHO, 2010).

Over the years, the efficacies of almost all antimalarial drugs have been interrupted by the rise of resistant *Plasmodium* strains. Recent studies highlight the importance of mutations in transporter molecules as major contributors to drug resistance and focus on three transporters: the chloroquine resistance transporter *Pf*CRT, the multi-drug resistance-associated protein *Pf*MRP, and the multi-drug resistance transporter 1 *Pf*MDR1 (Sanchez *et al.*, 2010). The multiple polymorphic alleles of *pfcrt* can confer different levels of chloroquine resistance (Sa *et al.*, 2009). Because lower amounts of CQ are observed in the food vacuoles of CQ-resistant parasites (Fitch, 2004), access of CQ to its target under the control of *Pf*CRT and a transport model of CQ drugs were proposed (Sanchez *et al.*, 2010). Single nucleotide polymorphisms of *pfmdr1* encoding an ATP-binding cassette (ABC) transporter and a homolog of P-glycoprotein in humans regulate drug susceptibility (Reed *et al.*, 2000; Sidhu *et al.*,

2005). A recent study demonstrated that *Pf*MRP may transport multiple antimalarial drugs, including CQ and QN, out of the parasites, thus playing a role in antimalarial drug resistance (Raj *et al.*, 2009). Besides these transporters, one to four point mutations in dihydrofolate reductase (DHFR) have been demonstrated to contribute to *P. falciparum* resistance to antifolates, while the mutations of dihydropteroate synthase (DHPS) are connected to the resistance to sulfonamides and sulfones (Le Bras *et al.*, 2003).

Besides the antimalarial drugs for malaria control, development of a safe and effective vaccine against malaria will be a vital step towards control, prevention, and eradication of malaria. Although acquisition of natural immunity appears limited only to blood stages in the human host, vaccines against parasites in three stages, the sporozoite and liver stage (pre-erythrocytic vaccines), the asexual blood stage (blood stage vaccines), and the sexual gametocyte/gamete stage (transmission blocking vaccines), are being developed (Figure 1.3) (Ashley *et al.*, 2012). A pre-erythrocytic vaccine is expected to evoke an immune response targeting all sporozoites or the vital proteins that prevent the invasion of hepatocytes, and/or to eliminate parasites within the hepatocytes. The immunization of mice with X-irradiated sporozoites of *P. berghei*, which cannot complete liver stage development, led to the development of protective immunity in mice (Nussenzweig *et al.*, 1967).

RTS,S vaccination, which is a recombinant protein-containing region of circumsporozoite protein (CSP), was shown to diminish clinical malaria by 30–50%, which has been the most promising result so far (Agnandji *et al.*, 2011). However, the goal in the Malaria Vaccine Technology Roadmap of 50% or greater efficacy against severe malaria or death that lasts at least one year is still hard to achieve through RTS,S, not to mention the long-term goal that a vaccine must be > 80% effective against disease (Nussenzweig *et al.*, 2011).

Even though it is unlikely that a blood stage vaccine will be completely effective in eliminating parasites, considering the fast speed of replication and destruction malaria brings to the immune system, it is still worth developing it as a powerful tool for malaria control and eradication. Up until now, the candidate antigens in the blood stage comprise merozoite surface protein 1-3 (MSP1-3), apical membrane antigen 1 (AMA-1), erythrocyte-binding surface antigen 175 (EBA-175), glutamate-rich protein (GLURP), ring-infected erythrocyte surface antigen (RESA), and serine repeat antigen 5 (SERA5) (Ashley *et al.*, 2012). The observation that low concentrations of anti-basigin antibodies can completely block the invasion of malaria (Crosnier *et al.*, 2011) suggested conserved merozoite ligands as candidate antigens. A vaccine at the sexual stage could directly benefit blocking the transmission of malaria, thus having a role in malaria elimination. Transmission-blocking vaccines (TBVs) target the developmental stages in the mosquito vector, therefore not attracting as much attention as other vaccines (Dinglasan *et al.*, 2008). Studies of Pfs25, a protein expressed on the surface of the zygote and ookinete form of the parasites, showed that high anti-Pfs25 IgG titers and sera from immunized mice inhibited the transmission of *P. falciparum* to the mosquito in mice (Goodman *et al.*, 2011). However, TBVs alone are obviously not capable of entirely eradicating malaria.

Even though much effort has been devoted to malarial research for centuries, malaria has yet to be conquered in its bastion. With the emergence of both drug and insecticide resistance and no effective vaccine, the identification of new promising targets is urgently needed.

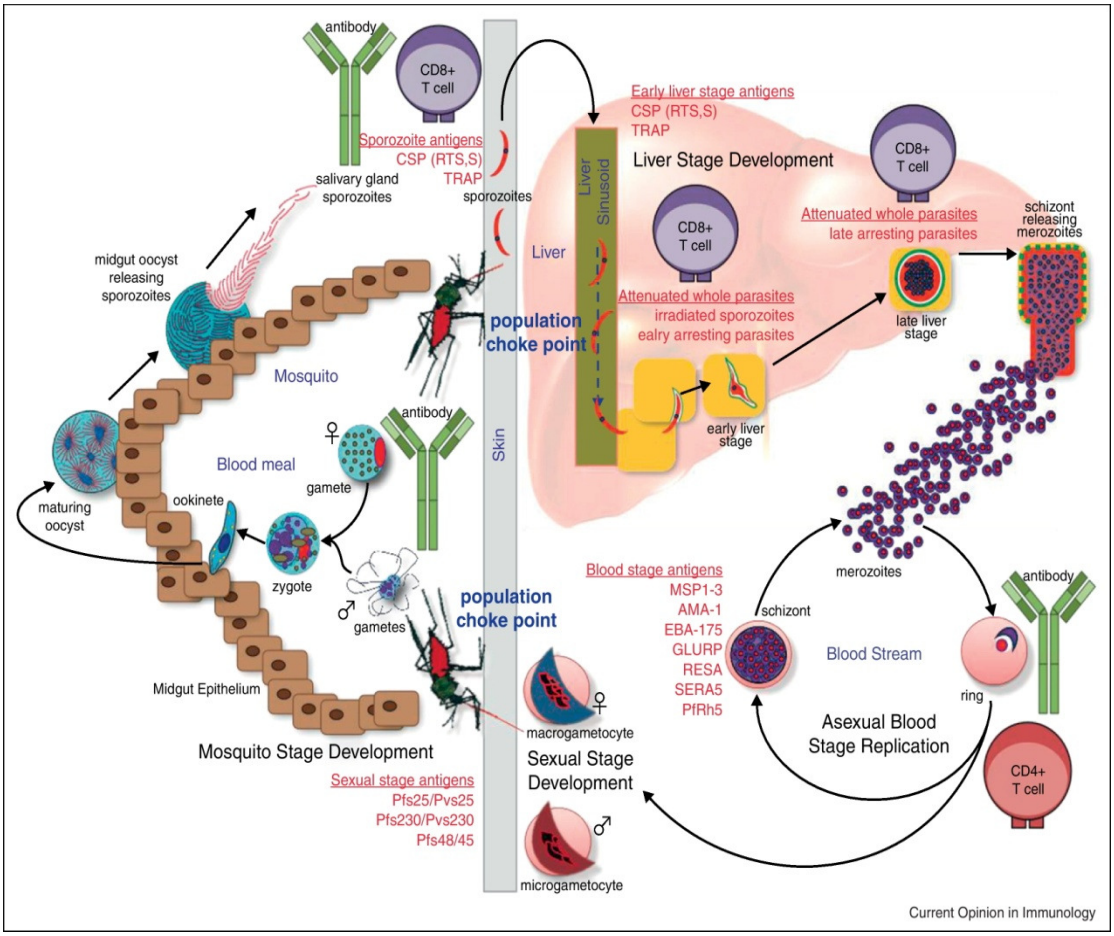

Figure 1.3 Parasite targets in different stages of the malaria life cycle used for vaccine development (Ashley *et al.*, 2012). Apical membrane antigen 1 (AMA-1), circumsporozoite protein (CSP), erythrocyte-binding surface antigen 175 (EBA-175), glutamate-rich protein (GLURP), merozoite surface proteins 1-3 (MSP1–3), reticulocyte-binding family homolog 5 (PfRh5), ring-infected erythrocyte surface antigen (RESA), serine repeat antigen 5 (SERA5), and thrombospondin-related adhesion protein (TRAP).

1.2 Adenylate kinase

The malaria parasite *Plasmodium* requires highly active adenylate kinase to fulfill its energetic and synthetic demands due to its fast metabolic rate and rapid multiplication. Adenylate kinase (AK, EC 2.7.4.3, ATP + AMP ⇔ 2 ADP), belonging to the nucleoside monophosphate kinase (NMPK) family, catalyzes the reversible high energy phosphoryl transfer from ATP to AMP, forming 2 ADP. This enzyme has been thoroughly studied to exemplify a model for catalytic mechanisms, the intracellular phosphoryl transfer system, and signal pathways.

1.2.1 Molecular and biochemical properties of adenylate kinase

It has been more than 60 years since adenylate kinase, initially called myokinase, was first reported by Colowick and Kalckar (Colowick *et al.*, 1943; Kalckar, 1944; Kotel'nikova, 2001). It was identified in many species such as *Escherichia coli* (Barzu *et al.*, 1983), yeast (Chiu *et al.*, 1967), rice (Kawai *et al.*,

1995), pig (Sato *et al.*, 1982), and other organisms. In mammals, there are eight isoenzymes of AK encoded by separate genes and located on different chromosomes. AK1 and AK2 are localized in the cytosol and the mitochondrial intermembrane, respectively, and prefer ATP rather than other nucleotide triphosphates as substrate, while AK3 is found in the mitochondrial matrix and uses GTP as a substrate (Tomasselli *et al.*, 1979; Walker *et al.*, 1982; Tanabe *et al.*, 1993; Janssen *et al.*, 2004). Acetylation and myristoylation in yeast AK1 and mouse AK2 were discovered to facilitate their binding to cell membranes (NODA, 1973; Klier *et al.*, 1996; Janssen *et al.*, 2004). AK4 and AK5 are found in the mitochondrial matrix and cytosol, respectively, with tissue specificities (Yoneda *et al.*, 1998; Noma, 2005). Human AK4 was initially designated AK3 due to its 58% homology to bovine AK3, which was then renamed AK4 when it was found in the mammalian central nervous system (Yoneda *et al.*, 1998). Thus, there are two AKs in the mitochondrial matrix, but no AK activity can be detected *in vitro* for human AK4 (Noma *et al.*, 2001). AK4 could interact with the mitochondrial ADP/ATP translocator, through which it exerts protective properties for cell survival and proliferation as a stress responsive protein (Liu *et al.*, 2009). Further studies show that a glutamine to arginine (Q159R) mutation in human AK4 recovers the adenylate kinase activity with GTP as a substrate (Liu *et al.*, 2009). AK5 is expressed in human pancreatic beta-cells and regulated in the K-ATP channel (Stanojevic *et al.*, 2008). Human AK6 is found in the nucleus and belongs to a distant subgroup of the AK family (Ren *et al.*, 2005) with an unusually broad substrate specificity, nuclear localization, and structural features of ATPase/GTPase proteins (Drakou *et al.*, 2011). The nuclear protein Rad50 in the DNA repair RAD50/MRE11/NBS1 protein complex (RMN) exhibits AK activity besides ATP hydrolysis facilitating efficient tethering between different DNA molecules (Bhaskara *et al.*, 2007). NBS1, the Nijmegen breakage syndrome gene product, is required for enzymatic activities of Rad50 and the whole RMN complex function (Paull *et al.*, 1999). Recently human AK7 and AK8 have been characterized, and both have cytosolic localizations with a much larger size of AK7 compared to other isoforms (Panayiotou *et al.*, 2011). The blast program reveals an NAD(P) binding site at its N-terminus, implying the other potential functions of human AK7.

1.2.2 Structure and catalysis of adenylate kinase

Structure and conformational transitions during the catalytic process of adenylate kinase have been investigated intensively. The general structure of adenylate kinase is composed of a CORE domain with a peripheral NMP-binding domain and a LID domain as shown in Figure 1.4. The CORE and NMP-binding domains are conserved in all AKs, whereas the LID domain is quite different. Depending on the size of the LID domain, AKs are divided into two groups: short form AKs including AK1, AK5, and AK6 in which the LID is simply a variable loop; and long form AKs such as AK2, AK3, and AK4 in which the LID is a four-stranded anti-parallel b-sheet. Prokaryotes exclusively have the long variant while both short and long AK variants are found in the cytoplasm and mitochondria of eukaryotes (Yan *et al.*, 1999).

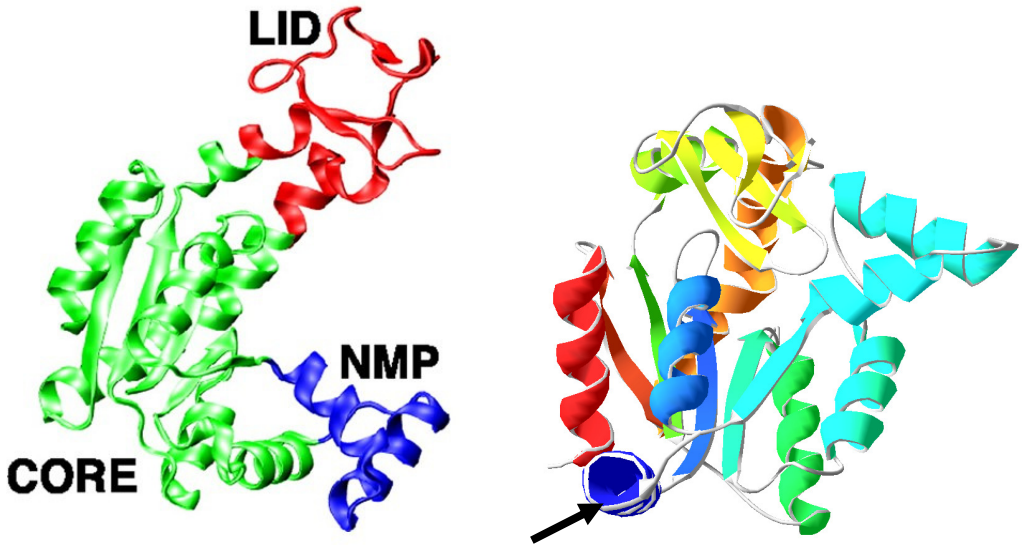

Figure 1.4 3D structure of adenylate kinase with closed and open conformations. Structure of apo/open conformation of AK from E. coli (left) (Arora *et al.*, 2007). The LID domain is in red, the AMP-binding domain in blue, and the core domain in green. The structure of the closed conformation of AK1 from *P. falciparum* (right) (3TLX from PDB) was partly predicted due to several missing amino acid residues in databank. A unique structure at the N-ternimus is labeled by an arrow.

NMR spectroscopy, X-ray crystallography and temperature-stability studies combined with site-directed mutagenesis have been employed for investigating structurally and catalytically important residues in adenylate kinases. Lysine[13] of AK from *E. coli* may play a vital role in catalysis (Reinstein *et al.*, 1990). Arg[132,138] and Arg[149] of cytosolic AK1 from the pig were important in transition-state stabilization, while Arg[44] and Arg[97] interacted with AMP specifically, and Asp[93] was critical to Mg^{2+} binding (Tsai *et al.*, 1991). Construction of a stabilized pentaco-ordinated transition state based on the crystal structure of *E. coli* AK with a bi-substrate inhibitor AP_5A was demonstrated as well (Figure 1.5).

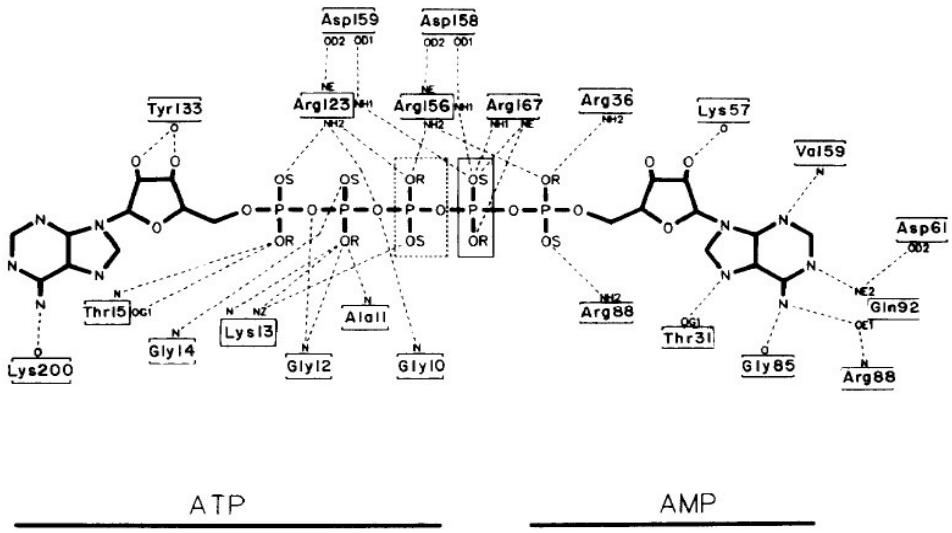

Figure 1.5 Schematic diagram of hydrogen bonds between Ap_5A and the polypeptide of AK (Muller *et al.*, 1992).

More research has focused on conformation transition of AK in the reaction since large conformational changes between active and inactive states are required for the activity of the enzyme. Conformational changes in the LID and NMP domains of adenylate kinase are demonstrated to be pivotal to ligand binding.

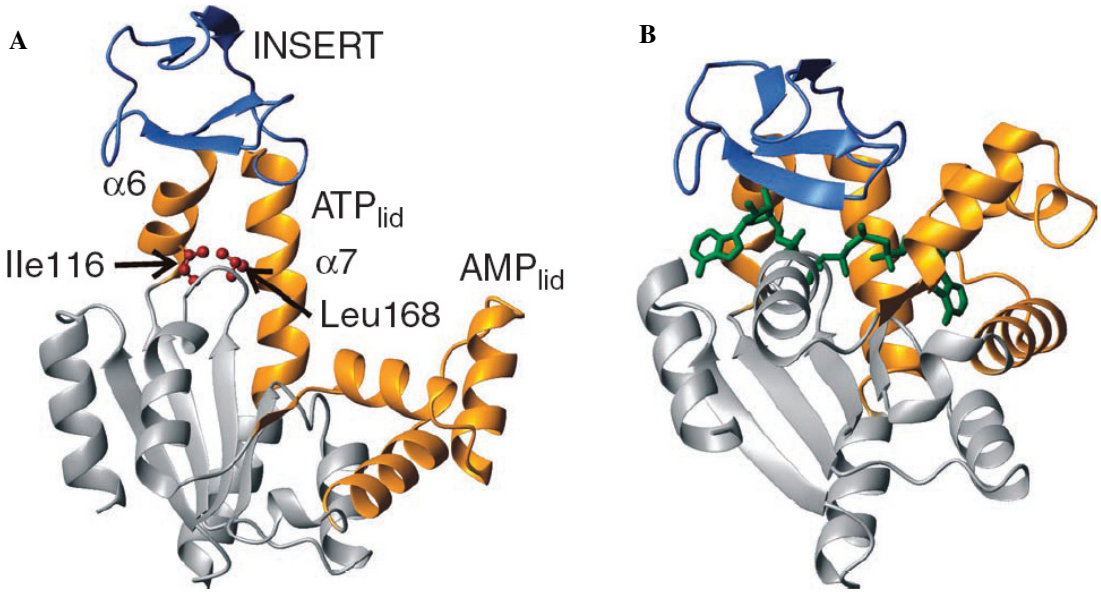

Figure 1.6 Structures of AK during the extreme stages of catalysis (Olsson *et al.*, 2010). (A) Substrate-free open AK; **(B)** Closed AK with bound Ap_5A.

Several models are proposed for elucidating the conformational changes in AK. In an induced-fit model, segments in between hinge regions' binding are spatially translated as rigid bodies (Gerstein *et al.*, 1993). Closure of ATP_{lid} resulted from rotation of the INSERT segment in helices α6 and α7, which in turn rotated the CORE domain (Figure 1.6) (Gerstein *et al.*, 1993; Olsson *et al.*, 2010). In another cracking model inferred from coarse-grained modeling and the principle of minimal frustration, high strain energy in the reaction was observed and released through localized regions of the protein unfolding during the functional transition (Whitford *et al.*, 2007). It was also suggested that LID motion signals NMP motion in a catalytic mechanism (Figure 1.7) (Whitford *et al.*, 2008). Unfolding/refolding of a partial subdomain in the enzyme is involved in the interconversion between open and closed states of the ATP-binding subdomain by using a combination of biophysical and mutagenic approaches (Olsson *et al.*, 2010).

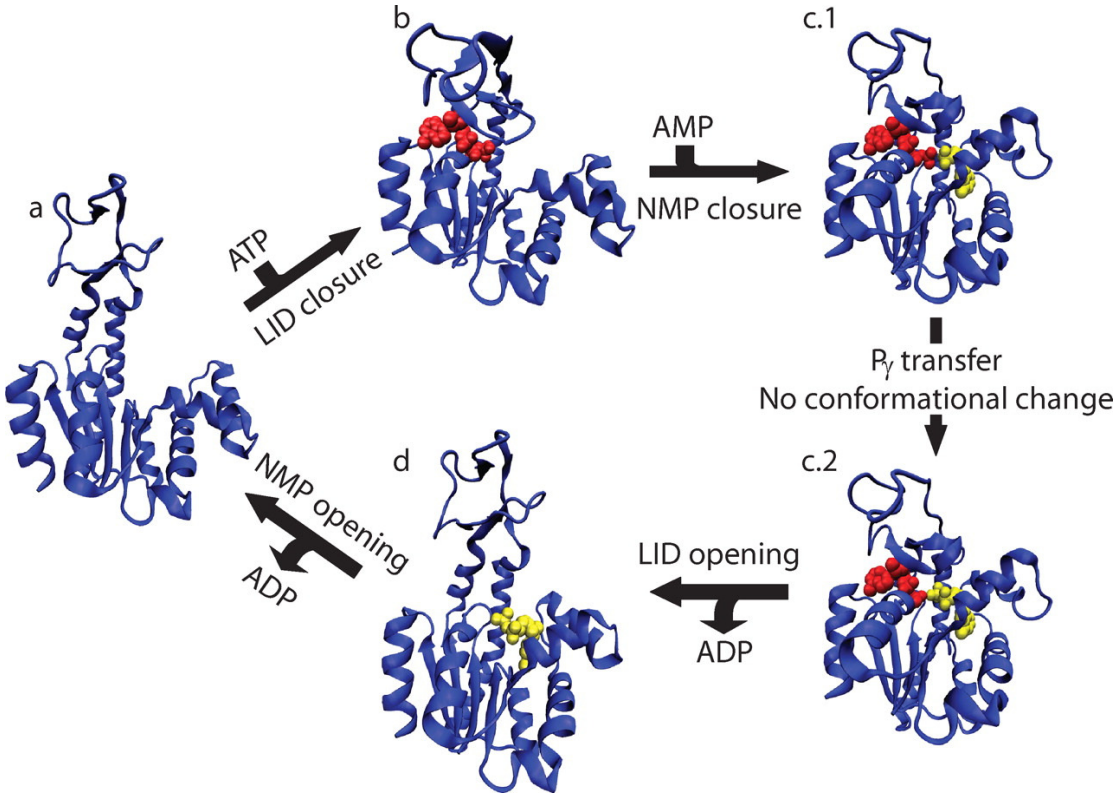

Figure 1.7 Proposed mechanism for AK catalysis (Whitford *et al.*, 2008).

1.2.3 Energy metabolism and signal pathway

The requirement of a significant concentration gradient in condensed mitochondrial and cellular structures makes them inefficient in energy transfer via diffusional exchange of adenine nucleotides (Dzeja *et al.*, 2003). The important role of adenylate kinase in cellular energy metabolism has been acknowledged, especially since the discovery that AK transfers and utilizes γ- and β-phosphoryls among adenosine phosphate molecules following a chain of sequential reactions (Dzeja *et al.*, 1985; Zeleznikar *et al.*, 1990; Dzeja *et al.*, 1996). The function of utilizing the second high-energy bond of the β-phosphoryl in the ATP molecule is crucial for the local compartment, which requires high and fluctuating energy. The networks of efficient energy transfer catalyzed by AK and ligand conduction circuit are gained by phosphoryl exchange measurements using ^{18}O-assisted ^{31}P-NMR techniques and biochemical, gene-knockout research (Janssen *et al.*, 2000; Dzeja *et al.*, 2002; Dzeja *et al.*, 2007b; van Horssen *et al.*, 2009). Figure 1.8 demonstrates the energy transfer shuttle catalyzed by AK from production to utilization within a cell. The energy transfer network of AK has multiple functions, which supply the driven force of high-energy phosphoryl flux. Contraction-mediated phosphorylation of AMP-activated protein kinase (AMPK) and muscle energetic economy were impaired in the skeletal muscle of AK-deficient mice (Janssen *et al.*, 2000; Hancock *et al.*, 2006). Energy supply to cell nucleus and cell motility was facilitated by functional energy transfer mediated by AK (Ren *et al.*, 2005; Cao *et al.*, 2006; Ford, 2006; Botta *et al.*, 2008). Adenylate kinase could modulate the activity of glycolytic and glycogenolytic enzymes and provide an integrative node for both pathways in order to respond rapidly to fluctuating energy demands (Dzeja *et al.*, 2007a). AK was shown to be involved in sperm motility through ATP delivery from mid-piece mitochondria to remote ATPases in the tail (Schoff *et al.*,

1989). Lower energetic efficiency, misrepresented signals to energy and metabolic sensors, including AMPK and K-ATP channels, and compromised adenosine generation were observed in AK1 knockout mice (Pucar *et al.*, 2000; Carrasco *et al.*, 2001; Pucar *et al.*, 2002; Hancock *et al.*, 2005; Hancock *et al.*, 2006).

A network of cellular energetic systems provides new angles for interpreting the relevant diseases from interruption aspects of energy metabolism, metabolic surveillance and sensor response (Weiss *et al.*, 2006; Dzeja *et al.*, 2007b). Heart failure was also shown to be related to compromised AK energy transfer (Dzeja *et al.*, 1999; Dzeja *et al.*, 2000; Dzeja *et al.*, 2007b).

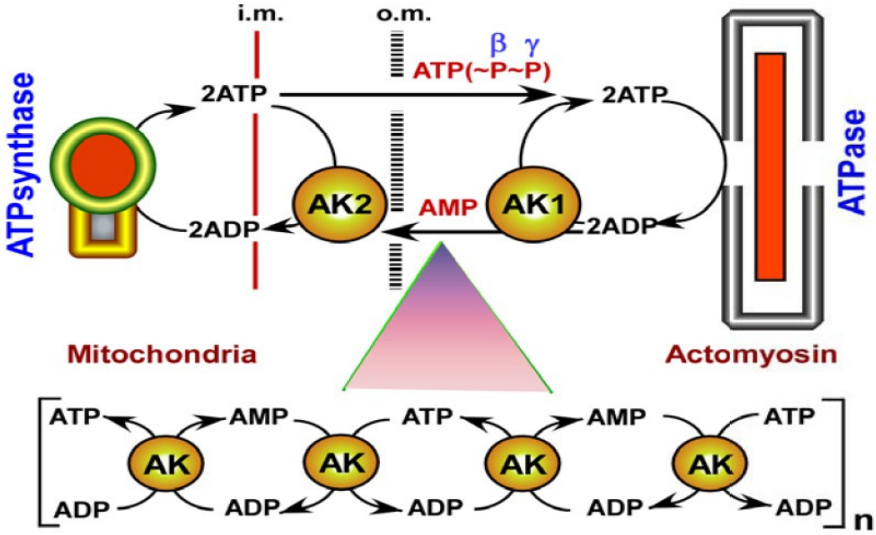

Figure 1.8 Energy transfer shuttle catalyzed by AK from production to utilization (Dzeja *et al.*, 2009). i.m. and o.m. – inner and outer membranes of mitochondria.

A membrane-associated isoform AK1 affected a tumor suppressor protein, p53, and low energy status in cells suppressed the malignant phenotype in tumor development (Collavin *et al.*, 1999; Swinnen *et al.*, 2005). Down-regulation of cytosolic AK1 transcription with siRNA resulted in increasing apoptosis in pancreatic cancer cells in human kinome profiling (Giroux *et al.*, 2006). The myristoylated AK1 was shown to be associated with the nuclear envelope, indicating a possible role in energy support of the nucleus (Janssen *et al.*, 2004). Mutations in the mitochondrial AK2 gene were discovered in the patients with reticular dysgenesis, which is the rare autosomal recessive form of inborn severe combined immunodeficiencies (SCID), which is associated with sensorineural deafness (Lagresle-Peyrou *et al.*, 2009; Pannicke *et al.*, 2009). It was shown that expression of AK2 was reduced significantly by AK2 gene defects identified in individuals with RD (Pannicke *et al.*, 2009). In contrast to the general concept that adenylate kinase mainly consumes ATP, the function of maintaining nucleotide pools was compromised in AK1 knock-out hearts under metabolic stress (Pucar *et al.*, 2000).

Since recent studies demonstrate that AMP signaling participates in diverse cellular processes (Hardie, 2008; Hardie *et al.*, 2012), AK is considered to play a critical role in metabolic pathways. Due to the catalytic properties of AK, a small decrease in ATP would result in a significant increase in AMP, thus representing AMP as an excellent energetic signal (Hardie *et al.*, 2012). For example, the catabolic

pathways producing ATP will be up-regulated, while the consumption of ATP is suppressed as a result of AK-mediated metabolic monitoring and downstream AMP signaling as activated by energetic stress (Figure 1.9) (Dzeja *et al.*, 2009). Adenylate kinase also promotes transmission of nucleotide signals in the compartment of intracellular and extracellular space through a sequence of spatially arranged enzymatic reactions. AK directly regulated the response of ATP-sensitive potassium channels K(ATP) to metabolic challenge and delivered mitochondrial signals to the cell membrane environment (Carrasco *et al.*, 2001). Due to the restriction of metabolite diffusion and spatial heterogeneity in the cell, the network of adenylate kinase is suitable for a high rate of phosphoryl exchange supported ligand conduction and signal transmission (Dzeja *et al.*, 2003). AK can cause AMPK activation, which has multiple cellular functions from adaptation to stress as shown in Figure 1.10 (Hardie *et al.*, 2012). An increase of AMPK activity in ischemia and protection of myocardium against ischemic injury by AMPK agonists were observed (Young *et al.*, 2005; Dyck *et al.*, 2006). Activation of AMPK by chemical compounds increases glucose transport activity in skeletal muscle both *in vivo* and *in vitro* (Bergeron *et al.*, 1999). The fact that mitochondrial content was significantly reduced in muscle tissue of double knockout mice lacking any AMPK activity demonstrated a vital role of AMPK in mitochondrial biogenesis (O'Neill *et al.*, 2011). The vital function of adenylate kinase in energetic signaling, which controls actin assembly in cell movement and chemotaxis, has been revealed (Kuehnel *et al.*, 2009). Above all, adenylate kinase regulates the signals for downstream AMPK, the energy metabolic pathways, and biomolecular synthesis through its unique β-phosphoryl utilization and nucleotide ratio adjustment.

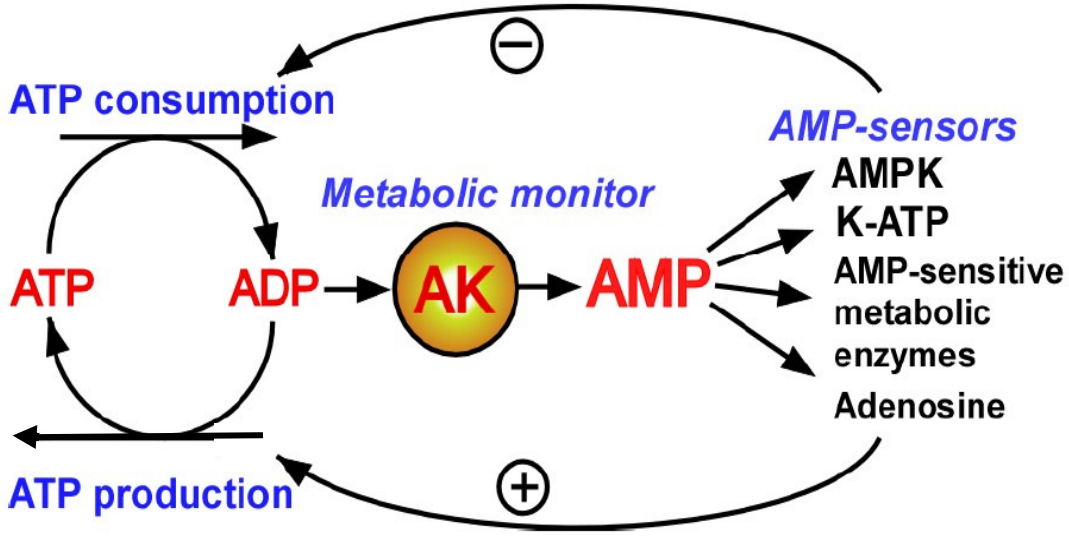

Figure 1.9 AK-mediated AMP signal pathways and monitor system (Dzeja *et al.*, 2009). AMP signal produced by AK, through which the energy status in cells is transmitted. AMP-sensors will up-regulate ATP production pathways and negatively regulate ATP utilization.

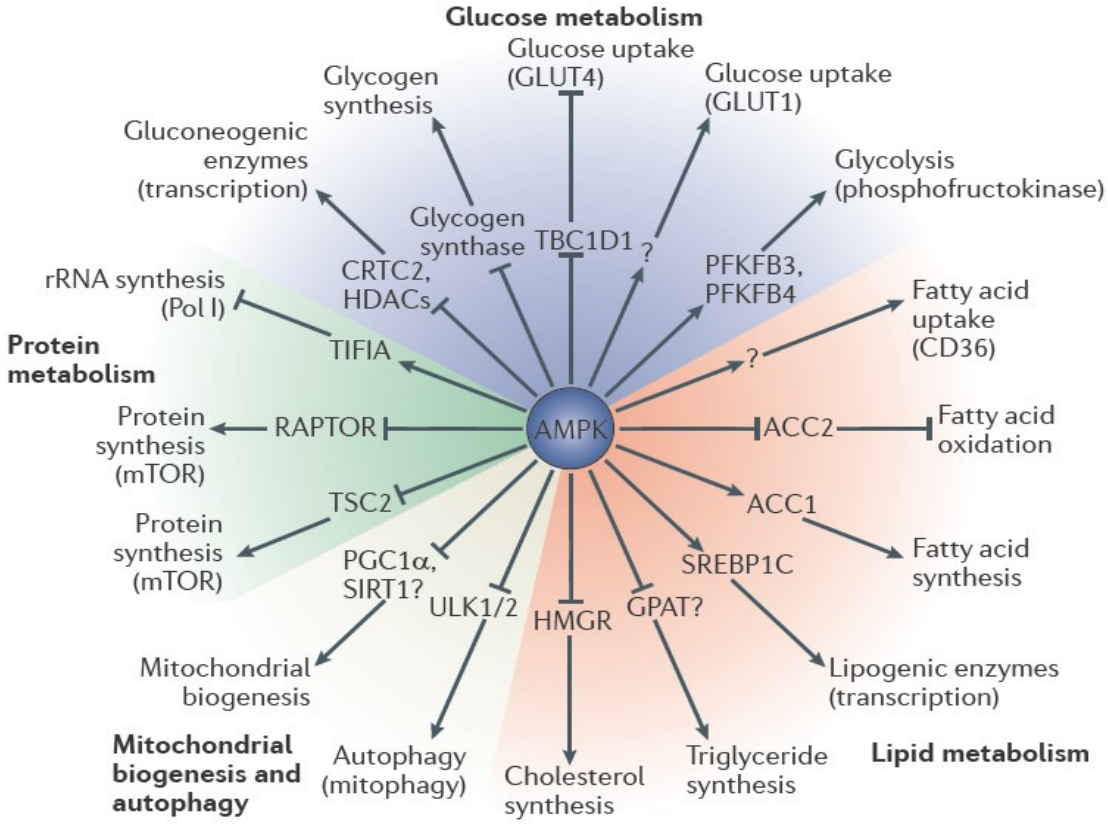

Figure 1.10 Effects of activation of AMPK on cellular metabolism (Hardie *et al.*, 2012).

The multiple isoforms of adenylate kinase with diverse subcellular localizations, tissue specificities, and kinetic properties are required for their local metabolic environment. There are variants of AK1-2 only found in Caucasian populations and hemophilia-A patients (Lee *et al.*, 1998) that have less than one third specific activity compared to variant AK1-1 with the same Michaelis constants (Luz *et al.*, 1990). AK3 and AK4 could be regulated by transcript factors called hypoxia-inducible factor 1(HIF-1) for cell survival (Semenza, 2000; Hu *et al.*, 2006). *In situ* compartmentation studies demonstrated that adenylate kinase was localized along with creatine kinase and glycolytic enzymes in skeletal muscle myofibrils, implying multiple multienzyme complex formation and energy supply for muscle contraction (Wegmann *et al.*, 1992). Using tagging GFP protein, myristoylated AK1 isoform was localized to the plasma membrane, while wild-type AK1 was in the cytosol (Ruan *et al.*, 2002). A study of intracellular localizations of AK isoforms in the parasite *Trypanosoma brucei* interpreted an unusually expended adenylate kinase family and provided insight for understanding the complexity of energy metabolism, demonstrating a sophisticated phosphotransfer network in this invasive parasite (Ginger *et al.*, 2005). By using Ty1 epitopes at the C-terminus of respective AKs, they demonstrated that one was targeted to the unique kinetoplastid-specific microbodies of the peroxisome class called glycosomes, where many reactions of carbohydrate metabolism are compartmentalized, and three isoforms were selectively built into either the flagellar axoneme or the extra-axonemal paraflagellar rod, which is essential for motility. Kinetic results from the only short form trypanosome adenylate kinase displayed a high activity and specificity toward CMP, revealing an adaptation to very low intracellular cytidine nucleotide concentrations (Ginger *et al.*, 2005). In a closely related species *Trypanosoma cruzi*,

six different genes of adenylate kinase isoforms were discovered via RT-PCR and Northern blot (Bouvier *et al.*, 2006). Thus this enlarged adenylate kinase gene family suggested a complex energy metabolism in this unicellular parasite. Strikingly, introduction of a Pro87Ser substitution in adenylate kinase renders *Yersinia pestis* avirulent (Munier-Lehmann *et al.*, 2003).

Therefore, adenylate kinase is a key component in the cellular bioenergetics network for regulating and maintaining energy homeostasis and AMP-mediated signal pathways.

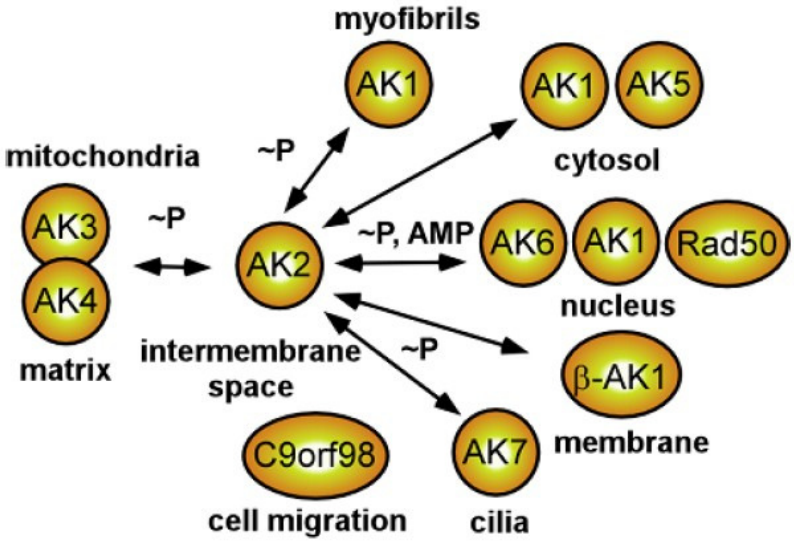

Figure 1.11 Adenylate kinase isoforms network and intracellular localizations (Dzeja *et al.*, 2009).

1.2.4 Adenylate kinase in *Plasmodium*

Plasmodium requires highly active adenylate kinase for rapid ATP turnover in order to cope with its energetic demand and biomolecular synthesis. Consumption of glucose in parasitized red blood cells has been shown to increase 50-100-fold compared to uninfected erythrocytes and is utilized during glycolysis to produce ATP (Roth, 1990). Parasites in the intraerythrocytic stage have also been suggested to export ATP to their host cell by means of an adenylate translocator and adenylate kinase, which is explained to maintain the minimum glycolysis pathway in the host cells so as to provide more glucose to the parasites (Kanaani *et al.*, 1989). Malaria parasites developed a unique TCA pathway according to their life cycle in order to meet their own needs. By using mass spectrometry combined with ^{13}C-labelled compounds, the tricarboxylic acid metabolism in *Plasmodium falciparum* has been shown to be disconnected from glycolysis and has its own features compared to the canonical pathway (Olszewski *et al.*, 2010). The notable characteristics of the TCA cycle in parasites are that the cycle is bifurcated and glutamate is required due to it lacking a pathway to convert pyruvate to acetyl-CoA as shown in Figure 1.12 (Olszewski *et al.*, 2010). Although ATP is believed to mainly be generated in the glycolytic pathway of parasites at least during the asexual stage, there is biochemical evidence to display mitochondrial function in ATP synthesis and Ca^{2+} transport in the trophozoite stage of the malaria parasite *Plasmodium berghei* (Uyemura *et al.*, 2000). Recent studies suggest that ATP synthase is localized to the parasite mitochondrion and seems essential for parasite survival in *Plasmodium falciparum* (Balabaskaran Nina *et al.*, 2011), indicating that a mitochondrial function in adenosine

triphosphate (ATP) production cannot be completely excluded. Atovaquone, one antimalarial drug, has been shown to inhibit electron transport and to collapse the mitochondrial membrane potential in malaria parasites (Srivastava *et al.*, 1997).

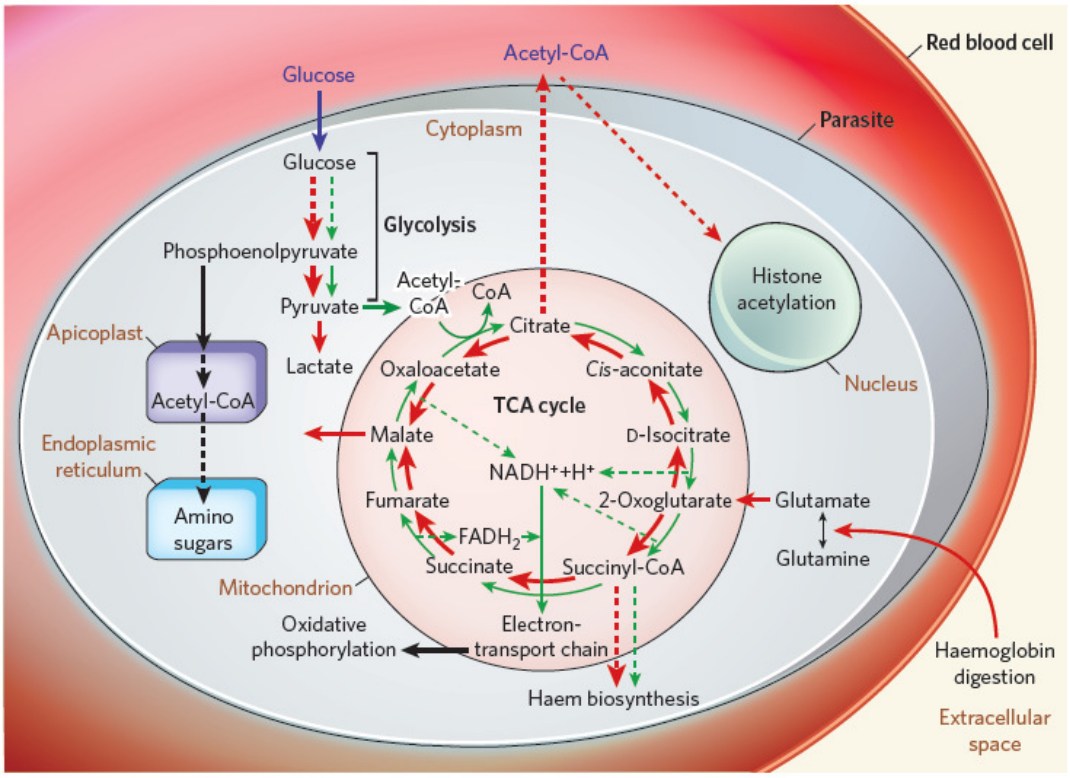

Figure 1.12 Metabolic and energetic pathways in *P. falciparum* (Ginsburg, 2010). Classic pathways are labeled in green; the unique pathways in *P. falciparum* are labeled in red.

Two AKs (*Pf*AK1, *Pf*AK2) and a GTP:AMP phosphotransferase (*Pf*GAK, EC 2.7.4.10, GTP + AMP ⇔ GDP + ADP) have been characterized in the malaria parasite *Plasmodium falciparum* (Ulschmid *et al.*, 2004; Rahlfs *et al.*, 2009). Heterologous overexpression in *E. coli* produces enzymatically active proteins of 28.9 (*Pf*AK) and 28.0 kDa (*Pf*GAK), the genes of which are located on chromosomes 10 and 4, respectively (Ulschmid *et al.*, 2004). Recombinant *Pf*AK1 displays the highest specificities for AMP and ATP as substrates with 75 U/mg, whereas *Pf*GAK exhibits a preference for GTP and AMP (Ulschmid *et al.*, 2004) with a specific activity of 100 U/mg. The bi-substrate analog inhibitors AP_5A and GP_5A inhibit *Pf*AK and *Pf*GAK at a K_i value of 0.1 µM and 0.2 µM, respectively (Ulschmid *et al.*, 2004). *Pf*AK2 with a molecular weight of 33 kDa displays 10 U/mg with ATP and AMP as a substrate pair and is inhibited by AP_5A with an IC_{50} value of approximately 0.2 µM (Rahlfs *et al.*, 2009). The properties of well-characterized AKs in *P. falciparum* are listed in Table 1.2 (Rahlfs *et al.*, 2009). Interestingly, *Pf*AK2 can be N-myristoylated and forms a heterodimer with N-myristoyltransferase when coexpressed with both proteins in *E. coli* (Rahlfs *et al.*, 2009). *Pf*AK1 has been hypothesized to be located in mitochondria, since it contains an N-terminal amphipathic helix (residues 118 to 130) that could function as a mitochondrial import signal (Ulschmid *et al.*, 2004). While most GAKs are located in the mitochondrial matrix, PfGAK is predicted (PlasmoAP4.4, PlasmoDB) to be targeted to the apicoplast, a non-photosynthetic plastid found in *Apicomplexa*. For *Pf*AK2, no target signals could be

identified when using the prediction programs PlasmoAP and PlasMit (Rahlfs *et al.*, 2009).

Properties	PfAK1	PfGAK	PfAK2
GenBank Accession number	AY118172	AF308612	AAV83966
Location in *P. falciparum* genome	Chromosome 10	Chromosome 4	Chromosome 8
Size of ORF (including start codon) (bp)	726	687	828
Amino acids	242	229	275
Molecular mass (kDa) (without His-tag)	27.6	26.7	32.5
Isoelectric point	8.97	9.38	7.49
ε_{280} ($mM^{-1}\,cm^{-1}$)	10.7	10.2	22.6
pH-optimum	5.5	6.0	8.0
V_{max} (U/mg) with AMP and ATP	75	≤1.0	10 ± 1.9[a]
k_{cat} (s^{-1})	35	47[b]	5.4 ± 1.0
K_M for AMP (μM)	50	210	290 ± 80
K_M for ATP (μM)	130	>5000	75 ± 15
IC_{50} for AP_5A	0.20	32.4	0.20 ± 0.05

Table 1.2 Properties of AK isozymes from *Plasmodium falciparum* (Rahlfs *et al.*, 2009). a, V_{max} for all studied forms of PfAK2; b. AMP and GTP as substrate.

Recently the structure of *Pf*AK1 was resolved and displays a similar structure to other adenylate kinases except for a unique helix structure at its N-terminus (PDB code 3TLX as shown in Figure 1.4). A crystal of *Pf*GAK was obtained through crystallization screening and was grown in 1.9-2.1 M ammonium sulfate, 0.1 M Tris-HCl pH 8.0 at 12 mg/ml, and the crystal structure of *Pf*GAK is currently being analyzed (Law *et al.*, 2012).

1.3 Myristoylation and N-myristoyltransferase

1.3.1 Protein lipidation

Diverse functions including driving proteins to various subcellular membrane domains, tracking protein subcellular localization, regulating activity and stability, and enhancing protein-protein interactions have been found by a protein modification, protein lipidation, thereby adding another level of functionality to many proteins (Resh, 2006). This process involves co- or post-translational modifications of proteins with a wide variety of lipids through covalent bounds. Protein lipid modifications can be classified based on the identity of the attached lipid moiety. Each type of lipid modification has unique features in terms of the nature of the covalent bond, the modified site of the lipid in the polypeptides, and the enzymes involved. There are five major types of protein lipidation: GPI-anchor addition, prenylation, cholesteroylation, palmitoylation, and myristoylation. The linkage of glycosyl-phosphatidylinositol (GPI) to the C-terminus of extracellular proteins takes place during GPI-anchor addition via transaminidase, which mediates their attachment to the plasma membrane (Paulick *et al.*, 2008). Addition of an isoprenoid lipid (farnesyl (C-15) or geranylgeranyl (C-20)) to one or two cysteines at or near the C-terminus by a thioether bond occurs in prenylation (Crowell *et al.*, 2009). In cholesteroylation, a cholesterol molecule is attached to a C-terminal glycine residue by an ester bond (Mann *et al.*, 2000). S-palmitoylation is defined as the attachment of long-chain fatty acids to cysteine residue and less frequently to serine and threonine residues of target proteins through a thioester linkage catalyzed by various protein fatty acyl transferases (PATs) such as the DHHC-PATs family (Linder, 2000; Resh, 2006; Tsutsumi *et al.*, 2008). A myristic acid is irreversibly attached to an

N-terminal glycine of the protein by N-myristoyltransferase by an amide bond after the removal of the first methionine residue, thus promoting weak protein-membrane association and protein-protein interaction (Towler *et al.*, 1987; Farazi *et al.*, 2001).

1.3.2 Protein myristoylation event

Protein myristoylation is initially considered co-translational on the nascent polypeptide upon removal of the lead methionine residue by a methionine aminopeptidase (Wilcox *et al.*, 1987). Interestingly, the methionine aminopeptidase has been shown to display high efficiency when the glycine is present after the initial methionine residue (Frottin *et al.*, 2006).

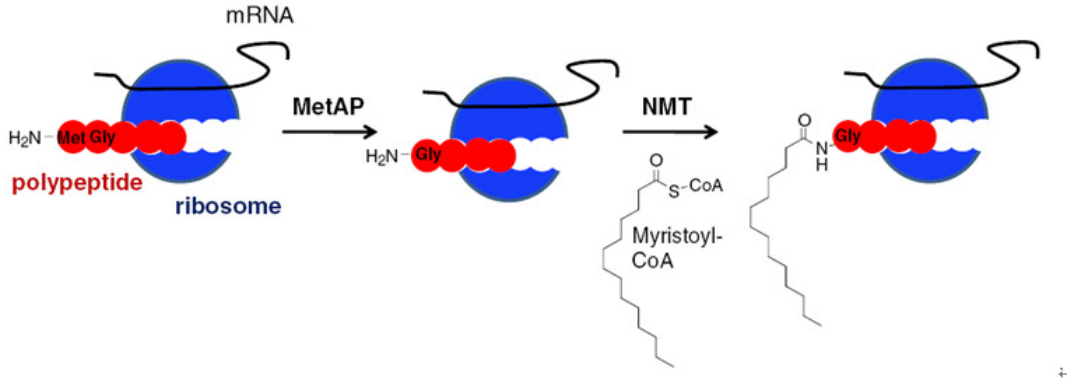

Figure 1.13 Process of protein myristoylation on the nascent polypeptide (Wright *et al.*, 2009). Ribosome, blue; polypeptide, red; mRNA, black.

The prevalence of myristoylated proteins naturally occurring in eukaryotes is predicted to be 0.5~3% of the whole proteome (Maurer-Stroh *et al.*, 2002). Several proteins have been reported to be myristoylated including tyrosine kinases, calcium-binding proteins, and MARCKS and are capable of protein-protein interaction, activity regulation, and membrane targeting (McLaughlin *et al.*, 1995; Hantschel *et al.*, 2003; Matsubara *et al.*, 2004). The 3D structure of cAMP-dependent protein kinase together with a myristoyl moiety demonstrated the important stability function of myristoylation (Zheng *et al.*, 1993). As myristoylation alone is not sufficient for membrane binding, adjacent palmitoylation or polybasic peptides are required (Cross *et al.*, 1984; Peitzsch *et al.*, 1993; Resh, 2004). A myristoyl switch is proposed and demonstrates the regulation of protein functions (Resh, 2006). The myristate moiety can exist in two states: the exposed state for facilitating membrane binding or in concealed mode in order to hide inside the protein, depending on the ligand binding and conformation change (Resh, 2006). The fact that GTP binds to the ADP ribosylation factor will lead to myristoyl exposure outside, therefore targeting the ADP ribosylation factor to the membrane (Amor *et al.*, 1994). The function of c-Abl tyrosine kinases can be regulated by a "myristoyl/phosphotyrosine" switch in a similar manner (Hantschel *et al.*, 2003). Considering the irreversibility of myristoylation, the reversible binding between myristoylated proteins and membrane domains in such models can be considered a regulator, allowing the regulation of such bindings according to the signal changes in the cell (Resh, 2006).

Myristoylated Src family tyrosine kinases such as $pp60^{src}$, $pp60^{yes}$, and $pp56^{lck}$ (Cross *et al.*, 1984)

exhibit elevated activity in many human cancers (Summy *et al.*, 2003). Studies that the inhibition of $pp60^{src}$ myristoylation reduced colony formation, cell proliferation and specific localization to the membrane reveal the vital function of pp60src myristoylation for tumorigenicity (Shoji *et al.*, 1990). Furthermore, these studies show that dephosphorylation and activity of $pp60^{src}$ are modulated by myristoylation (Bagrodia *et al.*, 1993). Recently, myristoylation and subsequent membrane targeting of $pp60^{src}$ is shown to regulate the ubiquitination and degradation of the protein and elevate the activity (Patwardhan *et al.*, 2010).

In 2000, Bid, a proapoptotic member of the Bcl-2 family, was the first protein shown to be post-translationally myristoylated on an internal glycine residue once this glycine was exposed at the N-terminus due to caspase cleavage during apoptosis (Zha *et al.*, 2000). Apoptosis is a rigorously controlled process where a series of sequential processes take place such as DNA degradation, mitochondrial dysfunction, and ultimately cell death (Wyllie, 1997). Myristoylated Bid will target to the mitochondrial membrane and react to Bak, resulting in mitochondrial dysfunction and cytochrome c release as a vital step in apoptosis (Zha *et al.*, 2000). The following study has identified 15 proteins cleaved by caspases that can be post-translationally myristoylated by a new metabolic labeling method with an azido-myristate analog (Martin *et al.*, 2008), which is illustrated in section 1.3.3 and enhances our knowledge of the role of myristoylation in the apoptotic process (Figure 1.14).

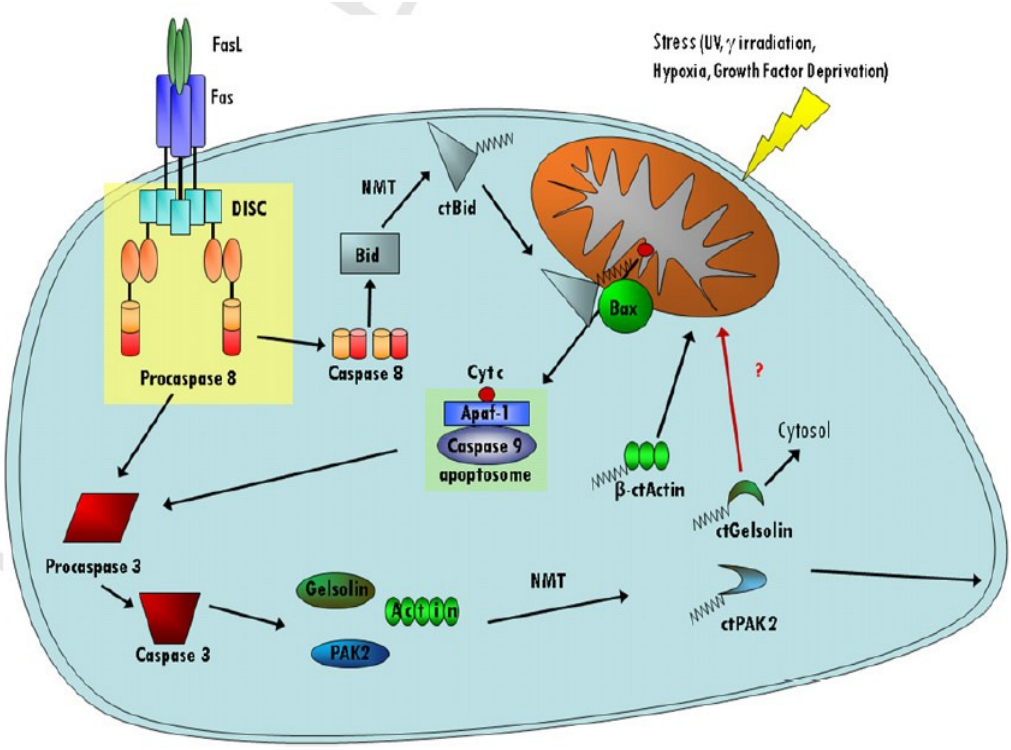

Figure 1.14 Post-translational myristoylation of proteins during apoptosis (Martin *et al.*, 2010). Fragments of Bid, Actin, PAK2, and Gelsolin cleaved by caspase can be myristoylated**.** See details in Martin's paper.

The first direct evidence that myristoylation is involved in human disease is the identification of aberrant myristoylation in the SHOC2 protein, which contains a glycine at position 2 in patients who develop a Noonan-like syndrome with loose anagen hair (Cordeddu *et al.*, 2009). The studies

demonstrated the incorporation of ^{3}H- myristic acid to mutant SHOC2, and mutant proteins were driven to the cell membrane rather than the nucleus in order to activate the Ras and the MAPK pathway (Mazzanti *et al.*, 2003; Schubbert *et al.*, 2007).

Some myristoylated proteins have been identified in protozoan parasites, including ADP ribosylation factors (Price *et al.*, 2003), CAP5.5 in *T. brucei* (Hertz-Fowler *et al.*, 2001), calcium-dependent protein kinase 1, and the 45-kDa gliding association protein in *P. falciparum* (Moskes *et al.*, 2004; Rees-Channer *et al.*, 2006). The importance of the ADP ribosylation factors in endocytosis and Golgi-lysosome trafficking in *T. brucei* has been revealed (Price *et al.*, 2003; Price *et al.*, 2007).

1.3.3 Click reaction in myristoylation research

The vital role played by myristoylation in cell signaling transduction warrants the identification of the myristoylation proteome. For a long time, metabolic labeling with ^{3}H-myristic acid combined with fluorography has been employed in order to investigate the myristoylated proteins. This time-consuming method is a laborious work, because it needs weeks or months of exposure time and has low sensitivity. Another method useed myristic acid analogs containing ^{125}I which greatly increases health hazards. Therefore, new methods need to be explored for such studies.

New concepts in chemical proteomics are emerging that benefit from the great progress in chemistry, proteomics, and biology, providing a new method to detect and identify protein modifications such as myristoylation. The bio-orthogonal chemical reporters are the key inventions in such methods. In our research, this reporter should be an analog of myristic acid without metabolically interrupting *in vivo* labeling and contain a biologically inert tag for downstream detection. The bio-orthogonal chemical reporters are employed, which can be specifically incorporated into proteins and then react initially with probes through Staudinger ligation between the alkyl azide and a phosphine (Hang *et al.*, 2007). The different chain length analogs of fatty acids containing azido groups were synthesized and used in the investigation of fatty acylated proteins in cells via the methods described here (Hang *et al.*, 2007; Martin *et al.*, 2008). The general procedure is as follows. A bio-orthogonal reporter of myristic acid (azido myristate) is incorporated into the N-terminal glycine of proteins, which should be myristoylated *in vivo*. The proteins comprising the azido group react with phosphine probes conjugated with biotin or FLAG. The last step is to detect the proteins in the Western blot against biotin or FLAG tag. The ultimate goal of the method is to purify the proteins through a pull-down assay and subsequently identify them via mass spectrometry. Later application of azide alkyne Huisgen cycloaddition known as click chemistry significantly optimized this method. Three types of reactions are used in this new technique as shown in Figure 1.15. Typically an alkynyl-myristic acid analog is metabolically ligated to a specific protein catalyzed by NMT. The azido probe containing a detection tag (biotin, rhodamine) could be added to the labeled proteins via click chemistry. Depending on the probe, various techniques such as Western blot, in-gel fluorescent scanning, or mass spectrometry can be applied for detection and identification (Figure 1.16) (Charron *et al.*, 2009). Charron and co-workers reported comparing the alkynyl and azido fatty acid chemical reporters for the metabolic labeling process (Charron *et al.*, 2009). They also employed a new CuI-catalyzed Huisgen [3 + 2] cycloaddition reaction and fluorescent tag for in-gel fluorescence scanning detection. The study showed that these optimizations obtained robust

and sensitive detection for analyzing the fatty-acylated proteins in cells (Charron *et al.*, 2009). The study then can provide a rapid and sensitive method for visualization of protein fatty-acylation, thereby enhancing our understanding of the functions and regulatory mechanisms of fatty-acylated proteins in physiology and disease.

In order to study S-palmitoylation in mammalian cells, 17-octadecynoic acid (17-ODYA) was exploited as a bio-orthogonal chemical reporter (Martin *et al.*, 2009). Both the Cu(I)-catalyzed azide alkyne [3 + 2] cycloaddition reaction and multidimensional protein identification technology (MudPIT) were employed in this method. They also used hydroxylamine to verify the palmitoylation modification through a thioester bond between 17-ODYA and proteins. Martin and Cravatt identified ~125 palmitoylated proteins including G proteins, receptors, and a family of uncharacterized hydrolases in mammalian cells. For validation, they constructed 12 high-confidence and 6 medium-confidence vectors that were overexpressed in 293T cells. As a result, only 2 targets cannot be palmitoylated in293T cells, therefore showing the high reliability of this method (Martin *et al.*, 2009).

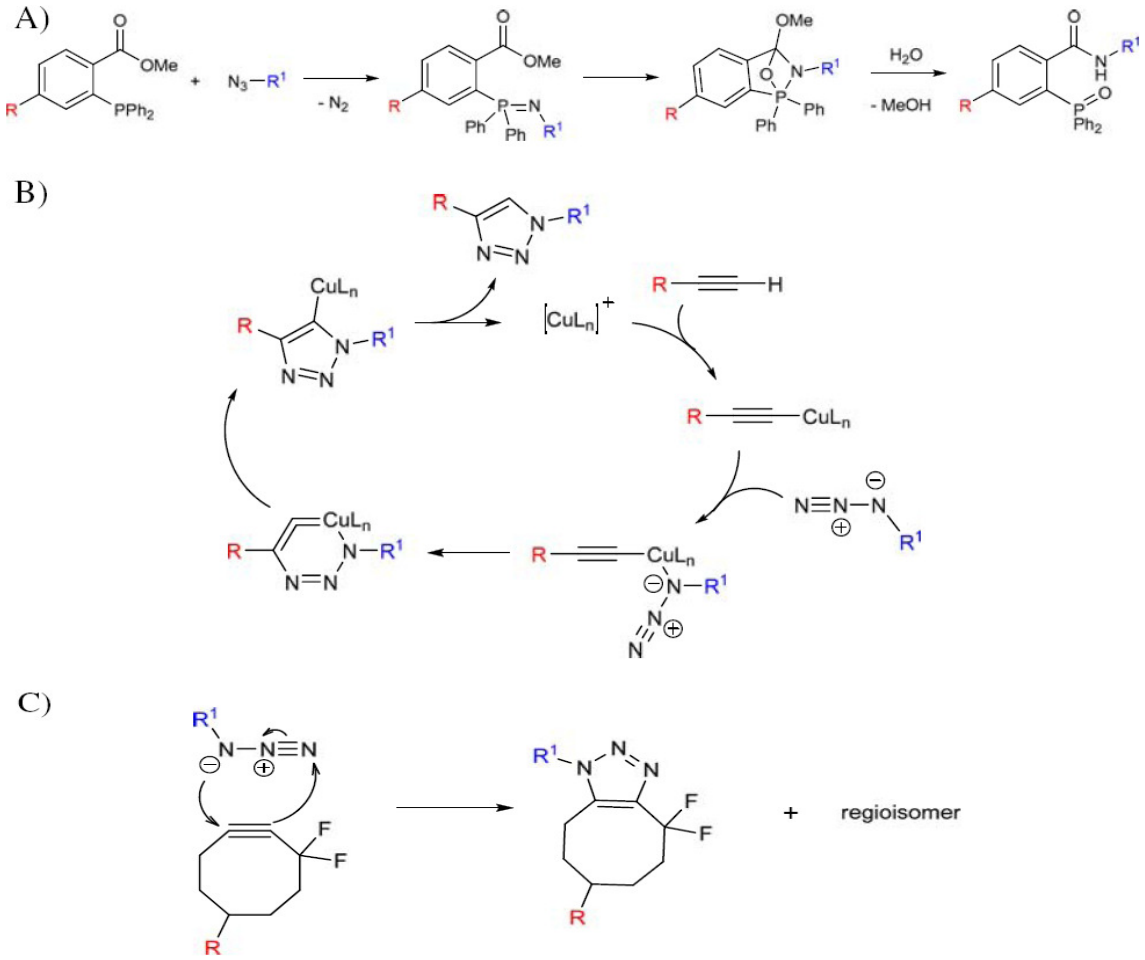

Figure 1.15 Three bio-orthogonal ligation reactions in use (Wright *et al.*, 2009). A) Staudinger ligation between a phosphine and an organic azide; **B)** Cu(I)-catalyzed 3+2 cycloaddition reaction between an alkyne and an azide; **C)** strain-promoted 3+2 cycloaddition reaction between a cyclooctyne and an azide. R and R1 can be any set of labels, proteins, DNA, or other biomolecules.

By using the new optimized method, fatty-acylated proteins in mammalian Jurkat T cells were investigated by using chemical reporters. The authors synthesized four types of chemical reporters and metabolically labeled mammalian cells for 8 hours. Total cell lysate then reacted with biotin or rhodamine for enrichment or visualization, respectively. The enriched proteins can be identified via mass spectrometry. It should be noted that they added a cleavable linker in the biotin tag so as to elute the proteins from streptavidin beads, specifically as the strong interaction between streptavidin and biotin significantly reduce the recovery of the binding proteins. The results demonstrated a novel S-acylation of histone H3 variants (Wilson *et al.*, 2011). The method can be adapted for the large-scale analysis of fatty-acylated proteomes in other cells.

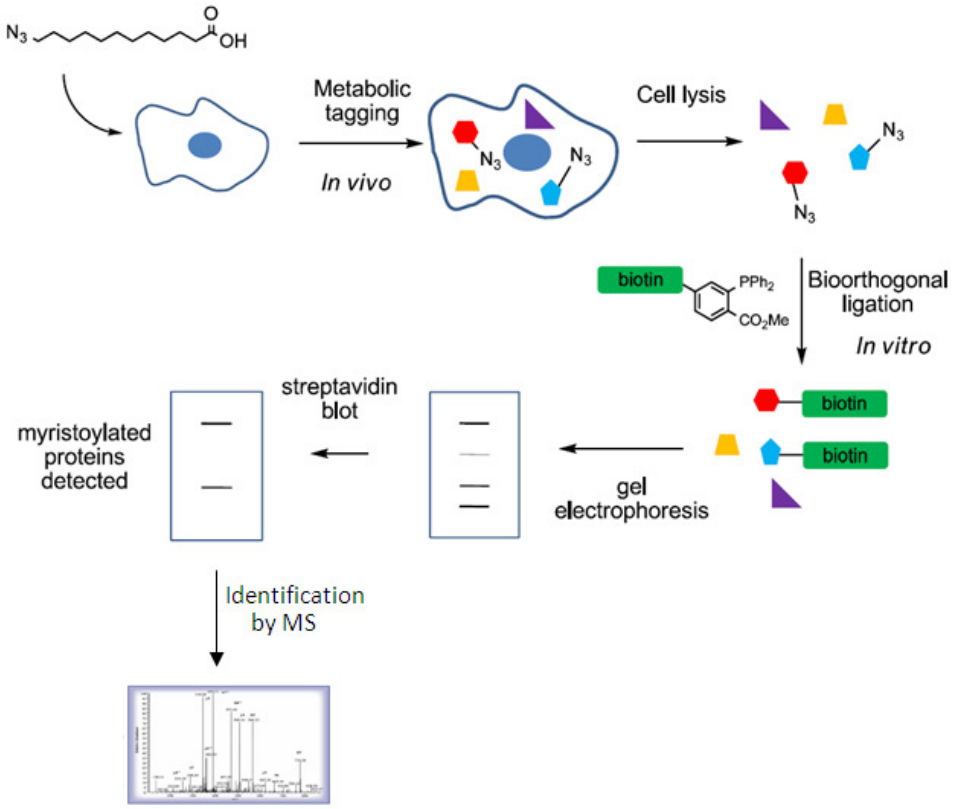

Figure 1.16 The complete procedure of identifying myristoylated proteins by bio-orthogonal analogs of myristic acid. Adapted from (Wright *et al.*, 2009)**.**

1.3.4 N-myristoyltransferase

N-myristoyltransferase belonging to the glycylpeptide N-tetradecanoyltransferase superfamily is universally present in many organisms including yeast, plants, and animals, but not in bacteria (Martin *et al.*, 2010). In vertebrates, two NMTs can catalyze the N-myristoylation reaction, while a unique one exists in lower organisms (Martin *et al.*, 2010). The catalytic mechanism of reaction catalyzed by NMT follows an ordered Bi-Bi model first to bind myristoyl-CoA with subsequent peptide binding (Figure 1.17) (Rudnick *et al.*, 1991). There is 76% identity of amino acids between two human NMTs with different substrate preferences resulting from the observation of NMT knock-out mice (Giang *et al.*, 1998; Yang *et al.*, 2005). NMT activity is regulated by phosphorylation, which is catalyzed by the Src

family tyrosine kinase members (Rajala *et al.*, 2001). Considering the fact that these Src family members can be myristoylated by NMT, there must be a complicated network of regulation.

The conserved motif for reorganization of NMT has been found to be Gly-X3-X4-X5-(Ser/Thr/Cys)6 (Utsumi *et al.*, 2004). The N-terminal Gly residue is absolutely essential for myristoylation, while Ser, Thr, Cys are more frequently observed at position X6 (Utsumi *et al.*, 2004). The first 17 amino acids at the N-terminus are predicted to be vital for myristoylation based on sequence alignment studies (Maurer-Stroh *et al.*, 2002). These studies also show that polar residues are preferred at positions 3 and 4, while large hydrophobic residues are favored at position 5 (Maurer-Stroh *et al.*, 2002). Small, polar residues at position 6 and the following lysine at position 7 are more frequent (Maurer-Stroh *et al.*, 2002). The MYR Predictor and MYRbase are two on-line tools for myristoylation prediction.

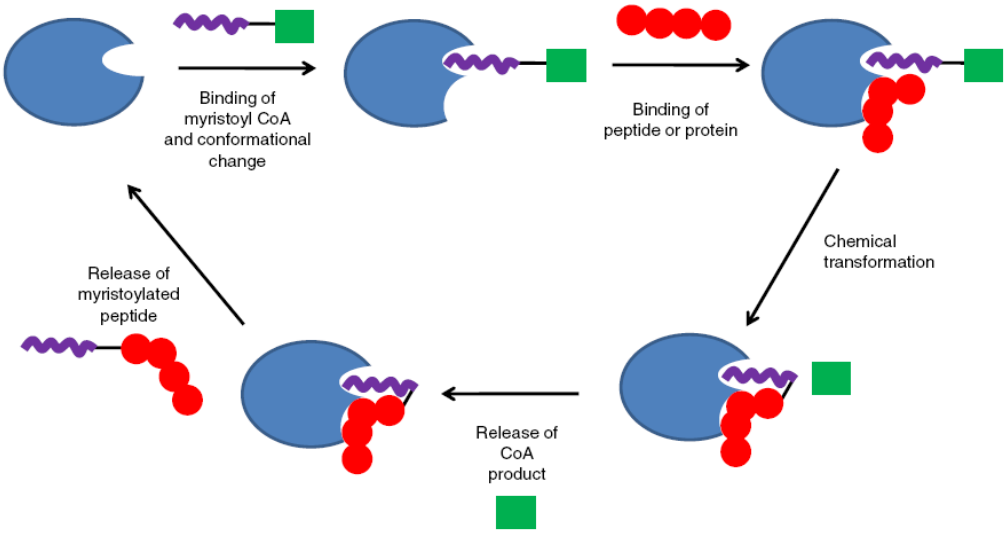

Figure 1.17 NMT catalytic mechanism (Wright *et al.*, 2009).

Structures of NMT with or without substrate analogs from several species such as *Leishmania donovani*, *Candida albicans*, *Saccharomyces cerevisiae*, and humans have been resolved (Bhatnagar *et al.*, 1998; Weston *et al.*, 1998; Brannigan *et al.*, 2010). The overall structures of NMT are quite similar and are composed of a saddle-shaped β-sheet as a core with a few surrounding α-helices as shown in Figure 1.18. This compact globular α/β protein forms a deep pocket in the center with two flanked grooves in a spatial structure. The protein seems to be symmetric in a three-dimensional structure, thereby divided into an N-terminal half and a C-terminal half (Weston *et al.*, 1998). The N-terminal half has been shown to form the groove for the myristoyl-CoA with only one residue from the C-terminus, while the peptides bind to the groove mostly formed by C-terminal half (Weston *et al.*, 1998; Farazi *et al.*, 2001). The binding of myristoyl CoA interacts with two amino residues to form an oxyanion hole. Then the carbonyl group is polarized to assist the nucleophilic attack on the carbon (Farazi *et al.*, 2001). The directing of the fatty acyl chain into the pocket of the enzyme where the methyl group interacts with the pocket floor will position the CoA and thioester properly (Farazi *et al.*, 2001). In this manner, NMT can specify the carbon chain length. As a result, all NMTs have a high specificity to myristoyl-CoA. The peptide binding site partially composed of the myristoyl CoA proves

the Bi-Bi ordered mechanism for catalysis (Farazi *et al.*, 2001). The N-terminal Gly ammonium group binds to the C-terminus of the enzyme. Both charges are neutralized, and resulting amine is ready for the nucleophilic attack on the thioester carbonyl of myristoyl CoA (Bhatnagar *et al.*, 1998). The rotation of the amine group is necessary for the approach to the thioester carbonyl for the proceeding reaction, thus making it impossible to substitute the Gly (Farazi *et al.*, 2001). The observation that the myristoyl CoA binding site is highly conserved among species probably indicates that it is not a wise strategy to design the inhibitor interacting with this site (Kishore *et al.*, 1993). According to studies of the specificity of the peptide substrate (Towler *et al.*, 1987; Duronio *et al.*, 1991; Rocque *et al.*, 1993), the peptide binding site is not highly conserved between species. A study of co-expression of the mammalian G protein alpha subunits and *S. cerevisiae* NMT in *E. coli* revealed that yeast NMT is unable to myristoylate mammalian G protein alpha subunits, which were supposed to be myristoylated in the mammalian cell (Duronio *et al.*, 1991), implying different protein substrates of NMT from different species as well. By using a group of 12 octapeptides, a distinct substrate preference between human NMT and *S. cerevisiae* NMT was shown, thus providing a chance to design the specific inhibitors against NMT from *S. cerevisiae* (Rocque *et al.*, 1993).

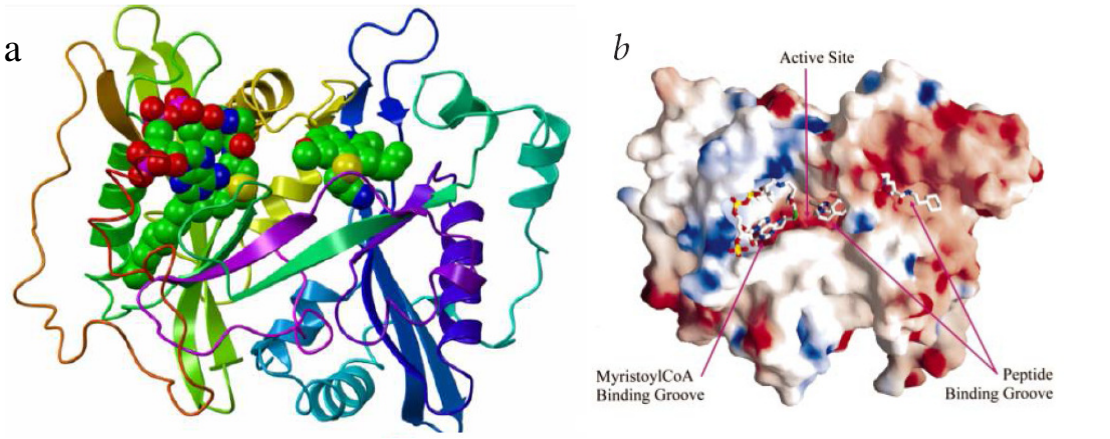

Figure 1.18 Crystal structure of NMT (Bhatnagar *et al.*, 1998; Goncalves *et al.*, 2012). a) Ribbon representation of chain A of the crystal structure of *Pv*NMT with bound NHM (S- (2- OXO) pentadecyl-CoA) (left) and inhibitor (right); **b)** Molecular surface of NMT from *Saccharomyces cerevisiae*.

1.3.5 N-myristoyltransferase as a drug target

Myristoylation, as an important cellular process, is involved in diverse metabolic pathways including cell signaling, apoptosis, and tumorigenesis as described above. Thereby, the enzyme NMT catalyzing the reaction is considered a promising target for treatment. Assembly and replication of some viruses including HIV also demand myristoylation (Maurer-Stroh *et al.*, 2004). Gag and Nef proteins in HIV, which are critical for virus replication, are myristoylated by host NMT and target to the plasma membrane (Schultz *et al.*, 1983; Spearman *et al.*, 1997). Due to the importance of these proteins in forming the viral capsid, the Gag precursor was found to be accumulated, and replication of competent viruses is blocked through the inhibition of myristoylation (Furuishi *et al.*, 1997). However, any anti-HIV inhibitors based on such studies have to target human NMT, causing a potential toxicity for uninfected cells. Searching for the specific substrate profile of human NMT 1 and 2 may circumvent

this problem (Seaton *et al.*, 2008). Since there are still many questions to be clarified, much more effort is required before this strategy can be applied against HIV infection.

Relying on the different substrate specificities between human and yeast NMTs (Rocque *et al.*, 1993) and their vital role in cell survival and vegetative growth of human pathogen *C. albicans* (Weinburg *et al.*, 1995; Price *et al.*, 2003; Yang *et al.*, 2005), they provide a promising drug target to develop novel inhibitors against NMT specifically from various fungus species such as *Candida albicans* and *Cryptococcus neoformans* (Lodge *et al.*, 1994; Devadas *et al.*, 1998). *C. albicans* with significantly reduced activity of NMT via genetic mutation cannot kill the animals in an immunosuppressed mouse model, unlike the wild-type NMT *C. albicans* strain (Weinburg *et al.*, 1995). Novel nonpeptidic inhibitors with bioavailability have been synthesized and display antifungal activity (Devadas *et al.*, 1998). Some parasitic protozoa including *Leishmania major* and *Leishmania donovani* (leishmaniasis disease), *Trypanosoma brucei* (African sleeping sickness), and *Plasmodium falciparum* (malaria) also possess their own NMTs that seem to be essential for their survival (Price *et al.*, 2003; Bowyer *et al.*, 2008). *T. brucei* in the bloodstream forms cells with knockdown NMT by RNAi lost virulence in a mouse model and has endocytic defects (Price *et al.*, 2010).

Recently, a pyrazole sulphonamide inhibitor against *T. brucei* NMT has been discovered (Frearson *et al.*, 2010). The selectivity between *T. brucei* and human NMT is over 100-fold, and a tight correlation between NMT activity and *T. brucei* proliferation has been observed. The inhibition of myristoylation *in vivo* has been shown by adding this leading compound, indicating that NMT is its target. By resolving the structure of *L. major* NMT with this compound, it can be demonstrated that pyrazole sulphonamide binds to the pocket of the peptide binding site. Moreover, this compound rapidly kills *T. brucei* below a detectable level in a mouse model of human African trypanosomiasis and eliminates the bloodstream form of *T. brucei* in cell culture. Therefore, optimization of this compound may lead to a real drug with promising therapeutic properties for treating African sleeping sickness (Frearson *et al.*, 2010).

P. falciparum NMT has been characterized (Gunaratne *et al.*, 2000), and a series of compounds containing a core benzothiazole scaffold were shown to inhibit the activity of *P. falciparum* NMT in the micromolar range by using a scintillation proximity assay suitable for high throughput screening, and two compounds were found to reduce the parasitemia by >80% at 10 μM in cultured parasites *in vitro* (Bowyer *et al.*, 2007). However, a strong overlap between the structure-activity relationships (SAR) for *Plasmodium* NMT and both human NMTs indicated the potential challenge in obtaining an appropriate selectivity profile according to the programs that target N-myristoyltransferases as starting points for treating tropical diseases (Bell *et al.*, 2012). Very recently, a series of inhibitors against *Plasmodium vivax* NMT has been discovered through high-throughput screening and the high-resolution crystal structure of NMT in complex with the leading compound. These studies provide the opportunity to understand the binding mode of the inhibitors and to further improve rational drug design (Goncalves *et al*., 2012).The sequence alignment showed 80% identity of amino acids between *Pf*NMT and *Pv*NMT, therefore probably demonstrating similar structure and inhibition patterns.

1.4 Objective of study

Due to the absence of a vaccine and increasing resistance to current drugs, new chemotherapeutic approaches fighting malaria are urgently needed (Dondorp *et al.*, 2010). This thesis aims to explore energy homeostasis mediated by adenylate kinase and the potential of targeting N-myristoyltransferase as a drug target. The following specific objectives are explored:.

1.4.1 Adenylate kinase networks

The first aim of my work was to characterize two new members of the AK family and to investigate the subcellular localization of all AKs in *P. falciparum*, thereby mapping the energy metabolism network catalyzed by AK isoforms.

1.4.2 Myristoylation

The second aim was to investigate the possibility of using chemical reporters to label the myristoylated proteins in *P. falciparum*, to detect the naturally occurring myristoylated proteins, and to identify them via mass spectrometry by using the new bio-orthogonal chemical reporter method, thus better understanding the myristoylation function in *P. falciparum*. The experimental results are compared with the protein list obtained via bioinformatic methods in order to reveal new myristyolated targets in *P. falciparum*.

1.4.3 N-myristoyltransferase

A heterologous expression and purification system of *Pf*NMT was established to obtain the highly pure NMT for crystallization studies. Different screenings were tried to crystallize NMT in order to resolve its structure so as to compare it to human NMT and to study SAR (structure-activity relationship) for novel inhibitor discovery.

2. Materials

2.1 Antibiotics

Antibiotic	Source	Stock concentration	Working concentration
Carbenicillin	Roth	50 mg/ml in 50% Ethanol	100 µg/ml
Chloramphenicol	Roth	25 mg/ml in 100% ethanol	25 µg/ml
Kanamycin	Roth	25 mg/ml in water	50 µg/ml

2.2 Antibodies

Antibody	Source
Mouse anti-histidine$_6$-tag antibody	Dianova, Hamburg
HRP Anti-mouse IgG antibody	Pearce, Rockford
Anti-GFP antibody	Roche, Mannheim
Anti-Exp 1 antibody	Dr. Przyborski, Marburg
Anti-Hsp 70 antibody	Dr. Przyborski, Marburg
Anti-SERP antibody	Dr. Przyborski, Marburg
HRP Streptavidin	GE Healthcare, München

2.3 Buffers and solutions

2.3.1 Buffer for DNA electrophoresis

DNA Sample buffer	0.1%	Bromophenol blue
	60%	Saccharose
	1 mM	Tris
	pH 8.3	HCl (adjustment)
10 X TBE (electrophoresis buffer)	1 M	Tris
	1 M	Boric acid
	20 mM	EDTA
	pH 8.0	Acetic acid (adjustment)

2.3.2 Buffer for extraction of *P. falciparum* parasites

Saponin lysis buffer	7 mM	K_2HPO_4
	1 mM	$MgCl_2$
	1 mM	NaH_2PO_4
	11 mM	$NaHCO_3$
	58 mM	KCl
	56 mM	NaCl
	14 mM	Glucose
	0.02%	Saponin
	pH 7.4	HCl (adjustment)

Cytomix	12 mM	KCl
	5 mM	$MgCl_2$
	10 mM	KH_2PO_4
	10 mM	K_2HPO_4
	25 mM	HEPES
	0.15 mM	$CaCl_2$
	2 mM	EGTA
	pH7.6	KOH (adjustment)
Parasite cell lysis buffer	137 mM	NaCl
	2.7 mM	KCl
	8 mM	Na_2HPO_4
	1.46 mM	KH_2PO_4
	1%	Triton
	pH 7.6	HCl (adjustment)

2.3.3 Buffer for AK assay

AK assay buffer	1.5 mM	$MgCl_2$
	90 mM	KCl
	110 mM	TEA-HCl
	pH 7.6	HCl (adjustment)

2.3.4 Buffer for protein purification

Lysis buffer	50 mM	Na_3PO_4
	300 mM	NaCl
	pH 8.0	NaOH (adjustment)
Tris-NaCl buffer	50 mM	Tris
	300 mM	NaCl
	pH 7.6	HCl (adjustment)

2.3.5 Buffer for SDS-PAGE electrophoresis

Electrophoresis buffer	193 mM	Glycine
	25 mM	Tris
	0.1% (w/v)	SDS
	pH 8.3	HCl (adjustment)
SDS Sample buffer (4x)	240 mM	1 M Tris-HCl, pH 6.8
	8% (w/v)	SDS
	40% (v/v)	Glycerol
	5% (v/v)	14.7 M β-Mercaptoethanol
	0.04% (w/v)	Bromophenol Blue

Coomassie staining solution	0.2% (w/v)	Coomassie brillant blue R250
	40% (v/v)	2-Propanol
	10% (v/v)	Acetic acid
Coomassie destaining solution	10% (v/v)	Acetic acid
	40% (v/v)	Methanol

2.3.6 Western blot buffer

Anode buffer I	300 mM	Tris
Anode buffer II	25 mM	Tris
Cathode buffer	40 mM	6-aminohexanoic acid
TBS buffer	10 mM	Tris
	155 mM	NaCl
	pH 8.0	HCl (adjustment)
TBS-Tween (TBST)	0.05%	Tween 20 (in TBS buffer)
Ponceau staining solution	1% (w/v)	Ponceau S
	5% (v/v)	Acetic acid
Ponceau destaining solution	5% (w/v)	Acetic acid
Luminol solution (store in dark	1.25 mM	Luminol
at 4 °C)	0.0093% (v/v)	H_2O_2
	0.1 M	Tris-HCl, pH 8.6

2.3.7 Stock solutions

Compound	Concentration	Solvent	Storage
APS	10% (w/v)	H_2O	-20 °C
L-Arabinose	20% (w/v)	H_2O	Filter sterilized, -20 °C
IPTG	1 M	H_2O	Filter sterilized, -20 °C
Rhamnose	20% (w/v)	H_2O	Filter sterilized, -20 °C

2.4 Biological materials

2.4.1 Plasmids

Plasmids	Antibiotic resistance	Source
pARL-1a+	Carbenicillin	Prof. Alan F. Cowman, Melbourne University
pET24	Kanamycin	Novagen, Darmstadt
pET28	Kanamycin	Novagen, Darmstadt
pGEM-T Easy	Carbenicillin	Promega, Mannheim
pGRO7	Chloramphenicol	TaKaRa, Göttingen
pQE30 (no His-tag)	Carbenicillin	Qiagen, Hilden (Lab modified)
pRAREII	Chloramphenicol	Novagen, Darmstadt
pSK	Carbenicillin	Stratagen, La Jolla, USA

2.4.2 *E. coli* strains

***E. coli* strain**	**Usage**	**Source**
XL-1 Blue	Cloning and plasmid preparation	Stratagene, Amsterdam
KRX	Overexpression	Promega, Mannheim
BL21	Overexpression	Invitrogen, Karlsruhe
C41	Overexpression	Avidis, France

2.4.3 *Plasmodium falciparum* strain

***Plasmodium falciparum* strain**	**Source**
3D7 (Chloroquine-sensitive)	Prof. Lanzer, Heidelberg University

2.5 Chemicals

Most chemicals used in the study were of highest purity available.

Chemical	Producer
Acetic acid	Roth, Karlsruhe
Acrylamide and bis-acrylamide solution (30/0.8%)	BioRad, München
Adenosine monophosphate (AMP)	Sigma Aldrich, Steinheim
Adenosine triphosphate (ATP)	Sigma Aldrich, Steinheim
Agarose	PeqLab, Erlangen
Albumax	Gibco, Karlsruhe
Alkynyl biotin	Invitrogen, USA
6-Aminohexanoic acid	Roth, Karlsruhe
Ammonium persulfate (APS)	Sigma Aldrich, Steinheim
Ammonium sulfate	Roth, Karlsruhe
L-Arabinose	Sigma Aldrich, Steinheim
Azido myristic acid	Invitrogen, USA
Bradford reagent	BioRad, München
Bacto-Agar	Roth, Karlsruhe
Boric acid	Roth, Karlsruhe
Bovine serum albumin	Roth, Karlsruhe
Bromophenol blue	Sigma Aldrich, Steinheim
Calcium chloride	Roth, Karlsruhe
Carbenicillin	Roth, Karlsruhe
Chloramphenicol	Roth, Karlsruhe
Coomassie brilliant blue R250	Sigma Aldrich, Steinheim
Coumaric acid	Sigma, Steinheim
Cupric sulfate ($CuSO_4$)	Sigma Aldrich, Steinheim
Cystatin	Roth, Karlsruhe

Cytidine monophosphate (CMP)	Sigma Aldrich, Steinheim
1,4-Dithiothreitol (DTT)	Roth, Karlsruhe
Dimethyl sulfoxide (DMSO)	Roth, Karlsruhe
Dipotassium phosphate (K_2HPO_4)	Roth, Karlsruhe
Disodium hydrogen phosphate (Na_2HPO_4)	Roth, Karlsruhe
dNTPs	Fermentas, St. Leon-Rot
Ethanol	Roth, Karlsruhe
Ethidium bromide	Sigma Aldrich, Steinheim
Ethylenediaminetetraacetic acid (EDTA)	Roth, Karlsruhe
Ethylene glycol tetraacetic acid (EGTA)	Roth, Karlsruhe
Gentamycin	Invitrogen, Karlsruhe
Giemsa (0.4%, w/v)	Sigma Aldrich, Steinheim
Glucose	Merck, Darmstadt
Glycerol	Roth, Karlsruhe
Glycin	Roth, Karlsruhe
Guanosine monophosphate (GMP)	Sigma Aldrich, Steinheim
Guanosine triphosphate (GTP)	Sigma Aldrich, Steinheim
Hydrochloric acid	Roth, Karlsruhe
4-(2-hydroxyethyl)-1-piperazineethanesulfonic acid (HEPES)	Roth, Karlsruhe
Hydrogen peroxide	Sigma Aldrich, Steinheim
Imidazole	Roth, Karlsruhe
Inosine monophosphate (IMP)	Sigma Aldrich, Steinheim
Inosine triphosphate (ITP)	Sigma Aldrich, Steinheim
Isopropanol	Roth, Karlsruhe
Isopropyl-β-D-thiogalactopyranoside (IPTG)	Roth, Karlsruhe
Kanamycin	Roth, Karlsruhe
Luminol	Sigma Aldrich, Steinheim
Methanol	Roth, Karlsruhe
Magnesium chloride	Roth, Karlsruhe
β-Mercaptoethanol	Roth, Karlsruhe
Milk powder	Roth, Karlsruhe
β-Nicotinamide adenine dinucleotide, reduced disodium salt (NADH)	Sigma Aldrich, Steinheim
Nickel-nitrilotriacetic acid (Ni-NTA)	Qiagen, Hilden
PEG 3350 (Polyethylene glycol)	Roth, Karlsruhe
PEG 6000	Roth, Karlsruhe
Pepstatin A	Sigma Aldrich, Steinheim
Phenylmethylsulfonylfluoride (PMSF)	Sigma Aldrich, Steinheim
Phosphoenolpyruvate (PEP)	Sigma Aldrich, Steinheim
Ponceau	Sigma Aldrich, Steinheim
Potassium chloride (KCl)	Roth, Karlsruhe

Potassium dihydrogen phosphate (KH_2PO_4)	Roth, Karlsruhe
Potassium hydroxide (KOH)	Roth, Karlsruhe
Rhamnose	Sigma Aldrich, Steinheim
RPMI 1640 Gibco	Invitrogen, Karlsruhe
Saccharose	Roth, Karlsruhe
Saponin	Roth, Karlsruhe
Sodium acetate	Roth, Karlsruhe
Sodium chloride (NaCl)	Roth, Karlsruhe
Sodium dihydrogen phosphate (NaH_2PO_4)	Roth, Karlsruhe
Sodium hydrogen carbonate ($NaHCO_3$)	Roth, Karlsruhe
Sodium dodecyl sulphate (SDS)	Merck, Darmstadt
Tetramethylethylenediamine (TEMED)	Sigma Aldrich, Steinheim
Triethylamine hydrochloride (TEA-HCl)	Sigma, Steinheim
Tris[(1-benzyl-1H-1,2,3-triazol-4-yl)methyl]amine (TBTA)	Sigma Aldrich, Steinheim
Tris(2-carboxyethyl)phosphine (TCEP)	Sigma Aldrich, Steinheim
Tetramethylethylenediamine (TEMED)	Sigma Aldrich, Steinheim
Tris(hydroxymethyl)aminomethane (Tris)	Roth, Karlsruhe
Triton X-100	Sigma Aldrich, Steinheim
Trypton	Roth, Karlsruhe
Tween 20	Merck, Darmstadt
Uridine monophosphate (UMP)	Sigma Aldrich, Steinheim
Uridine triphosphate (UTP)	Sigma Aldrich, Steinheim
Yeast extract	Oxoid LTD, U.K

2.6 Enzymes

2.6.1 Restriction Enzymes

Enzyme	Cleavage sequence	Source
AvrII	5' C↓CTAGG 3'	Fermentas, St. Leon-Rot
BamHI	5' G↓GATCC 3'	Fermentas, St. Leon-Rot
BglII	5' A↓GATCT 3'	Fermentas, St. Leon-Rot
HindIII	5' A↓AGCTT 3'	Fermentas, St. Leon-Rot
NdeI	5' CA↓TATG 3'	Fermentas, St. Leon-Rot
XhoI	5' C↓TCGAG 3'	Fermentas, St. Leon-Rot

2.6.2 DNA Polymerase

Enzyme	Company
AccuPrime™ Taq DNA Polymerase	Invitrogen, Karlsruhe
Pfu DNA Polymerase	Promega, Mannheim
RedTaq® DNA Polymerase	Sigma Aldrich, Steinheim

2.6.3 Other enzymes

Enzyme	Source	Function
DNaseI	Roche, Mannheim	DNA digestion
DpnI	Fermentas, St. Leon-Rot	Methylated DNA digestion
Lactate dehydrogenase	Roche, Mannheim	AK assay
Lysozyme	Sigma Aldrich, Steinheim	Cell lysis
Pyruvate kinase	Roche, Mannheim	AK assay
T4 Ligase	Fermentas, St. Leon-Rot	Nucleotide fragment ligation
Thrombin	Novagen (Merck), Darmstadt	Cleavage of His-tag from fused protein

2.7 Instruments

Instruments	Producer
Analytical Balance	Scaltec Instruments, Göttingen
Autoclave	Webeco, Bad Schwartau
Beckman DU 650 Spectrophotometer	Beckmann, München
Beckman Optima Max Ultracentrifuge	Beckmann, München
Bio Photometer	Eppendorf, Hamburg
Eppendorf Research® Plus Pipettes	Eppendorf, Hamburg
Eppendorf Thermomixer	Eppendorf, Hamburg
FPLC-Software Unicorn	Amersham Bioscience, Freiburg
FPLC System ÄKTA-FPLC	Amersham Bioscience, Freiburg
Fraction Collector Frac-100	Pharmacia Biotech, Freiburg
Freezer -86 °C	Heraeus Instruments, Hanau
Gene Pulser Xcell Electroporation	BioRad, München
GEL DOC 2000 System	BioRad, München
HeraCell CO_2 Incubator for *P. facliparum* Culture	Heraeus Instruments, Hanau
Hitachi U-2001 Spectrophotometer	Hitachi, Schwäbisch Gmünd
Honeybee 961 Crystallization robot	Zinsser Analytic, Frankfurt
Magnetic Stirrers RCT basic	IKA Werke, Staufen
Mastercycler® Thermal Cyclers	Eppendorf, Hamburg
Megafuge 1.0R Centrifuge	Heraus Instruments, Hanau
Mini-PROTEAN 3 cell Electrophoresis Module	BioRad, München
Minispin® Centrifuge	Eppendorf, Hamburg
Mitsubishi P91 Photo Printer	Mitsubishi, Ratingen
Neolab Heating Block	NeoLab, Heidelberg
Optima™ TLX Ultracentrifuge	Beckmann, München
OptiMax X-ray Film Processor	Protec, Oberstenfeld
QuadroMACS® Magnetic Separator	Miltenyi Biotec GmbH, Bergisch

	Gladbach
Owl EasyCast B1A Mini Gel Electrophoresis Systems (Agraose)	Thermo Scientific, Dreieich
pH Meter	Beckman, München
Pharmacia LKB Multiphor II NovaBlot	Amersham Pharmacia Biotech, Freiburg
Rotor Sorvall SLA 3000, SS34	Thermo Fisher Scientific, Waltham, USA
Shaker KS 500	Junke & Kunel, Ika Werke
Sonopuls GM 70 Ultrasonicator	Bandelin Electronics, Berlin
Sorvall® RC5BPlus Centrifuge	ThermoScientific, Waltham, USA
Thermomixer Comfort	Thermo Life Sciences, Egelsbach
Ultra Pure Water System	MembraPure, Bodenheim
UV/Vis-Spectrophotometer Beckman DU® 650	Beckmann, München
Vortex Minishaker MS2	IKA Werke, Staufen

2.8 Kits

Bradford kit	Biorad, München
HiSpeed® Plasmid Maxi kit	Qiagen, Hilden
JCSG Core Suite kit	Qiagen, Hilden
QIAprep Spin Miniprep Kit	Qiagen, Hilden
QIAquick PCR Purification Kit	Qiagen, Hilden
Western lightning chemiluminescence reagent	Perkin Elmer, Boston, U.S.A

2.9 Materials of affinity chromatography

Nickel-Nitrilotriacetate-Agarose (Ni-NTA)	Qiagen, Hilden
Protino® Ni-TED	Machery-Nagel, Düren
Soft-link avidin agarose	Proemga, Mannheim
SuperdexTM 200 prep grade (HiLoad 16/60)	GE Healthcare, Freiburg

2.10 Media for *E. coli* culture

Lysogeny Broth Medium (LB), 1 L	10 g Tryptone 5 g Yeast extract 10 g NaCl
Terrific Broth Medium (TB), 1 L	12 g Tryptone 24 g Yeast extract 9,4 g K_2HPO_4 2,2 g KH_2PO_4 4 ml Glycerol
2x YT Medium, 1 L	16 g Tryptone 10 g Yeast extract

	5 g NaCl
Modified LB, 1 L	12 g Tryptone 24 g Yeast extract 5 g NaCl 5 g K_2HPO_4 0,142 Na_2SO_4 40 ml Glycerol

2.11 Protease inhibitors

Inhibitor	Stock concentration	Working concentration
Protease Inhibitor Cocktail Tablets	/	50 ml solution / one tablet
Cystatin	40 µM in buffer	80 nM
Pepstatin A	0.3 mM in DMSO	3 µM
PMSF	100 mM in ethanol	0.1 mM

3. Methods

3.1 General methods

3.1.1 Agarose gel electrophoresis

Via agarose gel electrophoresis, DNA fragments were separated based on their sizes and shapes. The DNA sample was mixed with 6x loading buffer and loaded into the gel slots. The separation of DNA sample was often performed in 1% agarose gel, which was horizontally placed in an electrophoresis chamber containing 1 x TBE buffer. The size of the sample was compared with Fermentas 1 kb DNA size standard. The electrophoresis was carried out initially at a voltage of 70 V and then adjusted to 100 V for approximately 50 minutes. Then the gel was soaked in an ethidium bromide buffer for 15 minutes. Finally, the DNA bands were visualized under UV via the Gel Doc 2000 system.

3.1.2 Cleavage of double strand DNA by restriction endonuclease

The DNA fragments of PCR products or plasmids were cleaved by the restriction endonuclease (Roberts, 1976), which has the function of cutting DNA at a specific nucleotide sequence known as the restriction site. The DNA fragments were digested by one or more Fermentas restriction enzymes at an optimized buffer and temperature for 1 hour according to the manufacture's instruction. The mixture can be purified by QIAquick PCR Purification Kit and be further used for the ligation step.

3.1.3 Determination of DNA concentration

The concentration of DNA fragments from purified PCR products or the plasmids was determined via absorption at 260 nm. H_2O_{dd} was used as a blank. A value of one measured by absorption at 260 nm is equal to 50 ng/µl of DNA concentration (Sambrook *et al.*, 2001). The purity of the DNA sample could be examined via absorption at 280 nm. The ratio of A_{260nm}/A_{280nm} for a pure DNA sample ranges from 1.8 to 2.0.

3.1.4 Preparation of competent cells

The *E. coli* cells that would be used for transformation were inoculated into a liquid LB medium (3 ml) and grown overnight (~ 15 hours) in a shaking incubator at 37 °C. Then 150 ml LB medium was inoculated with the overnight culture and cultured until the OD_{600} value reached 0.6. The culture was placed on ice for 10 minutes and transferred into the Falcon tubes. The culture was then harvested at 4 °C for 10 minutes with a speed of 4,000 *g*. The pellet was resuspended in 10 ml ice-cold 0.1 M $CaCl_2$ containing 15% glycerol, which was then put on ice for 30 minutes. Again the resuspended pellet was centrifuged at 4,000 *g* at 4 °C for 10 minutes. The pellet was resuspended in 1.5 ml ice-cold 0.1 M $CaCl_2$ containing 15% glycerine. The competent cells were aliquoted into sterile Eppendorf tubes and frozen in liquid nitrogen for 3 minutes. The cells were stored at -80 °C ready to use.

If pGro7 or pRARE II plasmid was used in the heterologous expression system, a fresh transformation procedure as described in 3.1.5 was required before starting the above protocol for preparing the competent cells. The chloramphenicol antibiotic should be added to the medium for the whole

procedure because of the plasmid resistance.

3.1.5 Ligation and transformation

T4 ligase can catalyze the reaction to form a phosphodiester bond between the 5' phosphate group of one fragment and the 3' - hydroxyl group of the other. The molar ratio of the insert to the vector can vary from 3:1 to 7:1, and the amount of insert can be calculated as follows:

$$\text{Insert (ng)} = \frac{\text{Vector (ng) x Insert (kb)}}{\text{Vector (kb)}} \text{ x desired molar ratio of insert:vector}$$

The ligation mixture contained DNA fragments (insert), vector, and T4 ligase in a proper buffer. The reaction was performed at 16 °C for 3 h or 4 °C overnight (~ 15 h). 50 µl competent cells were incubated with 5 µl of the ligation mixture on ice for 30 minutes. The cells were placed at 42 °C for 90 seconds for heat shock and later cooled on ice for 5 minutes. 400 µl LB medium was added to the transformed cells, and the culture was grown at 37 °C for 1 hour. The bacterial suspension was spread on the agar plates with the appropriate antibiotic according to the plasmids, which then were incubated at 37 °C overnight.

The colonies on the agar plates were examined the next day, which were inoculated in 3 mL LB medium with the right antibiotics and grown overnight (~ 15 hours). The cells were harvested and plasmids were prepared by using the Qiagen Miniprep plasmid kit following the protocol from the manufacture's instruction. The plasmids could be further identified by the cleavage of proper restriction enzymes described in 3.1.3. The positive ones were sent for DNA sequencing for precise checking.

3.1.6 SDS-polyacrylamide gel electrophoresis

SDS-PAGE, sodium dodecyl sulfate polyacrylamide gel electrophoresis, is a technique used to separate protein mixtures based on their molecular weight under denaturing conditions. The detergent SDS would linearize and impart the negative charge to the polypeptide. The distribution of SDS covered on the protein surface mostly correlates to the molecular weight of the protein, therefore allowing them to be separated by their sizes.

Resolving gels (12%)	
1.5 M Tris pH 8.8	3.75 ml
SDS (10% in water)	0.15 ml
Acrylamide (Rotiphorese® gel 30)*	6 ml
TEMED	7.5 µl
APS (10%)	75 µl
H_2O	5.1 ml

Resolving gels (10%)	
1.5 M Tris pH 8.8	3.75 ml
SDS (10% in water)	0.15 ml
Acrylamide (Rotiphorese® gel 30)*	4.95 ml
TEMED	7.5 µl
APS (10%)	75 µl
H_2O	6.25 ml

Stacking gels (4%)	
1.5 M Tris pH 6.8	1.25 ml
SDS (10% in water)	0.05 ml
Acrylamide (Rotiphorese® gel 30)*	0.65 ml
TEMED	5 µl
APS (10%)	25 µl
H_2O	3.05 ml

Table 3.1 Composition of SDS-PAGE gels.

The solution of the resolving gel prepared as described above was poured into a Bio-Rad® casting apparatus. First, 70% ethanol was overlaid on the top of the solution. After cross-linking between polyacrylamide molecules for 40 minutes, the ethanol was removed. The stacking gel solution was filled on the top of the resolving gel, and the gel combs were inserted immediately. After polymerization for 20 minutes, the gel could be used directly after the polymerization of the stacking gel or stored at 4 °C for 3 weeks.

SDS-PAGE was performed according to the following steps. Protein samples were mixed with 4x sample buffer and denatured at 95 °C for 4 minutes. The sample mixture was loaded on 10% or 12% SDS-PAGE and run at 200 V in an electrophoresis buffer. The proteins were first concentrated in the stacking gel and further separated in the resolving gel on the basis of their molecular weight. After electrophoresis, the gel was stained in Coomassie blue solution for 20 minutes at RT with shaking. The destaining solution was changed several times in order to destain the gel so that the protein bands could be visualized. If Western blot was required, the gel was directly transferred into the cathode buffer without the Coomassie blue staining step.

3.1.7 Western blot

In our Western blot analysis, the proteins separated by SDS-PAGE were transferred into a polyvinylidene difluoride (PVDF) membrane. The target protein can be detected by a specific antibody through an immunological reaction. Semi-dry Western blot was used in our experiments (Towbin *et al.*, 1979). After the completion of the gel electrophoresis as described in 3.1.6, the gel was subjected to cathode buffer. The PVDF membrane was dipped in pure methanol for activation. Then 3 filter papers, 2 filter papers and the activated PVDF membrane, and 5 filter papers including the gel were soaked in anode buffer I, anode buffer II, and cathode buffer, respectively, for about 10 minutes. Then the total transfer stack composed of 5 filter papers from cathode buffer, the gel, the PVDF membrane, 2 filter papers from anode buffer II, and 3 filter papers from anode buffer I laid out from cathode to anode was set up as demonstrated below. The transfer process was performed at 0.8 mA/cm^2 of gel electrogram for 55 minutes.

After the transfer, the PVDF membrane was stained in Ponceau staining solution for 30 seconds and destained with 1% acetic acid until protein bands appeared. Then the PVDF membrane was washed in TBST solution until no protein band was visible. The PVDF membrane was then blocked by 5% milk TBS solution at RT for 1 hour with shaking or at 4 °C overnight in order to prevent non-specific

adsorption of antibodies. The membrane was washed 3 times for 10 minutes each in TBST solution and incubated with the primary antibody such as anti-histidine antibody for 1 hour at RT. After rinsing with TBST solution 3 times for 10 minutes each, the PVDF membrane was incubated for 1 hour at RT with a secondary antibody against the primary antibody. Again repeating the washing step with TBST solution, the membrane was immunostained by adding an enhanced chemiluminescence mixture containing 1 ml luminal solution and 10 µl coumaric acid to the PVDF membrane for 1 minute. The membrane was then placed in a film cassette and exposed to an X-ray film for an appropriate amount of time ranging from 30 seconds to 10 minutes. The film was developed by using an X-ray film exposure machine, and the signal was detected.

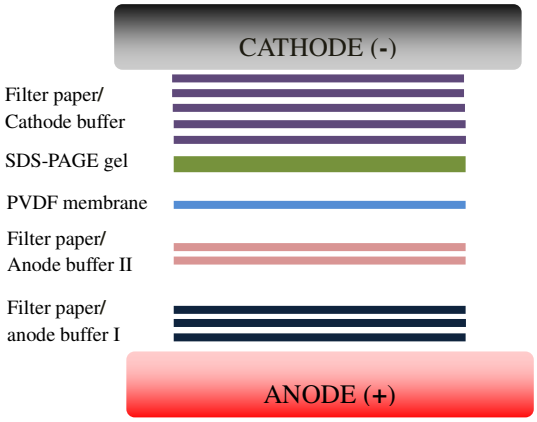

Figure 3.1 Transfer stack in semi-dry Western blot. Arrangement of the transfer stack from cathode to anode: 5 filter papers in cathode buffer, SDS-PAGE gel in cathode buffer, PVDF membrane in anode buffer II, 2 filter papers in anode buffer II, and 3 filter papers in anode buffer I.

3.1.8 Determination of protein concentration

The Bradford method for determining protein concentration is based on the shift of absorbance maximum of Coomassie Brilliant Blue G-250 dye from 465 nm to 595 nm when the protein-dye complex is formed (Bradford, 1976). An increase in absorbance at 595 nm correlates with the amount of protein, hence providing a measurement for the determination of protein amount.

In order to determine the protein concentration, a series of BSA concentrations as standards was prepared to plot a calibration curve. Then, 5 µl of each standard was mixed with 495 µl ddH_2O. To this mixture, 125 µl Bradford reagent was added with an immediate vortex and incubated for 15 minutes at RT. The absorption in a cuvette at 595 nm was observed using a photometer. Thus, the calibration curve of absorption against protein concentration was plotted. The absorption of a sample following the above procedure was obtained, and the sample concentration could be calculated using the previous calibration curve.

3.1.9 Cell culture of *P. falciparum*

The *P. falciparum* 3D7 strain in intraerythrocytic stages was cultured as described before with slight

modification (Trager *et al.*, 1976). The RPMI 1640 medium plus 0.5% Albumax, 9 mM glucose, 0.2 mM hypoxanthine, 2.1 mM L-glutamine, and 22 µg/ml gentamycin was used to culture the parasites supplemented with RBC (A+) at 3.3% hematocrit. The culture was maintained in an incubator containing 3% O_2, 3% CO_2, and 95% N_2 at 37 °C. The parasite growth was monitored by checking the parasitemia with Giemsa staining (10% Giemsa, 20 minutes). Normally parasites propagate 3 to 8-fold every 48 hours. High parasitemia should be avoided in order to obtain a standard growth unless experiments are required.

3.1.10 Magnetic purification of *P. falciparum* in trophozoite stage

The parasites in the trophozoite stage were purified by magnetic MACS® columns (Ribaut *et al.*, 2008). The hemozoin that exists in the trophozoite, schizont, and gametocyte stages binds to the magnetic column, resulting in the separation of parasites in these stages from the other parasites and non-infected RBCs. An LD magnetic column was connected to a 3-way stopcock and was set into a QuadroMACSTM separation system (Miltenyi Biotec, Germany). The LD column was first incubated with warmed (37 °C), complete RPMI 1640 medium. One plate of *P. falciparum* cell culture was harvested by centrifugation. The pellet was resuspended in 5 ml RPMI 1640 medium. The suspension was loaded on the top of the column, and the column was then washed more than twice with pre-warmed culture medium until the flow-through was almost free of RBCs. The column was removed from the magnetic support. Then, 10 ml culture medium was used to elute the parasites from the column. The eluate was centrifuged, and the pellet was directly used for further analysis or stored at -80 °C.

3.2 Adenylate kinase

3.2.1 Cloning of *Pfaklp1* and *Pfaklp2*

From a gametocytic cDNA library of *P. falciparum* 3D7 as well as blood stage cDNA library, the gene of *Pfaklp1* was cloned by PCR-amplification using the primers (5‘-AACATATGAAAAGAAAAGTAC CGAATATAAT-3‘, 5‘-AACTCGAGTATATATGAGAGAACCCAATTTTTTA-3‘) with *NdeI* and *XhoI* restriction sites (underlined). The following PCR program was employed, and the PCR product was ligated into a pGEM-T easy vector (Promega) and transformed into *E. coli* KRX cells. The colonies containing the plasmids were inoculated into 3 mL LB medium containing carbenicillin (100 µg/ml) to be grown overnight (~ 15 hours). The plasmids were prepared by using the Qiagen Miniprep plasmid kit and identified by the cleavage of *NdeI* and *XhoI* restriction enzymes on the agarose gel. The plasmids were further sent to sequence for verification. The correct *Pfaklp1* gene without a stop codon (558 bp) was then cleaved from the pGEM-T easy vectors and subcloned into the expression vector pET24a (*Pfaklp1*/pET24a) with a C-terminal hexahistidyl (His)-tag.

PCR mixture	
Component	Volume (µl)
10x buffer	5
Template (~80 ng)	1
dNTP (2 mM)	4
Primer forward (100 µM)	1
Primer reverse (100 µM)	1
Polymerase	0.5
H_2O_{dd}	37.5

PCR program	
Program	Time and Temperature
Initialization	94 °C for 3 min
Denaturation	94 °C for 30 s
Annealing	55 °C for 45 s
Elongation	72 °C for 90 s
Cycles	30 cycles
Final elongation	72 °C for 10 min

In order to clone the *Pfaklp1* into a N-terminal His-tag, two primers (5'-AACATATGAAAAGAAAAG TACCGAATATAAT-3', 5'-AACTCGAGTCATATATATGAGAGAACCCAATTTTTTA-3') with *NdeI* and *XhoI* restriction sites amplified an approximate 560 bp fragment. The PCR products were ligated into a pGEM-T easy vector and transformed into *E. coli* KRX cells. The colonies grown on agar plates were inoculated into 3 ml LB medium containing carbenicillin (100 µg/ml). The plasmids were prepared from overnight culture and identified by the digestion of *NdeI* and *XhoI* restriction enzymes. The plasmids containing the inserts were sent for sequencing. After sequencing, the *Pfaklp1* gene was subcloned into the pET28a (*Pfaklp1*/pET28a) vector with an N-terminal His-tag.

PCR mixture	
Component	Volume (µl)
10x buffer	5
Template (~80 ng)	1
dNTP (2 mM)	4
Primer forward (100 µM)	1
Primer reverse (100 µM)	1
Polymerase	0.5
H_2O_{dd}	37.5

PCR program	
Program	Time and Temperature
Initialization	94 °C for 3 min
Denaturation	94 °C for 30 s
Annealing	57 °C for 45 s
Elongation	72 °C for 90 s
Cycles	30 cycles
Final elongation	72 °C for 10 min

For amplification of the *Pf*AKLP2-encoding sequence, two primers (5'-ATATGGATCCGAAACACTT CTACATAGCGAAATAT-3' and 5'-ATATCTCGAGTTACCTTATATAGGAAAGAACTTGG-3') with restriction sites of *BamHI* and *XhoI* (underlined) were used and amplified an approximately 790 bp product by PCR from a blood stage cDNA library of *P. falciparum* 3D7. The amplified sequence was ligated into a pGEM-T easy vector. After the ligation, the mixture was added to competent *E. coli* XL-1 Blue cells for transformation. The colonies observed on the agar plates were picked up to be cultured in 3 ml LB medium containing carbenicillin (100 µg/ml) overnight (~ 15 hours). The plasmids were then prepared by using Qiagen Miniprep plasmid kit. After verified by restriction enzymes, the sequence was performed, and the results were compared with the data in the NCBI databank in order to check the whole sequence. The fragment with the correct sequence was then subcloned into pET28a (*Pfaklp2*/pET28a) with an N-terminal His-tag.

PCR mixture	
Component	Volume (µl)
10x buffer	5
Template (~80 ng)	1
dNTP (2 mM)	4
Primer forward (100 µM)	1
Primer reverse (100 µM)	1
Polymerase	0.5
H_2O_{dd}	37.5

PCR program	
Program	Time and Temperature
Initialization	94 °C for 3 min
Denaturation	94 °C for 30 s
Annealing	55 °C for 45 s
Elongation	72 °C for 90 s
Cycles	30 cycles
Final elongation	72 °C for 10 min

3.2.2 Overexpression and purification of *Pf*AKLP1 and *Pf*AKLP2

The construct *Pfaklp1*/pET24a or *Pfaklp1*/pET28a was transformed into *E. coli* KRX cells. Cells were grown at 37 °C in TB medium containing 50 µg/ml of kanamycin. The culture was induced by 0.1% (w/v) rhamnose at an optical density (OD600nm) of 0.6. The culture was further grown at 30 °C overnight for about 15 hours. Cells were harvested by centrifugation at 10,000 g for 15 minutes at 4 °C and resuspended in 50 mM sodium phosphate, 300 mM NaCl, pH 8.0. After adding protease inhibitors composed of pepstatin, cystatin, and PMSF, cells could be stored at -20 °C or directly be lysed for purification.

The cells were lysed by the addition of lysozyme and DNase I and stirred on ice for 30 minutes, followed by 6 times for 20 seconds, with each sonication in the presence of protease inhibitors (100 µM PMSF, 3 µM pepstatin, and 80 nM cystatin). After centrifugation at 38,000 g for 30 minutes at 4 °C, the supernatant containing all soluble proteins was deposited onto a 1 ml nickel-nitrilotriacetate (Ni-NTA) column that was equilibrated with buffer containing 50 mM sodium phosphate, 300 mM NaCl, pH 8.0. The recombinant protein was eluted with 20-200 mM imidazole after the column was washed with 10 ml buffer. The fractions were observed on the SDS-PAGE. The samples were concentrated with a 10 kDa viva spin column and further purified by gel filtration.

Overexpression and purification of *Pf*AKLP2 were carried out as described for *Pf*AKLP1, but Protino® Ni-TED resin was used instead of Ni-NTA for the purification.

3.2.3 Gel filtration of *Pf*AKLP1 and *Pf*AKLP2

The proteins can be separated according to their molecular mass during gel filtration. The large proteins pass through the gel filtration medium faster than the small ones.

*Pf*AKLP1 and *Pf*AKLP2 were further purified by gel-filtration chromatography on a HiLoad 16/60 Superdex 200 prep-grade column connected to an ÄKTA FPLC system (Amersham Pharmacia Biotech). The column was first calibrated with a gel-filtration standard (Amersham Pharmacia Biotech). Before loading the sample, the column was rinsed by 1 column volume of ultrapure water and then equilibrated with the buffer containing 50 mM sodium phosphate, 300 mM NaCl, pH 8.0. *Pf*AKLP1 or *Pf*AKLP2 was applied onto the column and the proteins in eluate fractions were detected spectrophotometrically at 280 nm. The protein fractions containing *Pf*AKLP1 and *Pf*AKLP2 were

concentrated with a 3 kDa viva spin column. Protein concentrations were determined using the Bradford protein assay (Bradford, 1976) using bovine serum albumin as a standard sample. Purity of the recombinant proteins was verified by SDS-PAGE. After use, the column can be washed with buffer and ultrapure water and stored in 20% ethanol water.

3.2.4 His-tag cleavage of recombinant proteins by thrombin enzyme

N-terminal His-tag cleavage of *Pf*AKLP1 and *Pf*AKLP 2 was carried out by using a thrombin kit from Novagen. This endoprotease could recognize the sequence of Leu-Val-Pro-Arg-Gly-Ser and cut between Arg and Gly, which exist between the His-tag and our recombinant proteins due to the design of the pET28a vector. Therefore, the protein without the His-tag can be obtained. In our study, about 3-4 mg of *Pf*AKLP1 and *Pf*AKLP 2 mixed with 10x thrombin cleavage buffer and 0.1 ml of thrombin per mg of protein was used, and the whole reaction was performed for 16 hours at 4 °C. Subsequently, the mixture was again loaded onto the affinity column in order to remove the uncleaved proteins. The resulting protein without His-tag could be obtained in the fraction of flow through. The proteins can be detected via SDS-PAGE gel and the cleavage of the tag can be confirmed by Western blot with the His-tag antibody.

3.2.5 Enzyme assay

The AK assay used in our study is based on the determination of ADP with pyruvate kinase and lactate in a coupled assay system as shown in Figure 3.2. Generally, ADP produced by AK can be utilized by PK, yielding the pyruvate. The third reaction catalyzed by LDH could use pyruvate and NADH as the substrate. The consumption of NADH is measured by the change of absorbance at 340 nm. The enzyme assay mixture contained 200 µM NADH, 10 U/ml lactate dehydrogenase (Roche), 10 U/ml pyruvate kinase (Roche), 2.3 mM NMP, 0.8 mM NTP, and rate-limiting quantities of *Pf*AKLP1 or *Pf*AKLP2 in 1.5 mM $MgCl_2$, 90 mM KCl, 110 mM TEA-HCl, pH 7.6, at 25 °C. The consumption of NADH (ε_{340nm} = 6.22 $mM^{-1}cm^{-1}$) was measured spectrophotometrically at 340 nm. In order to determine the substrate specificity, we tested AMP, CMP, UMP, IMP, and GMP as substrates while using ATP as the phosphate donor. The NTPs were also studied by testing ATP, GTP, ITP, and UTP as phosphate donors with AMP.

$$\text{ATP} + \text{AMP} \overset{\text{AK}}{\Longleftrightarrow} 2\,\text{ADP} \qquad \text{ADP} + \text{PEP} \overset{\text{PK}}{\Longleftrightarrow} \text{ATP} + \text{Pyruvate} \qquad \text{Pyruvate} + \text{NADH} \overset{\text{LDH}}{\Longleftrightarrow} \text{NAD}^+ + \text{Lactate}$$

Total reaction: $\text{AMP} + 2\,\text{PEP} + 2\,\text{NADH} \rightarrow \text{ATP} + 2\,\text{Lactate} + 2\,\text{NAD}^+$

$\varepsilon_{NADH} = 6.22\ mM^{-1}cm^{-1}$

$$V_A = \frac{\triangle A/\text{min} \times V_0}{6.22 \times V_i}\ [\text{U/ml}]$$

V_0 is the total volume of assay, and V_i is volume of enzyme used.

Figure 3.2 Overall reaction in an adenylate kinase-coupled assay. PK, pyruvate kinase; LDH, lactate dehydrogenase; PEP, phosphoenolpyruvate.

3.2.6 GFP constructs of all wild type AKs

Green fluorescent protein (GFP) is a protein originally containing 238 amino acids that will emit green fluorescence at 509 nm when excited with blue or ultraviolet light (Shimomura *et al.*, 1962; Tsien, 1998). The vectors expressing target proteins fused with GFP can be transfected into *P. falciparum*, which can then be examined for subcellular localization of target proteins. Under a fluorescent microscope, immunofluorescence from a compartment-specific protein will co-localize with fluorescence from GFP, thus revealing unique compartment localizations of target proteins.

In order to investigate the localization of all AKs in *P. falciparum*, we designed primers (Table 3.1) to insert *BglII* and *AvrII* restriction sites at both ends of the genes of *Pfak1*, *Pfak2*, *Pfgak*, *and Pfaklp1*, respectively. The genes were then cloned into a pSK-GFP vector via *BglII* and *AvrII* restriction sites in order to obtain GFP-fused genes with the right orientation, which located AK genes in the upstream of the GFP gene. Digestion with *XhoI* yielded fragments containing the respective gene coupled to a downstream GFP gene. After sequencing, the correct fusion fragments were ligated into a pARL-1a+ shuttle vector, which has a low-expression CRT promoter and allows episomal expression as described previously (Kehr *et al.*, 2010). The transfection vectors containing the fusion constructs were verified by sequencing, transformed in *E. coli*, and purified from *E. coli* using a Qiagen Maxi Kit. After the preparation of DNA from the kit, a further precipitation step was required to obtain the sterile DNA with high purity. Normally 550 µl of DNA solution was transferred to a 2 ml EP tube. Then 55 µl (0.1 volume) of a 3 M sodium acetate solution (pH 5.8) was added to the DNA solution. Finally 1.35 ml (2.5 fold) of cold ethanol was mixed with the solution. During this step, the DNA precipitation appeared. Typically the precipitation process was performed at -20 °C for at least 30 minutes. Then the tube was centrifuged at 13,000 rpm for 15 minutes at 20 °C in order to pelletize the DNA. The DNA pellet was washed twice with 70% cold ethanol and dried at RT. Finally the pellet was dissolved in 60-90 µl of sterile TE buffer.

Gene		Primers
Pfak1		CATAGATCTATGAATGAAAATTTAGAAAATTTTTC CATCCTAGGacctgctgcACCGTCTATATGTTGAGAGATTT
Pfak2		CATAGATCTATGGGATCATGTTATAGTAGAA CATCCTAGGacctgctgcATTGGGGTTATCATCTATAATG
Pfgak		CATAGATCTATGAGAATTGTATTATTTGGAG CATCCTAGGacctgctgcTTTTAATTTTTCATTTTTTCTGTA
Pfaklp1		CATAGATCTATGAAAAGAAAAGTACCGAATATA CATCCTAGGacctgctgcTATATATGAGAGAACCCAATTTTT
Pfaklp2	**Mutant**	ATGTTAACTAT**t**CTAGGAACTAATAAAAAG CTTTTTATTAGTTCCTAG**a**ATAGTTAACAT
	GFP	CATAGATCTATGGAAACACTTCTACATAGC CATCCTAGGacctgctgcTATATCACCGTTTAAAGTCGA

Table 3.2 Primers for AK-GFP constructs. The *BglII* and *AvrII* restriction sites are underlined. Two pairs of primers are needed for *Pfaklp2* because an additional silence mutation was required. The mutated nucleotides are indicated as bold small letters.

Figure 3.3 AK protein-fused GFP for sublocalization. The GFP gene is placed on the C-terminus of the AK gene, hence the fused protein.

Because an *AvrII* restriction site exists in *Pfaklp2*, we first introduced a silent mutation to remove the *AvrII* restriction site. The introduced mutation was designed to eliminate the *AvrII* restriction site in the nucleotide sequence without changing the amino acids of PfAKLP2 so that we could use *BglII* and *AvrII* restriction sites for GFP vector construction. Site-directed mutagenesis was performed as described by the QuickChange® site-directed mutagenesis kit with some modifications. The *Pfaklp2/pET28a* and the mutant primers (shown in Table 3.1) were used to generate the silent mutation. PCR was performed according to the table listed below, and products were purified with a QIAquick PCR purification kit and then digested with *DpnI* (37 °C for 2 hours). The digestion step (see below) was used to destroy the template, a methylated DNA used in mutagenesis PCR. Since the *Pfaklp2/pET28a* as the template was prepared from *E. coli* culture, it was methylated and could be cleaved by *DpnI*. After this step, the mutagenic plasmids from the PCR reaction were transformed into *E. coli* XL-1 blue cells. A colony on the agar plate was inoculated in LB medium and grown overnight (15 hours), and plasmids were prepared by using the Qiagen Miniprep plasmid kit. The mutation was verified by sequencing the plasmids. Subsequently, a GFP fusion vector for *Pfaklp2* was constructed by following the procedure we described above for other AKs.

PCR Mixture	
Component	Volume (µl)
10x *Pfu* buffer	5
Template (~80 ng)	1
dNTP (2 mM)	4
Primer forward (100 µM)	1
Primer reverse (100 µM)	1
Pfu Polymerase	0.5
DMSO	2.5
H_2O_{dd}	35

PCR Program	
Program	Time and Temperature
Initialization	94 °C for 5 min
Denaturation	94 °C for 1 s
Annealing	55 °C for 1 s
Elongation	68 °C for 9 min
Cycles	18 cycles
Final elongation	68 °C for 15 min

DpnI digestion	
Component	Volume (µl)
PCR product	30
10 x Tango buffer	5
DpnI (10 U/µl)	2.5
H_2O_{dd}	12.5

3.2.7 GFP construction of a mutant *Pf*AK2 at the myristoylation site

Glycine in position 2, the N-myristoylation site of *Pf*AK2 [6], was mutated to an alanine. PCR for site-directed mutagenesis of *Pfak2* was performed with a *Pfu* polymerase (Promega) using primers carrying the respective mutated codon: 5'-GAGATCTATGGCATCATGTT ATAGTAGAAAAAAT-3', 5'-ATTTTTTCTACTATAACATGATGCCATAGATCTC-3'; the mutated codon is underlined. PCR templates were removed by digestion with *DpnI*, and the PCR product was subsequently transformed into competent *E. coli* XL1-Blue cells. The introduction of the correct mutation into the gene sequence was verified by sequencing, and a GFP-fusion construct of *Pf*AK2^{G2A} was created as described above.

PCR Mixture	
Component	Volume (µl)
10x *Pfu* buffer	5
Template (~80 ng)	1
dNTP (2 mM)	4
Mutant primer forward (100 µM)	1
Mutant primer reverse (100 µM)	1
Pfu polymerase	0.5
DMSO	2.5
H_2O_{dd}	35

PCR Program	
Program	Time and Temperature
Initialization	94 °C for 5 min
Denaturation	94 °C for 1 s
Annealing	55 °C for 1 s
Elongation	68 °C for 9 min
Cycles	18 cycles
Final elongation	68 °C for 15 min

3.2.8 Parasite transfection

Transfection was carried out with the *P. falciparum* 3D7 strain via the electroporation method (Crabb *et al.*, 2004). A 5 ml parasite culture at ring stage (8-10 hours) with 5-8% parasitemia was centrifuged at 1,500 g for 5 minutes. Cytomix buffer was mixed with 150 micrograms of plasmid (AK-GFP fusion gene in pARL-1a$^+$) in a total volume of 400 µl. Then parasite pellet was resuspended in 400 µl plasmid Cytomix solution. The suspension was transferred into a sterile electroporation cuvette. Subsequently, the parasites were electroporated at 310 V, 950 µF (Gene pulser, Bio-Rad) as described (Crabb *et al.*, 2004). The resulting time constant was about 13 milliseconds. Transfected parasites were immediately transferred into 15 ml of fresh pre-warm (37 °C) medium with 3.5% hematocrit. Six hours post transfection, 2 nM WR99210 was added as a selection marker for transfectant selection. After 3-4 weeks, the concentration of WR99210 can be increased to 5 nM. Parasites were maintained by changing the complete RPMI medium daily containing WR99210 and adding 100 µl of fresh erythrocytes weekly.

3.2.9 Immunofluorescence imaging

Immunofluorescence imaging was carried out in collaboration with Dr. Jude Przyborski's group at Philipps University in Marburg. The cells were fixed in 4% paraformaldehyde/0.0075% glutaraldehyde in PBS pH 7.4 for 30 minutes at 37 °C (Tonkin *et al.*, 2004). The fluorescence quenching was achieved by adding 100 mM glycine/PBS. To label the nucleus, Hoechst DNA binding dye (50 ng/ml) was used

while the MitoTracker probe was applied to reveal the mitochondrion. Anti-SERP antibody can display the parasitophorous vacuole where serine-rich protein (SERP) was localized and anti-EXP1 antibody can show the parasitophorous vacuole membrane. The BODIPY dye can stain the lipid membrane. The images were obtained on a Zeiss Axio Observer inverted epifluorescence microscope system.

3.2.10 Western blot analysis

The transgenic parasites were maintained as described [9]. Parasitized red blood cells with *P. falciparum* at the trophozoite stage (IRBC) were enriched using LD-columns (MACS, Miltenyi Biotec) [12]. IRBCs were harvested at 300 g for 3 minutes at room temperature and resuspended in 50 µl 10 mM Tris pH 7.4, containing complete cocktail protease inhibitors from Roche. IRBCs were lysed by three freezing-thawing cycles using liquid nitrogen. The pellet was vigorously mixed by using a table vortex and briefly centrifuged before soaking it into the liquid nitrogen. The lysate was centrifuged at 50,000 g for 30 minutes at 4 °C. The supernatant containing the erythrocyte cytosol and parasite cytosol was transferred to a new tube and centrifuged two more times in order to remove any remaining contamination with the membrane fraction. The membrane pellet derived from the first centrifugation of the lysate was washed once with 1 ml and twice with 100 µl of the Tris buffer.

The membrane pellet and the supernatant including proteins from the erythrocyte cytosol and parasite cytosol were separated by 12% SDS-PAGE and transferred to a PVDF membrane. Membranes were probed with anti-GFP (1:1,000, Roche), anti-Hsp70 (1:1,000, T. Blisnick, Paris), or anti-Exp1 (1:500, Jude Przyborski) antibodies, respectively, followed by HRP-conjugated secondary anti-mouse antibodies (1:10,000, Jackson ImmunoResearch). All antibodies were diluted in 5% non-fat milk in TBST buffer. The membrane was then incubated with enhanced chemiluminescence agents for detection and exposed to X-ray film for a proper time starting from 30 seconds to 10 minutes. The film was developed by using an OptiMax X-ray film processor and the signal was detected.

3.3 N-myristoylation in *P. falciparum*

3.3.1 Metabolic labeling of *P. falciparum* in cell culture with azido myristic acid

The bio-orthogonal chemical reporters have been discovered to be a powerful tool for studying the fatty acylation of proteins in cells. Due to the property tested in mammalian cells (Hang *et al.*, 2007), we employed azido myristic acid to investigate the myristoylation in *P. falciparum.*

The *P. falciparum* strain 3D7 was continuously cultured *in vitro* according to the method in 3.1.9. The azido myristic acid was dissolved in DMSO to obtain a 50 mM stock solution. 45 µl stock solution of azido myristic acid was pre-mixed with 45 ml warm (37 °C) complete medium (RPMI 1640 medium with supplements). The culture medium was then changed with this fresh medium containing azido myristic acid at 1.25% parasitemia at the schizont stage. After around 26 hours, the medium was changed once with the addition of the same concentration of azido myristic acid. After another 12-hour culture, the parasite was purified with the magnetic column as in the previously described method in 3.1.10. The pellet was incubated with saponin solution for approximate 45 s to burst the RBCs without lysing the parasites. The complete medium was used to wash the parasites several times. The parasites

were harvested by quick centrifugation and were ready to use. The same volume of DMSO was added in cell culture instead of azido myristic acid in order to obtain the parallel negative control. Different concentrations of azido myristic acid were added into the cell culture when the dose-dependent effect was investigated. During the whole labeling process, we tried to minimize the exposure of the sample to light because the azido myristic acid is photosensitive.

3.3.2 Preparation of parasite cell lysate and click reaction

The parasite pellet was resuspended in 1% Triton PBS buffer (pH 7.4) and lysed by freezing-thawing four times and three times for 5 seconds for each sonication. The lysate was centrifuged at 16,000 g for 30 min at 4 °C. The supernatant was transferred into another tube and centrifuged at 100,000 g for 30 min at 4 °C. The pellet and the supernatant were collected separately for later experiments. The samples during preparation should not be exposed to light.

The proteins labeled by azido myristic acid that have an azido group can react with alkynyl biotin. The Cu-catalyzed azide-alkyne cycloaddition reaction can form a triazole from a terminal alkyne and an azide, therefore resulting in the biotinylation of the proteins that are supposed to be myristoylated. The protein concentration of parasite lysate was determined by the Bradford assay (Bradford, 1976). The click reaction took place as follows:

Component	Stock concentration	Working concentration	Volume
Protein	/	1-2 mg	
Alkynyl biotin	4 mM	100 µM	12.5 µl
TCEP	50 mM	1 mM	10 µl
TBTA	10 mM	100 µM	5 µl
$CuSO_4$	50 mM	1 mM	10 µl
PBS buffer	/	/	Up to 500 µl

Table 3.3 Compositions of CuAAC click reaction

The reaction lasted for 3 hours at RT with shaking. After the click reaction, the proteins become biotinylated and are stable in the presence of light. The methanol:chloroform precipitation method was employed to terminate the reaction and remove excess biotin from the solution. Briefly, 600 µl of methanol was added to the 200 µl reaction solution following an addition of 150 µl chloroform to the mixture. Then 400 µl of ultrapure water was required for mixing. The vortex step was necessary after each addition. After centrifugation for 10 minutes at 15,000 g, the upper aqueous phase was discarded as much as possible without disturbing the interface layer. Then 450 µl of methanol was added to the tube and was centrifuged for 10 minutes at 15,000 g. The supernatant was removed afterwards and the protein pellet was washed three times with 600 µl methanol and was air-dried for 5 minutes. The pellet was resuspended in 1% Triton PBS and kept at -20 °C for around 3 days. The water-bath sonication may be required to fully solubilize the protein pellet. The negative control and the sample with the addition of azido myristic acid should simultaneously proceed following the same procedure as described above.

3.3.3 Visualization of myristoylated proteins by streptavidin-HRP blot

The general procedure is the same as the classic Western blot described in 3.1.7, except that no second antibody is required. Before the sample was loaded onto the SDS-PAGE, the protein concentration was measured using a Bradford assay (Bradford, 1976). The same amounts of proteins from negative control and sample were loaded into gel slots. After gel electrophoresis, the proteins were transferred into a PVDF membrane using the semi-dry method. The efficiency was checked by Ponceau staining, and the membrane was blocked in 5% milk TBST at 4 °C overnight. The streptavidin-HRP with 1:1,000 dilution in TBST solution was prepared and added to the membrane for 1 hour at RT after washing three times. The membrane was incubated with chemiluminescence reagent for 1 minute and visualized in an X-ray film.

3.3.4 Pull-down assay of myristoylated proteins with avidin beads from *P. falciparum*

The biotin-avidin system is a mainstay in most fields of biological sciences. The binding interaction between biotin and streptavidin is one of the strongest non-covalent ones known in nature. The strong interaction between avidin and biotin can be exploited to affinity-isolate biological molecules. In our study, we employed soft-link avidin beads in order to pull down the biotinylated proteins.

This soft-link avidin beads allow the neutral condition to elute the proteins from the beads. The 5 mM biotin was pre-incubated to the 100 µl bead slurry for 30 minutes in order to block all the binding sites of biotin in the avidin beads. After incubation, the biotin solution was discarded by centrifugation, and the beads were washed several times with PBS buffer. Then 1 ml 10% acetic acid was added to wash the beads with gentle shaking for 10 minutes. The acetic acid needed to be changed twice. During this step, the irreversible binding sites in avidin beads were still blocked by biotin while reversible binding sites were released by acid wash. Then the beads were washed five times with 500 µl $NaPO_4$ (pH 7.0) buffer, and the pH was monitored until it reached 6.8. The beads were equilibrated with 0.1 M $NaPO_4$ (pH 7.0) for 1 hour in order to let avidin refold. The beads were then equilibrated with 1% Triton PBS buffer. Then the protein sample was added to the beads for pull-down with shaking for 3 hours. The beads were centrifuged, and the supernatant was removed. After this, the beads were intensively washed 6 times with 1% Triton PBS buffer, and the biotinylated proteins were eluted by using the 5 mM biotin PBS solution. The eluants were collected for further analysis. The beads were boiled with 4x sample buffer at 96 °C for 10 minutes to check the elution efficacy.

3.3.5 Prediction of myristoylation in *P. falciparum*

Since a conserved motif for myristoylation exists, at least two prediction tools are available on the web. Myristoylator on ExPASy (Bologna *et al.*, 2004) web and the MYR Predictor provided by IMP Bioinformatics Group (Maurer-Stroh *et al.*, 2004) can predict the myristoylated proteins by bioinformatic methods based on the analysis of diverse NMT structures from different species and the recognition motif in the myristoylated proteins. The MYR Predictor is developed relying on a method that uses position-specific independent counts, redundancy-corrected profiles of known substrates in

combination with physicochemical constraints of enzyme-substrate interactions (Maurer-Stroh *et al.*, 2004). The MYR Predictor is designed to predict not only the N-terminal glycine myristoylation site but also a possible internal glycine. The myristoylator employs a neural network models that can distinguish the myristoylated proteins from nonmyristoylated ones for prediction and has a false positive error rate equal to 2.1%. The entire proteome of *P. falciparum* was obtained from the PlasmoDB web server, which contains a lot of information of *Plasmodium*. The sequences of the whole proteome were subjected to the web server of the MYR Predictor. Then the server returned prediction results. After this, the predicted proteins were repeatedly analyzed with the myristoylator tool.

3.4 Crystal screening of N-myristoyltransferase

3.4.1 Overexpression and purification of N-myristoyltransferase from *P. falciparum*

The *Pfnmt* gene was subcloned into pET28 from a *Pfnmt*/pQE30 construct (Rahlfs *et al.*, 2009) in order to overexpress *Pf*NMT with a His-tag. In brief, *BamH I* and *Hind III* were used to digest the *Pfnmt*/pQE30 and pET28. The ligation step was performed as described in the general methods section in order to construct a *Pfnmt*/pET28. The ligation mixture was transformed into competent KRX cells, and the plasmid was confirmed by digestion with *BamH I* and *Hind III* following the standard protocol described previously.

Heterologous overexpression of *Pf*NMT was optimized by varying the different parameters such as cell strain, medium, and helper plasmids. The overexpression conditions tested in my work are listed in Table 4.1 in the Results section.

The optimized protocol for *Pf*NMT overexpression employed in our experiment is described below. The vector *Pf*NMT/pET28 was transformed into a competent C41/pGro7 cell line. After inoculating the colony into 3 ml LB medium and subsequently into 50 ml medium as a pre-culture, one liter of TB medium was inoculated and shaken at 37 °C. The media each contained 50 µg/ml kanamycin and 25 µg/ml chloroamphenicol. L-arabinose with a final concentration of 1 mg/ml was added when starting the 1-liter culture. The addition of 1 mM IPTG was carried out when OD_{600} reached 0.8. Subsequently, the culture was grown at RT for 24 h with a shaking speed of 170 rpm. The cells were harvested by centrifugation at 8,000 *g* for 15 minutes at 4 °C. To resuspend the cells, approximately 30 ml of buffer (50 mM Tris, 300 mM NaCl, pH 7.6) was used in addition to the protease inhibitor (100 µM PMSF, 3 µM pepstatin, and 80 nM cystatin). The cell resuspension was stored at -20 °C.

The cells were lysed by the addition of lysozyme and DNase I for 40 minutes and then sonicated four times for 30 seconds each in the presence of protease inhibitors (100 µM PMSF, 3 µM pepstatin, and 80 nM cystatin). After centrifugation at 38,000 *g* for 30 minutes at 4 °C, the supernatant was loaded onto a 1 ml Protino-Ni-TED column that was equilibrated with a buffer composed of 50 mM sodium phosphate, 300 mM NaCl, and pH 8.0. The recombinant protein was eluted with 30-200 mM imidazole. The fractions were analyzed by SDS-PAGE.

For further purification of *Pf*NMT, the fractions containing PfNMT proteins were combined and concentrated with a 10 kDa viva spin column. Gel filtration was carried out as described in chapter 3.2.3 with only a minor modification. The buffer used for *Pf*NMTP purification was 50 mM Tris, 300 mM NaCl, pH 7.6. Purity of *Pf*NMT was confirmed by SDS-PAGE and the protein was concentrated

with a 10 kDa viva spin column. Protein concentration was determined by a Bradford assay (Bradford, 1976), which could be used for the following crystallization screen.

3.4.2 *Pf*NMT crystal screening

This experiment aims to produce crystals of *Pf*NMT that can be used for X-ray diffraction. X-ray diffraction data can then be collected for structure solution and structure refinement. Finally, the structure of the protein can be solved. Both hanging drop and sitting drop methods, which are schematically demonstrated in Figure 3.4, were applied in order to crystallize *Pf*NMT protein based on vapor diffusion. The principle of the method is based on vaporization of water or certain volatile agents between the droplet containing the protein and the reservoir solution with a large volume and higher precipitant. As water vaporizes from the droplet, the precipitant concentration of the droplet gradually increases until a crystal appears. Crystals can grow under these optimum conditions because the system is in equilibrium (McRee, 1993; Rhodes, 1993).

The initial trial of crystal screening of *Pf*NMT started with the JCSG Core Suite kit from Qiagen by using the Honeybee 961 robot from Zinsser Analytic, which automatically allows a minimum of one nanoliter of protein solution for screening and fast plate preparation within 2 minutes. The full set of the JCSG Core Suite kit is composed of four screens of 384 unique conditions that have three types of precipitants, salt, organic, and polymers, on the basis of analyzing over 500,000 crystallization experiments. Therefore, higher hit rates could be expected for the initial screening. The reservoir solution without the protein was also sitting on a pedestal above the reservoir solution (Figure 3.4B) as a comparison.

After the preliminary screening, several solutions were picked up for further testing using a manual hanging drop method. Reservoir solution drops 2.5 µl in size were mixed with a 2.5 µl *Pf*NMT solution sitting on the cover slips. These were then placed over a small well containing 800 µl of the reservoir solution. Silicon oil was used on the sides of the glass slip to seal the entire well.

Besides *Pf*NMT, the complex of the enzyme with myristoyl-CoA was also tried for crystal screening. After the pure protein was obtained, myristoyl-CoA was added at a molar ratio of 1:1.5 between

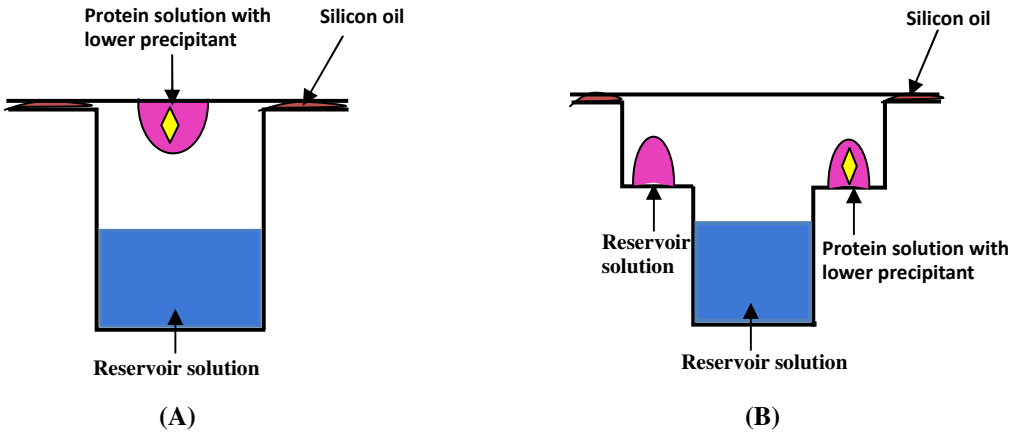

Figure 3.4 Schematic diagram of Hanging drop (A) and Sitting drop (B) for protein crystallization.

*Pf*NMT and myristoyl-CoA. The complex was ready to use for crystal screening after one night of incubation. The crystallization of *Pf*NMT with myristoyl-CoA was screened with the JCSG Core Suite kit from Qiagen by using a Honeybee 961 robot. Several conditions were further screened with a manual hanging drop method.

3.4.3 Homology modeling of *Pf*NMT

Homology modeling is a method to construct a 3D structure of the target protein based on its amino acid sequence and an experimental structure of its related homologous protein. The accuracy of the predicted structure depends on the identity of amino acids between the target proteins and the proteins with known structures. Homology modeling requires the following steps (Schwede *et al.*, 2003). First, the template will be chosen based on the sequence alignment in a database with the structure solved. Then the target sequence is aligned with the main template structures using a local pair-wise method. The backbone structure of the target protein will be constructed followed by side chain modeling. The energy minimization method is applied in order to normalize and improve the structure. The stereochemistry as well as geometric and energetic arrangement of the model should be considered in the evaluation process.

The structural model of *Pf*NMT was predicted via the homology modeling method with the Swiss-Model Server (Peitsch *et al.*, 1995). There are three modes to choose from: automated, alignment, and project mode. Due to the known structure of *Plasmodium vivax* NMT, which shares about 80% identity with *Pf*NMT, the automated mode can be applied in our experiment. The FASTA format of the amino acid sequence from *Pf*NMT was submitted to the Swiss-Model Server. Then best template structures from ExPDB were acquired relying on its sequence similarity to *Pf*NMT. This process was obtained by aligning the target protein sequence with all entries of the ExPDB sequence database by using the BLASTP tool. After this step, the best template was determined to be *Pv*NMT. Hence, the structural model was built on a crystal structure of *Plasmodium vivax* NMT (4a95A). Details of the structure model were displayed in a new interface. The model's coordinates and all analysis results can be sent to the user via e-mail.

3.4.4 Crystal screening of *Pf*NMT and the *Pf*AK2 complex

In our previous study, *Pf*AK2 and *Pf*NMT could form a heterodimer (Rahlfs *et al.*, 2009) in *E. coli* cells that lack myristoylation and NMT of their own and could be overexpressed and purified as a complex *in vitro*.

In brief, the *Pfnmt* gene was cloned into a special pQE30 vector, which was modified in our lab in order to eliminate the sequence encoding the His-tag. *Pfak2* was cloned into pET28 with a C-terminal His-tag. Both plasmids were transformed into competent C41 cells for coexpression. The complex of *Pf*NMT/AK2 was obtained by two-step purification. The Protino-Ni-TED column was used as a first step followed by gel filtration chromatography. The complex of *Pf*NMT/AK2 was concentrated by a 10 kDa viva spin column to approximately 6 mg/ml and the protein concentration was determined by the Bradford method (Bradford, 1976).

The crystal screening of *Pf*NMT/AK2 was initiated with the JCSG Core Suite kit from Qiagen by using the Honeybee 961 robot from Zinsser Analytic. The various PEG and pH buffers were also tested for the initial screening step.

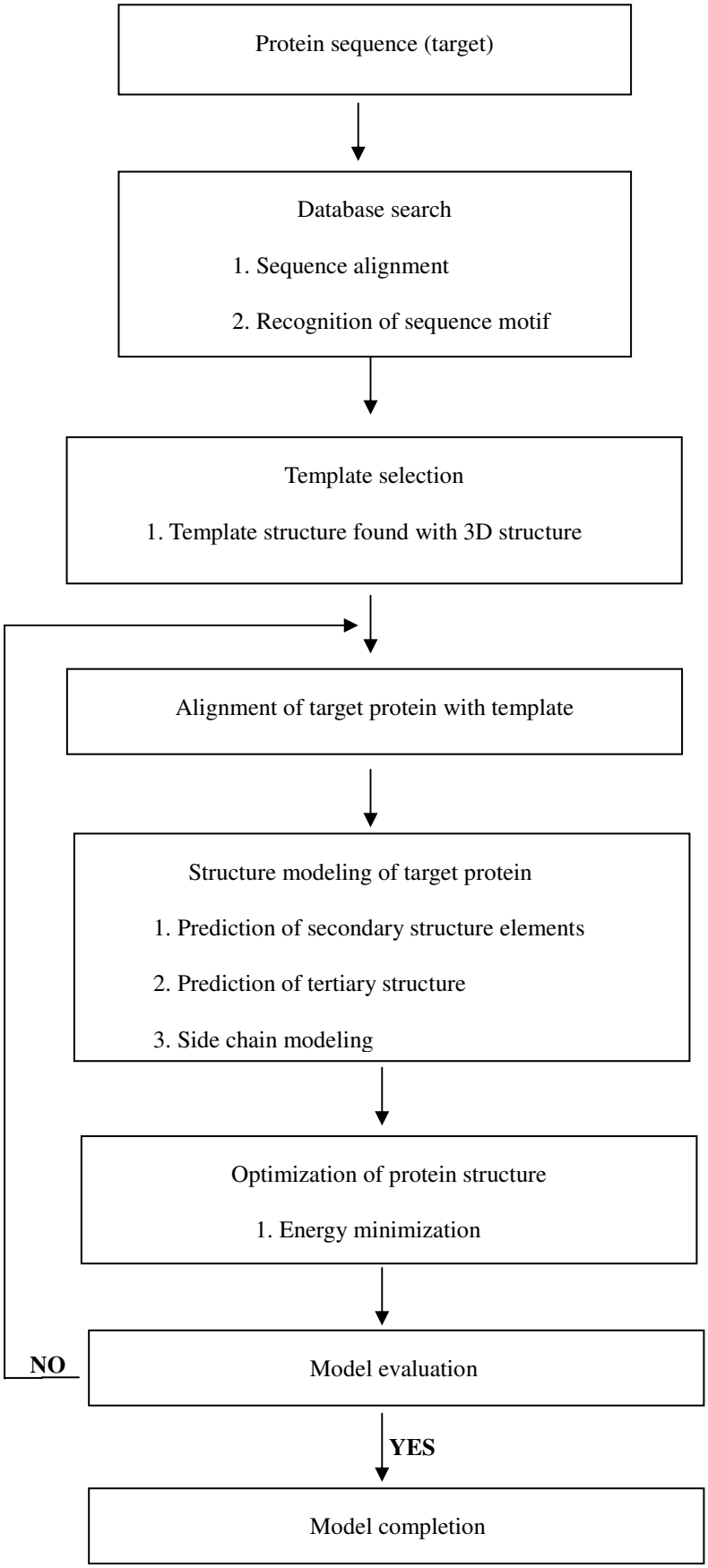

Figure 3.5 Flow chart of Protein 3D structure modeling.

4. Results

4.1 *Pf*AKLP1 and *Pf*AKLP2

In this study, new putative adenylate kinase isoforms have been identified, cloned, heterologously overexpressed, and tested in AK enzymatic assays. Besides this, the subcellular localization of AK isoforms has been systematically investigated in order to elucidate the AK-mediated, high-energy phosphotransfer network in *P. falciparum*.

4.1.1 Sequence alignment and phylogenetic tree

When searching for adenylate kinases in PlasmoDB, two new putative adenylate kinases were predicted. One gene (PFA0530c; PfAKLP1) is located on chromosome 1 and consists of one exon with 561 bp. The gene is expressed in intraerythrocytic stages as well as in gametocytic stages (PlasmoDB). A homology search on NCBI shows the highest similarity (64% identity) between *Pf*AKLP and a hypothetical protein related to nucleotide kinase in *P. knowlesi*, while the sequences of *Pf*AK1 and *Pf*AKLP1 only share 25% identity. Moreover, *Pf*AKLP1 shows similarity with 33% amino acid identity compared to human AK6, which has AK activity and is located in the nucleus (Ren *et al.*, 2005). A multiple sequence alignment (Figure 4.1) shows that most amino acids of the canonic phosphoryl-binding loop GxxGxGxxT in *Pf*AKLP1 (G12, G17, K18, T20 for ATP binding; K18 and L75 for AMP binding) are conserved (Rahlfs *et al.*, 2009), while a number of residues typically involved in AMP binding (L63, R64, G84, V87, V92, G113, R116, Q120 in PfAK1) are missing in *Pf*AKLP1. The arginine residue at position 127 and the spartate residue at position 172 contributing to transition state stabilization are conserved in *Pf*AKLP1 (Figure 4.1) (Reinstein *et al.*, 1990; Tsai *et al.*, 1991).

Additionally, a second protein (PFI1550c, *Pf*AKLP2) was predicted to belong to the AK family. The open reading frame of *Pfaklp2* positioned on chromosome 9 has 792 bp including 4 exons. The gene is expressed in all stages and has an expression peak in late schizonts (PlasmoDB). A homology search based on the BLASTP program predicts the enyme to belong to the P-loop-NTPase superfamily and shows that *Pf*AKLP2 has similarity with adenylate kinase from several species including *Trypanosoma brucei*, *Leishmania braziliensis*, and *Gallus gallus*. A sequence alignment revealed that the amino acids for substrate binding (Q95, K108) and transition stabilization (E138, E175) are hardly conserved in *Pf*AKLP2. While V111, I116, G139, and Q146 are reminiscent of AMP binding in *Pf*AKLP2, the sequence of the canonic P-loop is – apart from G65 – hardly noticeable (Figure. 4.1) (Reinstein *et al.*, 1990; Tsai *et al.*, 1991; Ulschmid *et al.*, 2004).

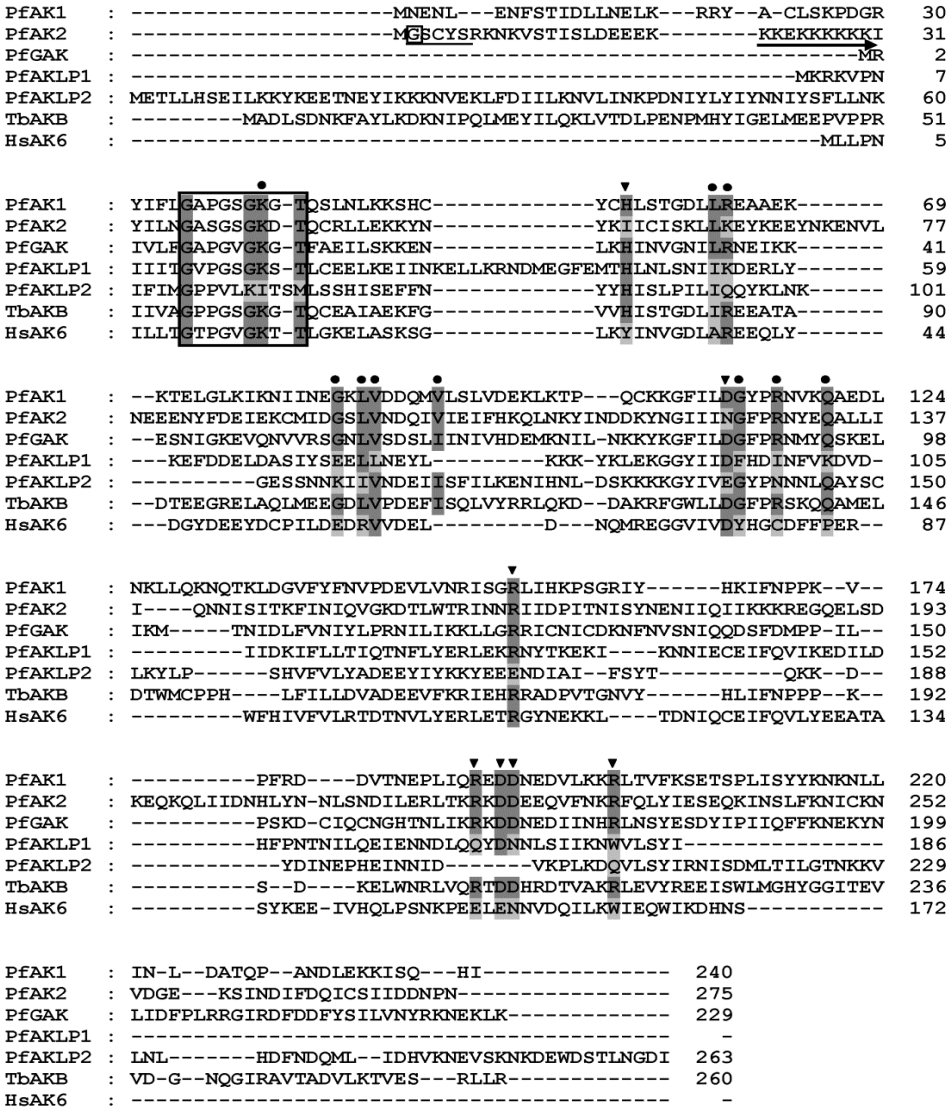

Figure 4.1 Multiple sequence alignment of AK family members (Ma *et al.*, 2012). *Pf*AKLP1 (XP_001351038), *Pf*AKLP2 (XP_002808979), *Pf*AK1 (XP_001347371), *Pf*AK2 (XP_001349355), *Pf*GAK (XP_001351464), human AK6 (NP_057367), and *Trypanosoma brucei* adenylate kinase B (XP_822341)**.** Amino acids forming the canonic phosphoryl loop (P-loop, GxxGxGxxT) are demonstrated in a frame; amino acids responsible for AMP binding are indicated by solid circles. The conserved residues labeled by solid triangles play a role in the catalytic mechanism of AKs. The polybasic stretch of amino acids related to membrane association is marked by a horizontal black arrow. The myristoylated glycine within the myristoylation motif of PfAK2 (underlined) is given in the box. The alignment was created by using Clustal Omega.

A phylogenetic tree (Figure 4.2) was constructed based on multiple sequences with high similarity of various AKs. It seems the AK members in *Plasmodium* can be classified into two subgroups. It became obvious that the subfamilies of *Pf*AK1 and *Pf*GAK are conserved in closely related organisms. Accordingly, *Pf*AK2, which has a novel myristoylated motif at its N-terminus, is clustered separately to

distant subgroups of AK when compared to *Pf*AK1 and *Pf*GAK,. The branch of *Pf*AKLP1 seems closer to the subgroup of human AK6 while *Pf*AKLP2 is clustered individually. In the phylogenetic tree, the branch of *Pf*AK2 is closer to the group including *Pf*AK1 and *Pf*GAK, while the cluster of *Pf*AKLP2 belongs to the group comprising *Pf*AKLP1 and human AK6.

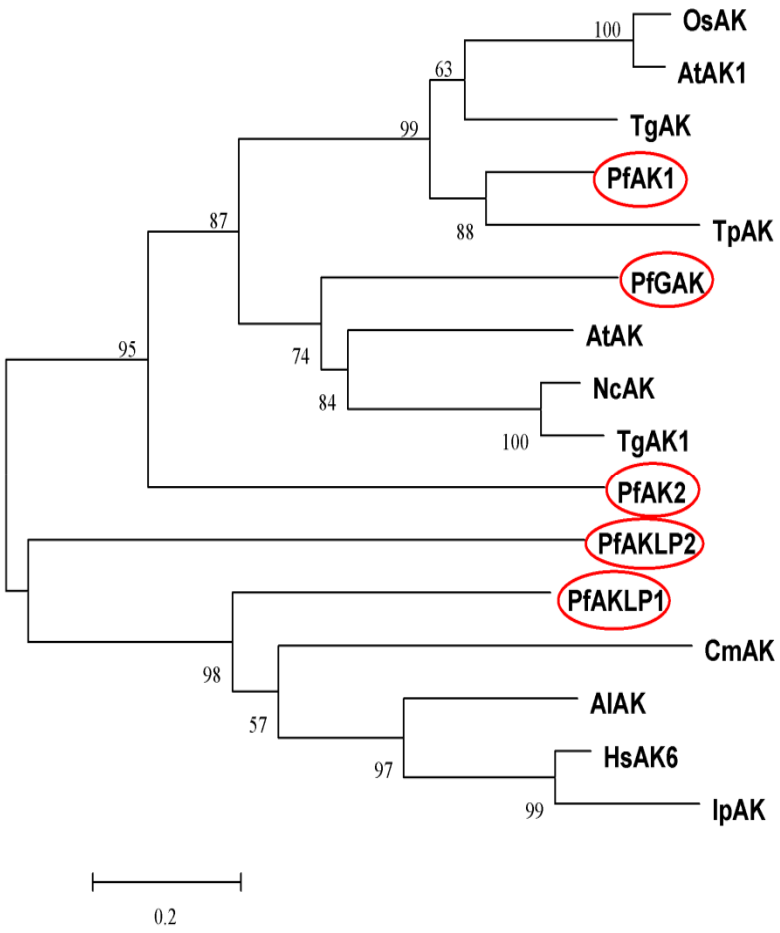

Figure 4.2 Radial phylogenetic tree generated by using the neighbour-joining method based on the results of multiple sequence alignments of AKs from various species (Ma *et al.*, 2012). Tg, *Toxoplasma gondii*, XP_002366164; Tp, *Theileria parva*, XP_766154; Os, *Oryza sativa*, NP_001067759; At, *Arabidopsis thaliana*, NP_201145; Nc, *Neospora caninum*, CBZ51007; Al, *Albugo laibachii*, CCA23523; Cm, *Cryptosporidium muris*, XP_002141495; Hs, *Homo sapiens*, NP_057367; Ip, *Ictalurus punctatus*, NP_001187781. Scale bar, evolutionarily indicated 0.2 substitutions per site. Numbers at the branches indicate the confidence level of a bootstrap analysis with 1,000 replications as a percentage value.

4.1.2 Cloning of *Pfaklp1* and *Pfaklp2*

Pfaklp1 was successfully amplified from a gametocytic cDNA library of *P. falciparum* 3D7 as well as blood stage cDNA library using the specific primers described in methods. The resulting 560 bp fragment was cloned to pET24 vector, therefore adding a C-terminal His-tag to the protein. In order to

cleave the His-tag, *Pfaklp1* was subcloned into the pET28a vector to obtain the recombinant *Pf*AKLP1 protein with a N-terminal His-tag.

PCR was performed to clone the *Pfaklp2* gene in order to construct the overexpression vector. The gene was then cloned into the pET28a vector so that the produced proteins contained an N-terminal His-tag for further purification and cleavage.

4.1.3 Overexpression and purification of recombinant *Pf*AKLP1 and *Pf*AKLP2

*Pf*AKLP1 has been successfully overexpressed and purified by the methods we described previously. *Pf*AKLP1 was purified by Ni-NTA affinity chromatography followed by gel filtration chromatography (Figure 4.3 A and Figure 4.4 A). Heterologous overexpression of *Pf*AKLP1 in *E. coli* yielded a 25 kDa

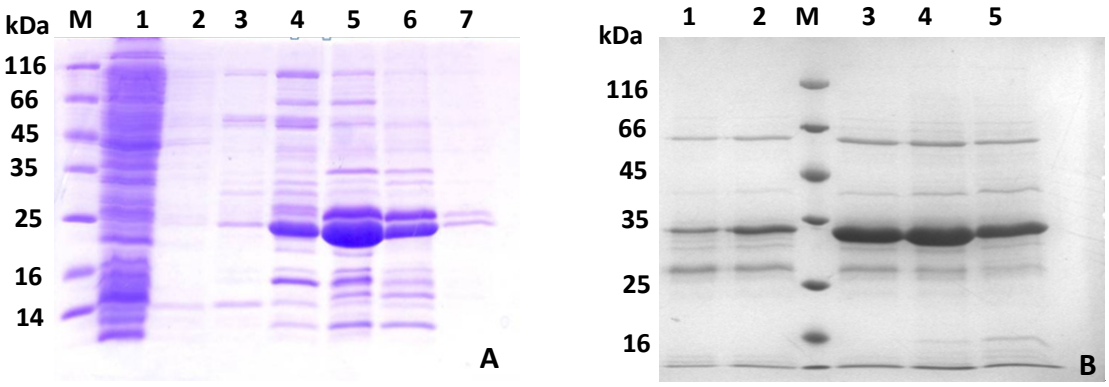

Figure 4.3 12% SDS-PAGE gel after affinity chromatography purification. A) SDS-PAGE gel of *Pf*AKLP1 after Ni-NTA purification. M, unstained molecular weight marker; 1: flow-through; 2: wash fraction; 3-7: elution with 10 mM, 50 mM, 100 mM, 200 mM, and 500 mM imidazole, respectively. **B)** SDS-PAGE gel of *Pf*AKLP2 after Protino Ni-TED purification. M, unstained molecular weight marker;1-5: elution with 10 mM, 50 mM, 100 mM, 200 mM, and 500 mM imidazole, respectively.

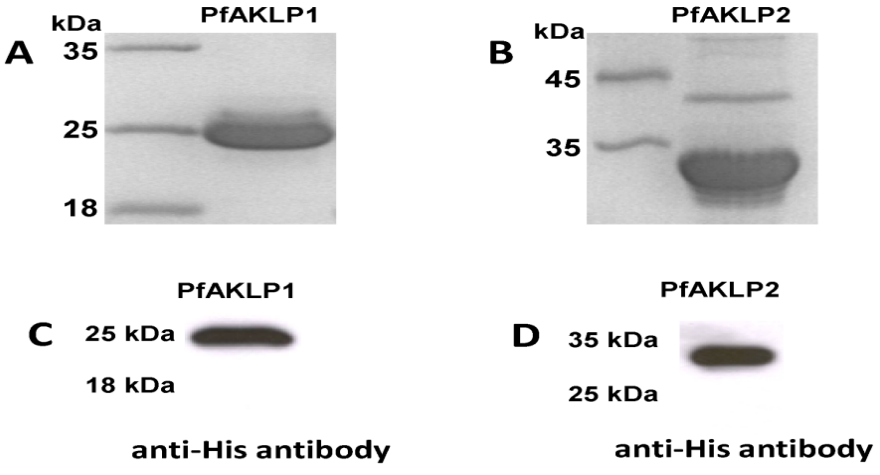

Figure 4.4 SDS-PAGE and Western blot of recombinant *Pf*AKLP1 and *Pf*AKLP2 (Ma *et al.*, 2012). (**A**) and (**B**), recombinant *Pf*AKLP1 and *Pf*AKLP2 on SDS-PAGE with Coomassie staining after gel filtration. (**C**) and (**D**), Western blot of recombinant proteins *Pf*AKLP1 and *Pf*AKLP2 using an anti-His antibody.

protein with a C-terminal His-tag. The maximum yield of pure protein reached about 4 mg/L *E. coli*

culture. *Pf*AKLP2 can be further purified by gel filtration chromatography after the first purification with Protino Ni-TED resin (Figure 4.3 B and Figure 4.4 B). The yield of recombinant *Pf*AKLP2 with 90% purity was about 1.5 mg/L *E. coli* culture (Figure 4.3 B and Figure 4.4 D).
Both recombinant proteins can be verified by Western blot with an anti His-tag antibody as shown in Figure 4.4 C and D.

4.1.4 Cleavage of His-tag of recombinant *Pf*AKLP1 and *Pf*AKLP2 by thrombin

In order to test the effect of the His-tag on the enzyme activity, the enzyme thrombin was used to cut the His-tag. Since both genes were cloned into the pET28 vector, recombinant proteins had a thrombin cleavage site between their N-terminal His-tag and the proteins. After affinity chromatography purification, the His-tags of recombinant proteins were cleaved, and the undigested proteins could be removed by an affinity chromatography column. The recombinant proteins were collected in the flow-through. As shown in Figure 4.5, the recombinant proteins without His-tag were a little smaller than the uncut ones (Figure 4.5 A and C). In a Western blot, such treated proteins were not recognized by the anti His-tag antibody, while the untreated ones showed the signals (Figure 4.5 B and D).

4.1.5 Enzyme assay

The enzyme activity of *Pf*AKLP1 was mainly determined by using the recombinant protein with a C-terminal His-tag. The specific activity of *Pf*AKLP1 was approximately 3 mU/mg with ATP and AMP as substrates. In order to study whether the His-tag affects the enzymatic activity of *Pf*AKLP1, the enzyme without His-tag was also tested in the enzyme assay. However, there was no difference in the specific activity of recombinant *Pf*AKLP1 with and without His-tag. We also tested different pH ranging from 6 to 9, but the activity was still low. Therefore, it was impossible to determine the K_m of the substrate in our assay. Different monophosphate nucleotides including AMP, CMP, UMP, IMP, and GMP were used as substrates while using ATP as the phosphate donor. Also the various triphosphate nucleotides such as ATP, GTP, ITP, and UTP were tested as phosphate donors with AMP. *Pf*AKLP1 showed the best enzyme activity with ATP and AMP as substrates.
Even though the different substrates were also employed to show substrate specificities, *Pf*AKLP2 was not found to be active in the enzymatic assay described above. After the cleavage of the His-tag by thrombin, there was still no detectable activity for *Pf*AKLP2 to demonstrate the His-tag effect. The low or absent enzyme activity for these two proteins is indicative that our purified proteins are not contaminated with *E. coli* AK.

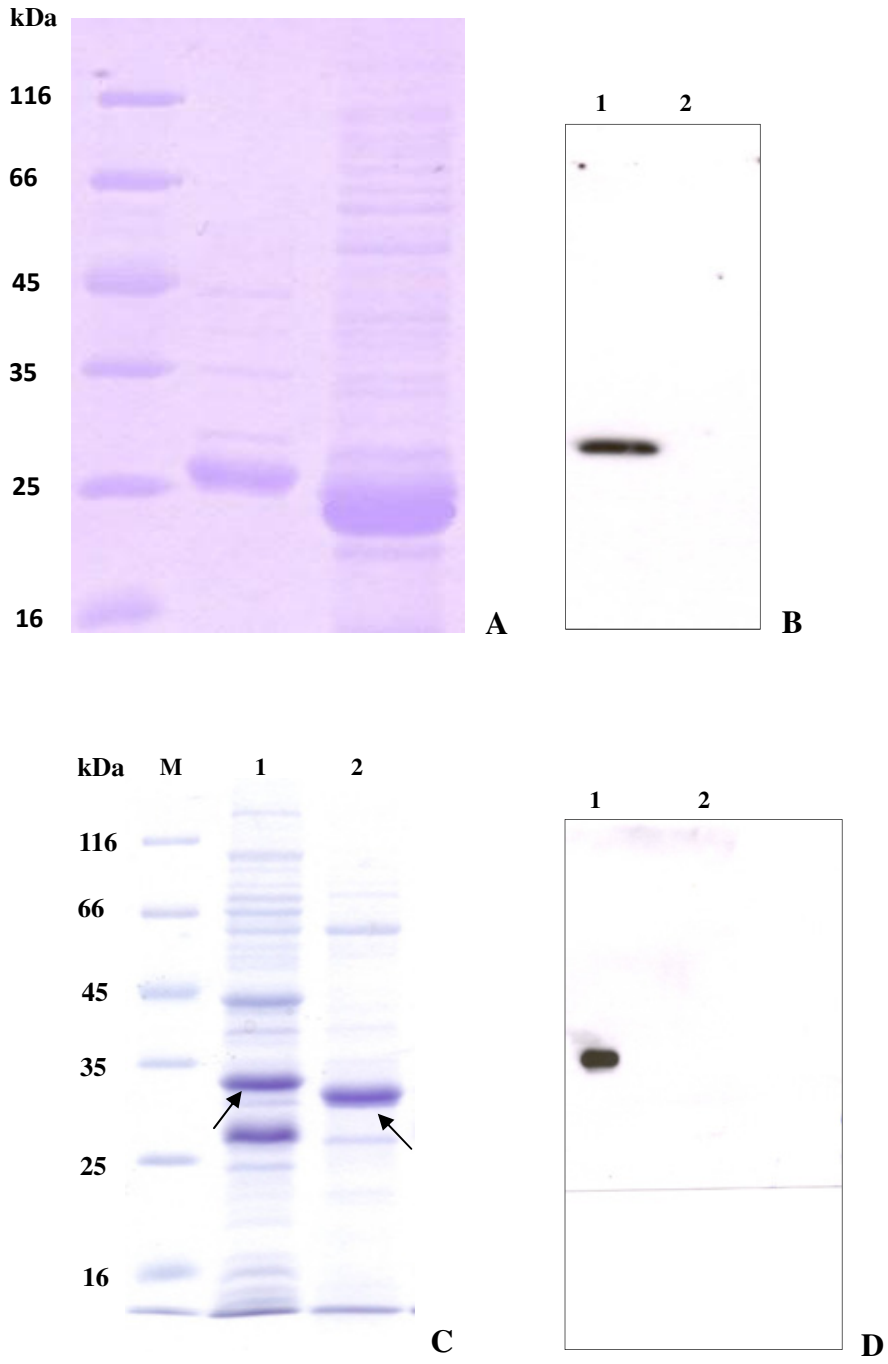

Figure 4.5 12% SDS-PAGE gel and Western blot after His-tag cleavage by thrombin. A) SDS-PAGE gel of recombinant *Pf*AKLP2. M, unstained molecular weight marker; 1, *Pf*AKLP1 with his-tag; 2, *Pf*AKLP1 without His-tag after thrombin treatment and Ni-NTA purification. **B)** Western blot of recombinant *Pf*AKLP1. 1, *Pf*AKLP1 with His-tag; 2, *Pf*AKLP1 without His-tag after thrombin treatment and Ni-NTA purification. **C)** SDS-PAGE gel of recombinant *Pf*AKLP2. M, unstained molecular weight marker; 1, *Pf*AKLP2 with His-tag; 2, *Pf*AKLP2 without His-tag after thrombin treatment and Ni-NTA purification. Black arrow, *Pf*AKLP2. **D)** Western blot of recombinant *Pf*AKLP2. 1, *Pf*AKLP2 with His-tag; 2, *Pf*AKLP2 without His-tag after thrombin treatment and Ni-NTA purification.

4.2 Localization of *Pf*AK1, *Pf*AK2, *Pf*GAK, *Pf*AKLP1, and *Pf*AKLP2

4.2.1 Localization of AKs and GAK in *Plasmodium*

The vector was constructed by adding a GFP gene downstream of full-length AK genes. Then different subcellular localizations of all *Plasmodium* AKs were demonstrated by examining transgenic parasites via immunofluorescence microscopy. It is clear that *Pf*AK1, *Pf*AKLP1, and *Pf*AKLP2 are located in the parasite cytosol (Figure 4.6 A-C). Immunofluorescence analyses suggest that *Pf*GAK is located in the mitochondrion, as seen by co-localization of the GFP and mitotracker signals (Figure 4.6 D).

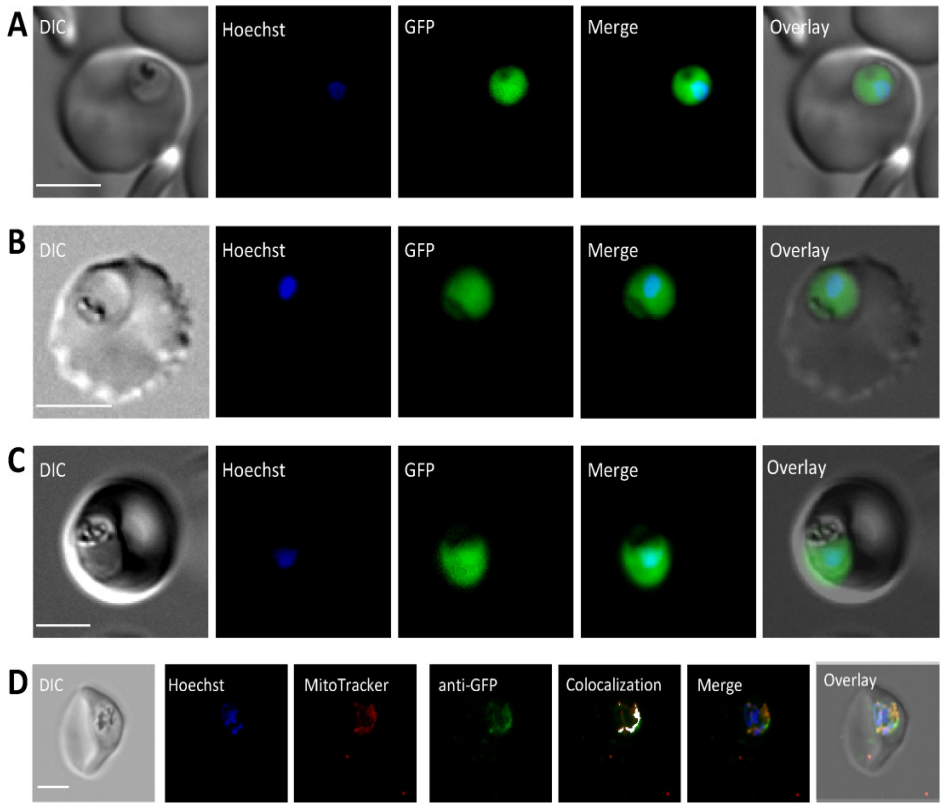

Figure 4.6 Localization of *P. falciparum* AKs fused to GFP (Ma *et al.*, 2012). Cytosolic targeting of *Pf*AK1 (**A**), *Pf*AKLP1 (**B**), and *Pf*AKLP2 (**C**). Line (**D**) illustrates mitochondrial targeting of *Pf*GAK as shown by co-localization with anti-GFP antibody and the mitochondrial dye MitoTrackerOrange. Hoechst, a nucleus dye. Scale bar, 3 µm.

4.2.2 Localization and N-myristoylation of *Pf*AK2

Interestingly, *Pf*AK2 localized to a ring-like structure around the parasite, and "loops" apparently connected to the PVM (Figure 4.7, Figure 4.8 A). This was highly indicative of localization to the PV. Indeed, co-localization analysis shows that *Pf*AK2-GFP co-localizes with the PV resident protein SERP (Figure 4.7 A). SERP seems to be excluded from the "loops," suggesting that *Pf*AK2-GFP in fact

actually associates with the membrane of the PV rather than being found in a soluble state in the PV lumen. Staining parasites with the membrane stain Bodipy-TR-ceramide indeed verified that the loops contain membranous material (Figure 4.7 B). Especially, the fluorescence images of *Pf*AK2-GFP can be merged well by using the anti-exp1 antibody (Figure 4.7 C). Taken together, these data suggest that *Pf*AK2 localizes to the PVM. Parasite proteins secreted beyond the boundary of the parasite's plasma membrane commonly contain an N-terminal secretory signal sequence. Since *Pf*AK2 lacked such a signal, we wished to study its mode of trafficking to the PVM. A mutant of *Pf*AK2 lacking the target site of N-myristoylation (*Pf*AK2^{G2A}) was constructed and transfected into *P. falciparum*. *Pf*AK2^{G2A} was clearly located in the cytosol (Figure 4.8 C), thus demonstrating that N-myristoylation of the protein is required in order to target *Pf*AK2 to the PVM. Western blots using an anti-GFP antibody confirmed that *Pf*AK2 is indeed associated with the membrane, while *Pf*AK2^{G2A} was found in the soluble fraction. To control the separation of membrane and cytosolic fractions of the parasite, antibodies reacting with the membrane protein Exp1 and the cytosolic protein Hsp70 were employed. As shown in Figure 4.8 B and D, both membrane and cytosolic fractions of transgenic parasites containing the AK2-GFP fusion protein can be separated, since only a little contamination by the two antibodies was observed. The majority of *Pf*AK2 was found in the parasite pellet, while most of *Pf*AK2^{G2A} could be detected in the cytosolic fraction of the parasitized erythrocytes by an anti-GFP antibody.

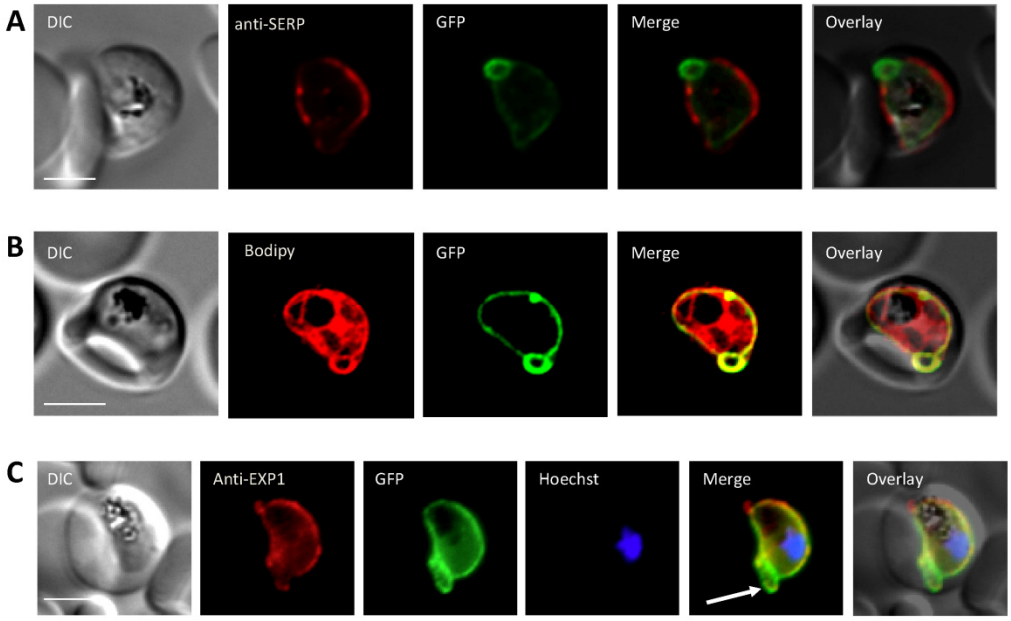

Figure 4.7 Localization of PfAK2 (Ma *et al.*, 2012). (**A**) Co-localization of *Pf*AK2-GFP with serine-rich protein (SERP). (**B**) A comparison of *Pf*AK2-GFP localization with Bodipy-TR-ceramide shows that the loops contain membranous material. (**C**) Co-localization of *Pf*AK2-GFP with *Plasmodium falciparum*-exported protein (EXP1). Bodipy, a lipid membrane dye; SERP, a protein localized in the parasitophorous vacuole; EXP1, a protein localized in the parasitophorous vacuole membrane. Scale bar, 3 µm.

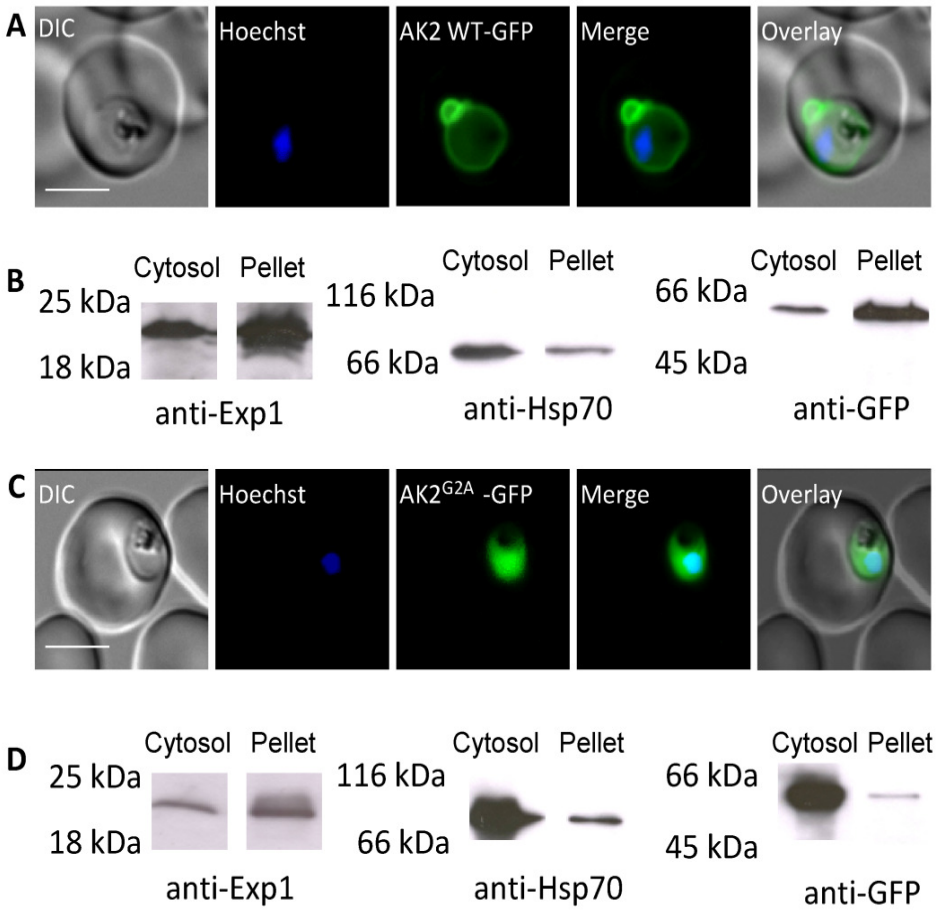

Figure 4.8 Subcellular localizations of *Pf*AK2 and *Pf*AK2G2A in *P. falciparum* (Ma *et al.*, 2012). (**A**) Localization of *Pf*AK2 in the parasitophorous vacuole membrane. (**B**) Western blot of parasites transfected with AK2-GFP constructs using anti-Exp1 as a marker for the membrane fraction, anti-Hsp70 as a marker for the cytosolic fraction, and anti-GFP antibodies. (**C**) Cytosolic localization of *Pf*AK2G2A. (**D**) Western blot of parasites transfected with the AK2G2A-GFP. Cytosol comprises erythrocyte cytosol and parasite cytosol; pellet includes the parasite membrane plus erythrocyte membrane plus parasitophorous vacuole membrane. Scale bar, 3 µm.

4.3 N-myristoyltransferase from *P. falciparum*

Pure *Pf*NMT was obtained by using the optimized expression and purification method described in this work with a 2-fold improvement in the amount compared to a previous study (Bowyer *et al.*, 2007). It was sufficient to be used for crystallization screenings.

4.3.1 Sequence alignment

Through multiple sequence alignment, NMT was shown to be highly conserved among different organisms.

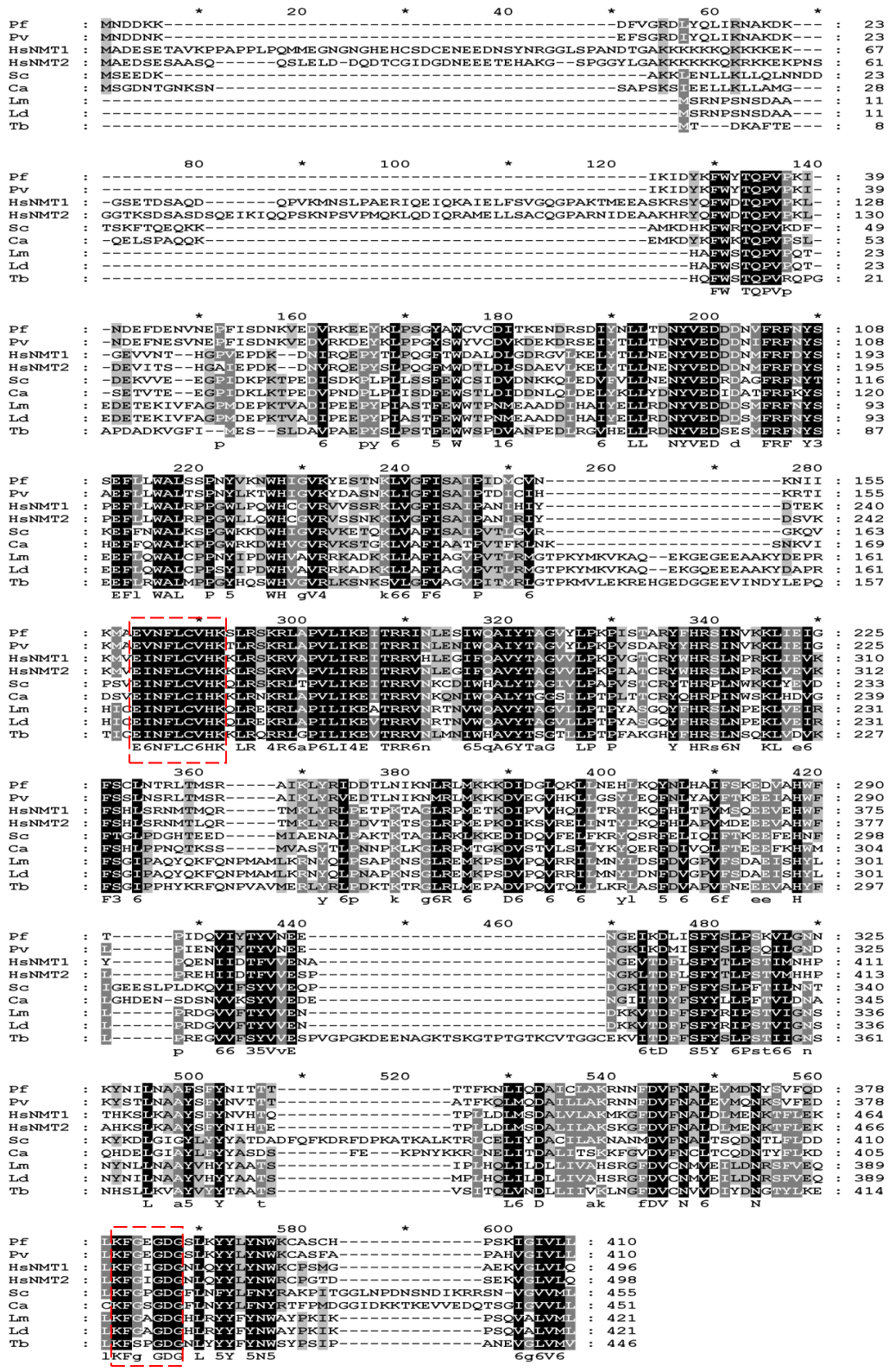

Figure 4.9 Multiple sequence alignment of NMT from various species. Pf, *Plasmodium falciparum*, XP_001348300; Pv, *Plasmodium vivax*, XP_001616826; Hs, *Homo sapiens*, NP_066565 (Type 1), NP_004799 (Type 2); Sc, *Saccharomyces cerevisiae*, NP_013296; Ca, *Candida albicans*, XP_722859; Lm, *Leishmania major*, XP_001685320; Ld, *Leishmania donovani*, XP_001467690; Tb, *Trypanosoma brucei*, CBH16561. Signature motifs of NMTs are labeled with red frames.

*Pf*NMT as well as others do not contain a long N-terminus, which exists in both types of human NMT and was shown to have a vital role in the subcellular localization of NMT in mammalian cells (Glover *et al.*, 1997). Also two signature motifs including [DEK]-[IV]-N-[FS]-L-C-x-H-K and K-F-G-x-G-D-G are found in all NMTs. The amino acid residues involved in the myristoyl-CoA binding are F40, W41, Y103, E105, N169, F170, L171, V173, R178, K180, R181, I187, T191, A202, Y204, and L210 in *S. cerevisiae* NMT (Farazi *et al.*, 2001). These residues are conserved in all NMTs including *Pf*NMT, showing that binding myristoyl-CoA is very strict. Y103, F111, F113, N169, T205, Y219, H221, F234, Y330, G416, D417, G418, and L455 residues in the peptide binding pocket of *S. cerevisiae* NMT are conserved in *Pf*NMT. However, the residues of R107, F334, I347, Y349, and M454 are not the same between *Pf*NMT and *S. cerevisiae* NMT.

4.3.2 Overexpression and purification of recombinant *Pf*NMT

The recombinant *Pf*NMT was initially overexpressed in KRX cells using LB medium at 37 °C for 4 hours. Then the 4 different media and three strains of *E. coli* were employed as the first optimization step for improving overexpression as shown in Table 4.1. The results showed that C41 combined with TB medium and overnight expression was the best condition for producing the recombinant *Pf*NMT. However, a Western blot demonstrated that small parts of the *Pf*NMT existed as an insoluble form in the cell debris, although the majority of recombinant protein was in the supernatant after cell lysis. Considering another study (Bowyer *et al.*, 2007), codon optimization may also enhance overexpression. Therefore, two plasmids were used for the next optimization step as shown in Table 4.1. Plasmid pGro7 contains several chaperones to help proteins properly fold so as to increase solubility, while the pRARE II plasmid was constructed to provide around ten tRNA genes that are rare in the expression systems of *E. coli* cells. This further step was conducted as shown in Table 4.1. The best yield could be obtained by using the pGro7 plasmid to co-express *Pf*NMT in the C41 cells at RT overnight. Meanwhile, two affinity chromatography columns were used to purify the protein. Impurity was significantly improved by using the Protino Ni-TED resin rather than Ni-NTA resin.

As shown in Figure 4.10, there were always three obvious protein-bands after the Protino Ni-TED column. However, these three proteins can hardly be eluted at different concentrations of imidazole. The purity of *Pf*NMT after this step was not satisfactory for further crystallization screening. Thus an additional purification step was applied by using a native gel filtration chromatography. Eventually, very pure *Pf*NMT as shown in Figure 4.11 could be obtained with a yield of 1 mg/ liter culture, which can be used in crystallization trials.

Optimization step	*E. coli* strain	Medium	Tempature/time	Results
Step 1	KRX	LB; 2xYT;	RT / overnight;	TB medium and overnight expression could slightly improve the final yield.
		TB; MLB	37 °C / 4 h	
	BL21	LB; 2xYT;	RT / overnight;	BL21 cell could enhance the overexpression combined with TB medium and overnight induction.
		TB; MLB	37 °C / 4 h	
	C41	LB; 2xYT;	RT / overnight;	C41 gave the best *Pf*NMT yield if *Pf*NMT was overexpressed in TB medium at RT overnight.
		TB; MLB	37 °C / 4 h	
Step 2	C41;	TB	RT / overnight	The solubility of recombinant *Pf*NMT could be increased, and there was no recombinant protein in the cell debris if the C41/pGro7 cell was used as shown by anti-His tag western.
	C41/pGro7; C41/pRAREII			

Table 4.1 Optimization of the heterologous overexpression of *Pf*NMT.

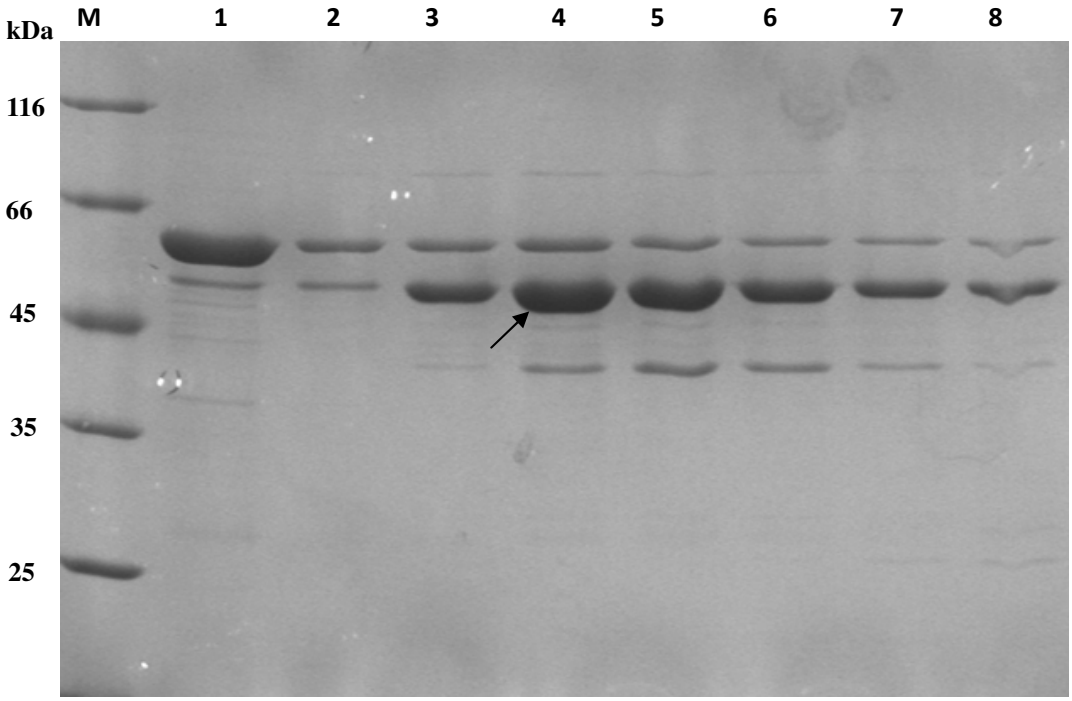

Figure 4.10 10% SDS-PAGE gel of *Pf*NMT after Protino Ni-TED purification. M, unstained molecular weight marker; 1-8: elution fraction with 10 mM, 30 mM, 50 mM, 75 mM, 100 mM, 150 mM, 200 mM, and 500 mM imidazole, respectively. Black arrow, *Pf*NMT.

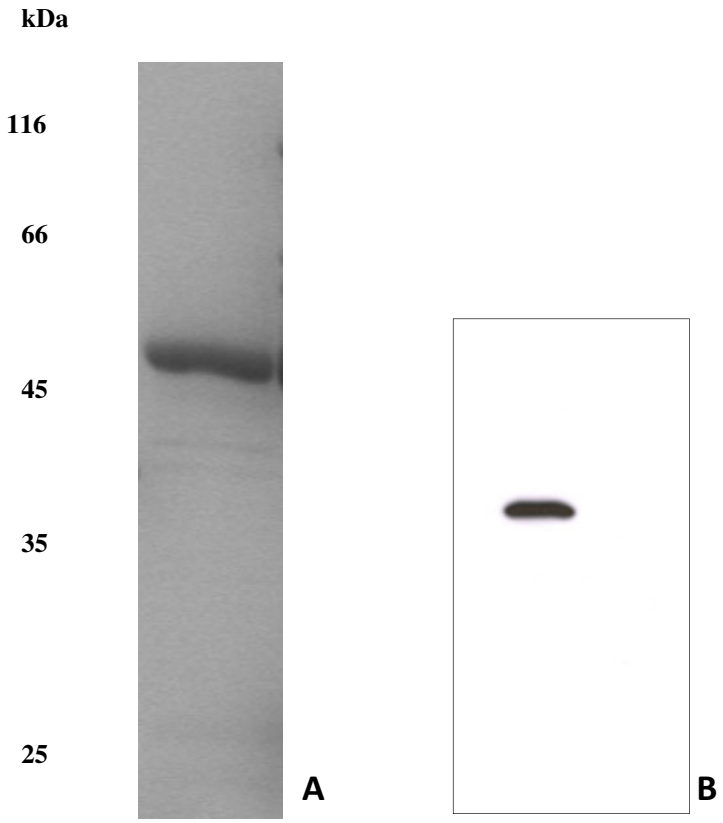

Figure 4.11 10% SDS-PAGE gel of *Pf*NMT after gel filtration purification. A) 7.5 µg of recombinant *Pf*NMT; **B)** Western blot of *Pf*NMT using the anti-His tag antibody.

4.3.3 Complex of *Pf*NMT/AK2

The complex of *Pf*NMT/AK2 can be obtained through a coexpression method described in the method part (Rahlfs *et al.*, 2009). The complex can be seen in the gel filtration analysis in Figure 4.12. P1 peak with retention time at 79.4 min represented the heterodimer of *Pf*NMT/AK2 which is shown in Figure 4.12B.

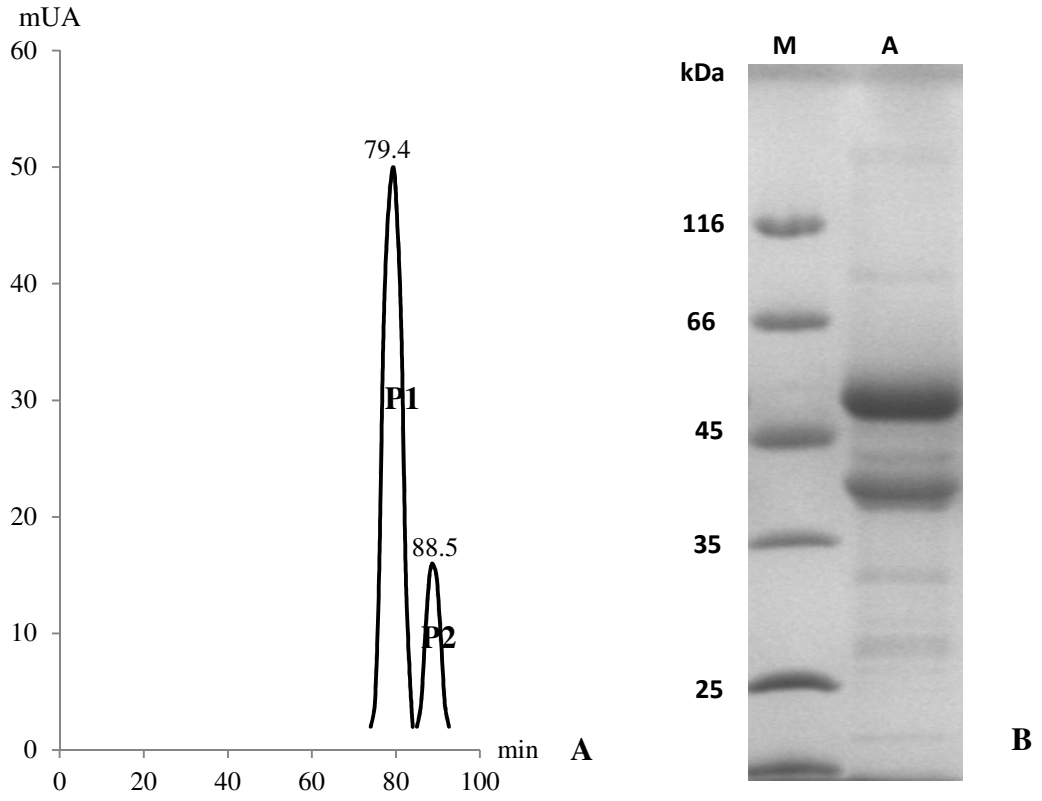

Figure 4.12 Gel filtration and SDS-PAGE gel analysis. A) Schematic diagram of gel filtration of the *Pf*NMT/AK2 complex after affinity chromatography purification. P1, peak of *Pf*NMT/AK2 heterodimer; P2, peak of *Pf*AK2 alone. **B)** 12% SDS-PAGE gel analysis. M, unstained molecular weight marker; A, *Pf*NMT/AK2 complex.

4.3.4 Crystallization of *Pf*NMT

4.3.4.1 Crystallization screening of *Pf*NMT in complex with myristoyl-CoA

The crystallization screening trials of *Pf*NMT were initiated with a JCSG Core Suite kit using a screening robot. Moreover different types and concentrations of PEG as well as various buffers with different pH were tested as a start point. Two concentrations of 9 mg/ml and 17 mg/ml were used for screening. *Pf*NMT was stored in the buffer containing 50 mM Tris, 300 mM NaCl, 2 mM DTT with pH 7.6. There was no significant impact with these concentrations. The complex of *Pf*NMT with myristoyl-CoA was also used for the crystallization test.

After the preliminary test, the complex and *Pf*NMT showed similar results. Four conditions seemed promising for further optimization listed in Table 4.2. By slightly varying the concentrations of components in these conditions, further screening could be tested manually. Even though there were some signs of crystals forming, no high quality crystal was obtained from these trials.

Drop 1	Drop 2	Drop 3	Drop 4
21% PEG 3350, 0.1 M Bis-Tris, pH 5.3	0.2 M ammonium acetate, 20% PEG 6000, 0.1 M HEPES, pH 7.5	20% PEG 3350, 0.1 M LiCl, 0.1 M HEPES, pH 7.5	20% PEG 6000, 0.1 M Tris, pH 8.5

Table 4.2 Promising conditions for crystallization screening.

Furthermore, we also tested buffer conditions used for the crystallization of NMT in other species. The conditions were listed in Table 4.3. Precipitation was observed in most drops after 5 days. No crystal was observed.

Condition 1	Condition 2	Condition 3	Condition 4	Condition 5
19% PEG 3350, 0.2 M ammonium citrate, tribasic anhydrous, pH 5.7	2.4 M ammonium sulfate, 20 mM HEPES, pH 7.5	10% PEG 4000, 50 mM zinc acetate, 0.1 M sodium cacodylate, 21% glycerol	18% PEG 3350, 0.2 M lithium sulfate, 50 mM HEPES, pH7.5	10% PEG 4000, 15% glycerol, 0.1 M Tris-HCl, pH7
Condition 6	**Condition 7**	**Condition 8**	**Condition 9**	
20% PEG 4000, 0.1 M ammonium acetate, 0.1 M sodium cacodylate	18% MME, 10 mM nickel chloride, 0.1 M sodium cacodylate	10% PEG 3350, 0.2 M ammonium acetate, 50 mM HEPES, pH7.5	26% PEG 1500, 0.2 M sodium chloride, 0.1 M sodium cacodylate	

Table 4.3 Crystallization conditions for NMT from other organisms.

4.3.4.2 Crystallization screening of the complex comprising *Pf*NMT with its natural substrate *Pf*AK2

The complex purified by gel filtration was used directly for crystallization screening. As with *Pf*NMT, the trial of *Pf*NMT started with the JCSG Core Suite kit using the screening robot. Different types and concentrations of PEG as well as various buffers with different pH were also screened. The protein concentration was 6 mg/ml. The proteins seemed to precipitate quickly, and no promising conditions could be further investigated.

4.3.5 Homology modeling of *Pf*NMT

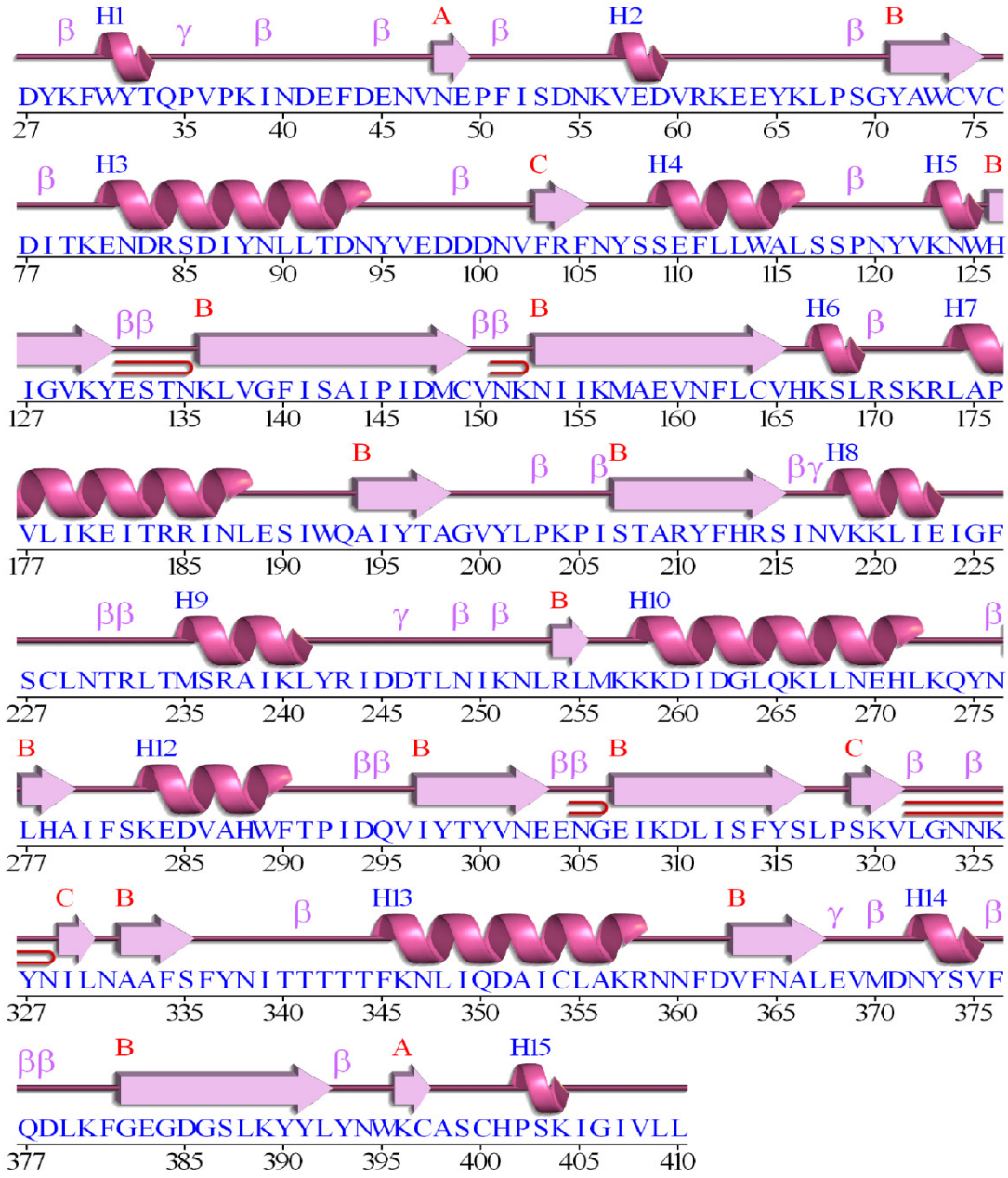

Figure 4.13 Secondary structure prediction of *Pf*NMT. helix, strand. β, beta turn; γ, gamma turn; , beta hairpin. The image was created by the PDBsum online server**.**

A model of *Pf*NMT was generated on the basis of the crystal structure of *P. vivax* NMT. Since the amino acid sequence of NMT between *P. falciaprum* and *P. vivax* shares 80% identity, the amino acid sequence was submitted to the Swiss-Model Server in automated mode in order to generate the *Pf*NMT model. Then the model was completed and provided as a PDB file. As shown in Figure 4.14, the predicted structure of *Pf*NMT was very similar to the known structure of NMT. Its core is composed of several compact stranded β-sheets surrounde features ranging from amino acid 325 to 340 were observed in this secondary structure profiles d by some α-helices (Figure 4.14). The tiny differen

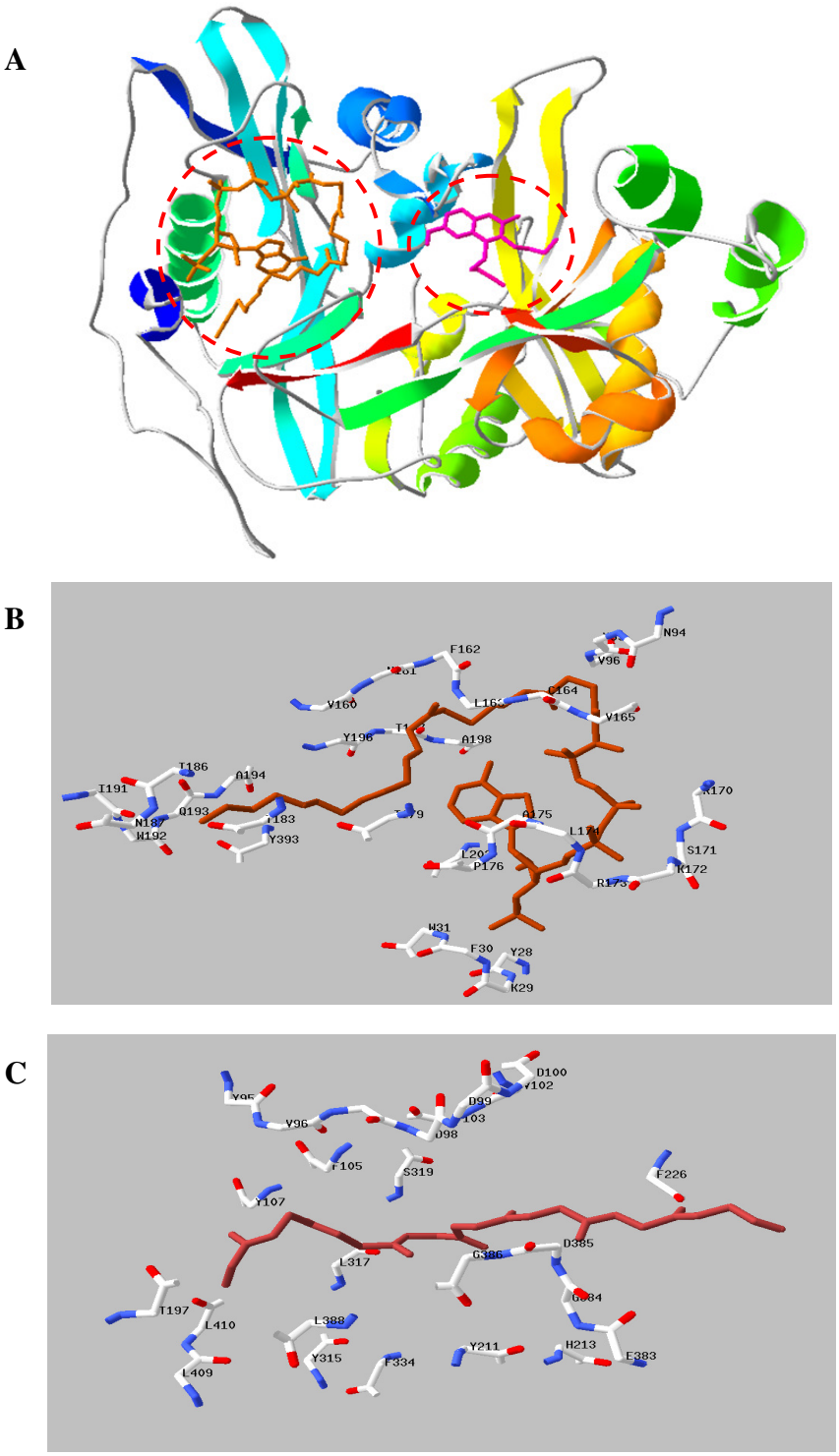

Figure 4.14 The *Pf*NMT model and details of substrate binding sites. A) The overall model of *Pf*NMT generated by the Swiss-Model Server. The brown molecule in the left red circle is the NHM, a myristoyl-CoA analog showing the myristoyl-CoA binding site. The purple molecule in the right red circle is an inhibitor known to bind to the peptide substrate pocket, indicating the peptide substrate binding site. **B)** Amino acids in the myristoyl-CoA binding pocket in comparison to the model of *Pf*NMT on the ternary complex of *Sc*NMT with NHM and the octapeptide GLYASKLA. **C)** Amino acids in the peptide binding pocket in comparison to the model of *Pf*NMT on the ternary complex of *Sc*NMT with NHM and the octapeptide GLYASKLA. All shown amino acids are within 4 Å of substrates.

compared to the well-defined NMT structure of NMT from *S. cerevisiae* (Wu *et al.*, 2007). The substrate binding site can be shown by superposing the model of *Pf*NMT onto the ternary complex of *Sc*NMT with NHM and the octapeptide GLYASKLA. The details of both substrate binding sites in the *Pf*NMT model are illustrated in Figure 4.14 B and C.

4.4 Myristoylation in *P. falciparum*

4.4.1 Metabolic labeling of myristoylated proteins in *P. falciparum*

The metabolic labeling method was demonstrated to study myristoylation in *P. falciparum*. As shown in Figure 4.15, the myristoylated proteins can be detected by a streptavidin-HRP blot. Three different concentrations including 25 µM, 50 µM, and 100 µM were tested to demonstrate dose-dependent effect and labeling optimization. The latter dose-dependent experiment showed that 50 µM was the best concentration for the labeling step (Figure 4.15).

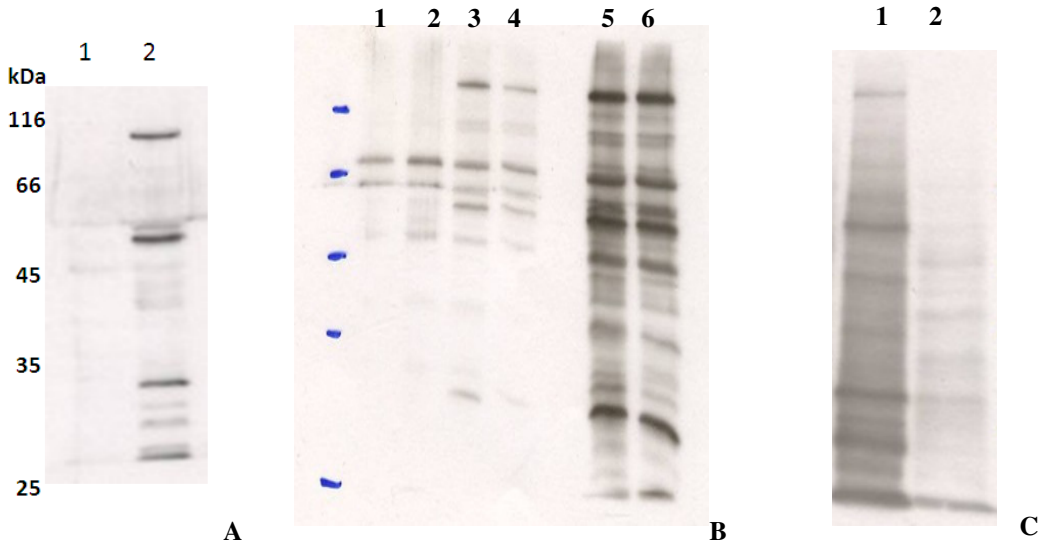

Figure 4.15 Streptavidin-HRP blot of myristoylated proteins in *P. falciparum* by metabolic labeling. A) Preliminary test with azido-myristic acid at the concentration of 25 µM. 1, DMSO negative control; 2, azido-myristic acid labeling. 5 µg of total lysate input for each sample. **B)** Dose dependent effect of azido-myristic aicd. 1, 2, 3, and 4 represented the treatment of DMSO control, 25 µM, 50 µM, and 100 µM azido-myristic acid and 3 µg was loaded for each sample. 5 and 6 represented the 50 µM, and 100 µM azido-myristic acid treatment samples with 15 µg input for each. **C)** 50 µM treatment with 10 µg input for each sample. 1, azido-myristic aicd treatment; 2, DMSO treatment as negative control.

4.4.2 Pull-down assay

The biotinylated proteins were incubated with soft-link avidin beads for enrichment. Although the biotinylated proteins should be eluted from the beads by 5 mM biotin according to the manufacture's instruction, it was not possible to elute the proteins under such conditions. From the Western blot result in Figure 4.16, it is obvious that the biotinylated proteins could be eluted with sample buffer at 95 °C for 5 minutes. However, the gel of the elution sample demonstrated that this elution condition cannot selectively elute the proteins. Thus, it is not possible to send these samples for mass spectrometry

identification. Even though different elution conditions including the acid elution, long-time elution, and alternative avidin beads have been employed, there is no significant improvement of the pull-down assay to achieve. So further optimization steps are required to elute the biotinylated proteins selectively, which then hopefully leads to the final identification of the myristoylated proteome in *P. falciparum*.

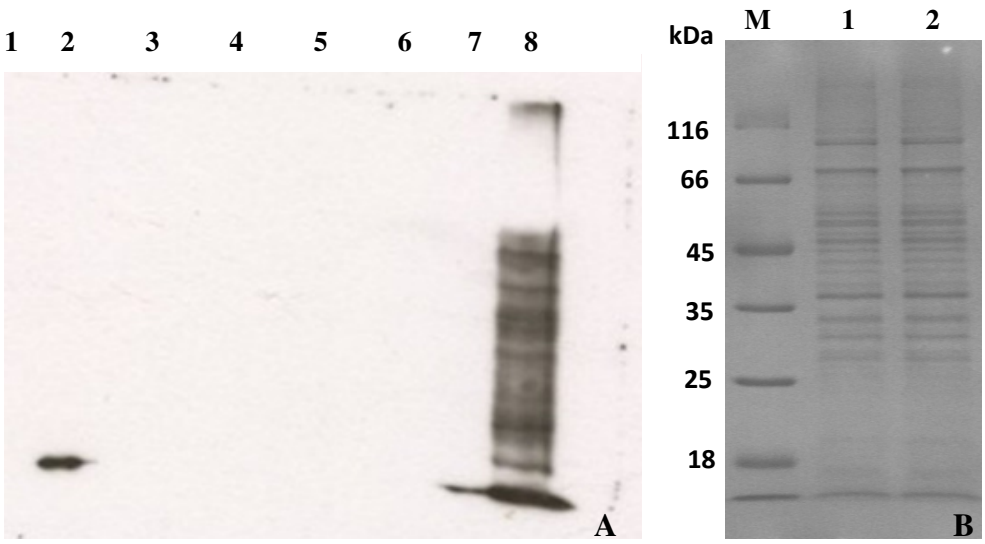

Figure 4.16 Pull-down assay of myristoylated proteins from *P. falciparum*. A) Streptavidin blot of a pull-down assay with soft-link avidin beads. 1, 5 mM biotin elution of DMSO negative control; 2, 5 mM biotin elution of azido-myristic acid treatment; 3, flow-through of DMSO negative control; 4, flow through of azido-myristic acid treatment; 5, wash fraction of DMSO negative control; 6, wash fraction of azido-myristic acid treatment; 7, boiling fraction with sample buffer of DMSO negative control; 8, boiling fraction with sample buffer of azido-myristic aicd treatment. **B)** SDS-PAGE gel of boiling sample. 1, boiling sample of DMSO negative control (Sample 7 in figure 4.16A); 2, boiling sample of azido-myristic acid treatment (Sample 8 in figure 4.16A); M, unstained molecular weight marker.

4.4.3 Prediction of myristoylated proteins in *P. falciparum*

The whole proteome of *P. falciparum* could be obtained from PlasmoDB. The MYR Predictor (Maurer-Stroh *et al.*, 2004) allows the submission of whole proteome sequences at once and claims to be capable of predicting the N-terminal and internal myristoylation site. The total number of proteins predicted by MYR Predictor is 42, while no internal myristoylation site is found. The percentage of myristoylation in the proteome is 0.76%. Among them, there are four targets that cannot be recognized by another tool – Myristoylator. The Myristoylator predicts (Bologna *et al.*, 2004) 65 myristoylated proteins in the *P. falciparum* proteome with a percentage of 1.1%. The protein information is summarized in Tables 4.4 and 4.5. It is shown that at least nine members in the *Pf*EMP1 family can be myristoylated. And another big group is the conserved proteins with unknown function, implying more efforts are required to reveal the multiple functions and pathways that myristoylation is involved in. Since only one sequence is permitted to be submitted to the server each time and no internal myristoylation can be predicted by the Myristoylator, we tested all the sequences which have glycine at their position 2 from *P. falciparum* proteome. Also the new ones in the Myristoylator table that the MYR Predictor cannot predict mostly have medium or low confidence. It seems that the results from

the MYR Predictor prediction are more reliable. However, two proteins (PF08_0062 and PF10_0203) that have been demonstrated to be myristoylated (Leber *et al.*, 2009; Rahlfs *et al.*, 2009) in the experiment cannot be reliably discovered with high confidence by the MYR Predictor, implying that much stricter laws for prediction by MYR Predictor may ignore the potential targets. Therefore, it is still worthwhile to experimentally explore myristoylation in *P. falciparum*, not only for the improvement of prediction tools, but also for the biological study and proof of NMT as a drug target against malaria.

Protein Name	Accession number (PlasmoDB)	Protein length (Amino acid)	Recognition motif	Tested by Myristoylator	Remarks
Rab GTPase 5b	PF3D7_1310600	207	GCSSSTERLTSTKNINI	Verified	
Protein phosphatase 2C	PF3D7_1138500	924	GAYLSSPKTNKESLDGG	Verified	
Serine/threonine protein kinase	PF3D7_1450000	376	GSTISKRKNNTDKNVKD	Verified	
Erythrocyte membrane protein 1 (PfEMP1)-like protein	PF3D7_0600400	1325	GSDYSSPGGNKSVNITE	Verified	False positive prediction: 2.39e-02
Erythrocyte membrane protein 1	PF3D7_1255200	2268	GGSNGGGGSSQEQDESV	Failed	False positive prediction: 2.07e-02
Protein phosphatase	PF3D7_0810300	550	GTCISFLKKNSVKEKKN	Verified	False positive prediction: 5.67e-03
Conserved *Plasmodium* membrane protein	PFL1825w	210	GCTVSNLKCVTNVAGLA	Verified	
Erythrocyte membrane protein 1	PFD1235w	3553	GNASSSEGEAKTPSLTE	Verified	
Golgi reassembly stacking protein 1	PF3D7_1017300.1	573	GAGQTKEIMGGYRILRI	Failed	Experimental proof (Struck *et al.*, 2005)
Conserved *Plasmodium* membrane protein	PFI1500w	4553	GNCKSYSSHFSVNKNNT	Failed	
Calcium-dependent protein kinase 2	PFF0520w	509	GNHLSVNKLKRKKKKKS	Verified	

Protein Name	Accession number (PlasmoDB)	Protein length (Amino acid)	Recognition motif	Tested by Myristoylator	Remarks
Calcium-dependent protein kinase 1	PFB0815w	524	GCSQSSNVKDFKTRRSK	Verified	Experimental proof (Moskes *et al.*, 2004)
Calcium-dependent protein kinase 4	PF07_0072	528	GQEVSSVNNTKNEHHKT	Verified	
Protein phosphatase 2c-like protein	PF3D7_1309200	827	GNCASVINHSKFKIKKK	Verified	
Conserved protein	PF10_0107	144	GNIVSCCSLDENKKYLN	Verified	
Erythrocyte membrane protein 1	PF11_0008	2994	GSQTSKFSKTVVGNETH	Verified	
Erythrocyte membrane protein 1	PF08_0141	2858	GSQGSKPVDTSDVKNES	Verified	
Erythrocyte membrane protein 1	PFE1640w	3164	GNEQSSSSSEGAKNPSI	Verified	
Erythrocyte membrane protein 1	PF13_0003	3346	GNTQSSEEEEAKSPSLT	Verified	
TPR-like domain containing protein	PFF0080c	285	GAFGSKNLEYYNYASMK	Verified	False positive prediction: 1.20e-02
Erythrocyte membrane protein 1	PFF0005c	259	GSQSSKSLEPIVDTNES	Verified	
Glideosome-associated protein 45	PFL1090w	204	GNKCSRSKVKEPKRKDI	Verified	Experimental proof (Rees-Channer *et al.*, 2006)
Erythrocyte membrane protein 1	PFD0020c	3467	GTGSSTPSVPKDVKNES	Verified	
Calpain	PF3D7_1362400	2048	GCINSKVKEKRKIKKRK	Verified	Experimental proof (Russo *et al.*, 2009)
Developmental protein	PFI0300w	195	GNKISTEDHIFRLKLKT	Verified	

Protein Name	Accession number (PlasmoDB)	Protein length (Amino acid)	Recognition motif	Tested by Myristoylator	Remarks
ADP-ribosylation factor-like protein	PF10_0337	178	GLIFSSIFSRLFSNKEV	Verified	False positive prediction: 1.57e-02
Conserved *Plasmodium* protein	PFI1430w	341	GNAMGFKDKNKNKENIS	Verified	False positive prediction: 1.20e-02
Conserved *Plasmodium* protein	PFI1455c	272	GQISSKEDEIEKQNIYA	Verified	
Conserved protein	PFL0095c	207	GSSSSSSDMFILKNHED	Verified	
Cleft lip and palate-associated transmembrane related protein	PF11_0384	689	GLSLSSPQLPANAGSNI	Verified	
Mitochondrial import receptor subunit	PFE1230c	105	GTALSKIITINEENRLV	Verified	False positive prediction: 1.57e-02
ABC transporter (MDR family)	PF13_0218	925	GNSLSLCLLRETSKDVF	Verified	False positive prediction: 7.44e-03
Conserved ARM repeats protein	PFD0720w	275	GNNCCAGRDLLYKNKLQ	Verified	
CAMP-dependent protein kinase regulatory subunit	PFL1110c	441	GNVCTWRQGKEKAGDDN	Verified	
Protein phosphatase 2b regulatory subunit	PF14_0492	177	GNTQAILSEKDQKDLLQ	Verified	
Conserved *Plasmodium* protein	PF3D7_0728700	720	GNTLSNSTLFRPTEPSY	Verified	

Protein Name	Accession number (PlasmoDB)	Protein length (Amino acid)	Recognition motif	Tested by Myristoylator	Remarks
Conserved *Plasmodium* protein	PF14_0578	148	GNLCCSNND IKNSKSNI	Failed	
Conserved *Plasmodium* protein	PFI0675w	86	GCRLSKAND PKEQKHTE	Verified	
Vacuolar protein-sorting protein	PF08_0064	209	GTYFSKDLQECLREEKR	Verified	
Adenylate kinase	PF08_0062	275	GSCYSRKNKVSTISLDE	Verified	False positive prediction: 1.57e-02; experimental proof (Rahlfs *et al.*, 2009)
Conserved *Plasmodium* protein	PF11_0100	155	GNTFSSYDEKERRGLIL	Verified	
ADP-ribosylation factor-like protein	PFI1005w	191	GNTVTTFFRDCCNRLFN	Verified	

Table 4.4 Myristoylated protein prediction of the whole proteome of *P. falciparum* via the MYR Predictor tool. Remarks, prediction with low reliability or the experimental evidence are labeled here. Recognition motif is given by the MYR Predictor tool.

Protein name	Accession number (PlasmoDB)	Protein length (Amino acid)	Recognition motif	Remarks
Erythrocyte membrane protein 1	PF11_0521	3119	MGNAIPATPDPIFINESY	
*Pf*MNL-2 CISD1-like iron-sulfur protein	PFD0807c	89	MGNNMLKAKSRNVFRKKG	
40S ribosomal protein S29	PF3D7_0705700	54	MGCILNVHPKKYGQGSRQ	Medium confidence
40S ribosomal protein S17	PFL2055w	137	MGRVRTKTIKRAARQIVE	Medium confidence
Alpha/beta hydrolase	PF3D7_0805000	245	MGNVLNRIIFNGPTEGYY	
Conserved *Plasmodium* protein	PF14_0149	590	MGNAMYAKSVYSSEGSEI	Medium confidence
Serine/threonine protein kinase	PF14_0227	284	MGNALNKLLKHYRNVEKK	
Conserved *Plasmodium* protein	PFF0960c	633	MGNTISERKQRQFVLYKD	
Conserved *Plasmodium* protein	PF14_0390	227	MGSKKNSNTVDSSENVEE	Medium confidence
Conserved *Plasmodium* protein	PF3D7_1317500	89	MGFFYSGFHKPNKKNMND	
Krox-like protein	PF3D7_1344100	805	MGEGYSKSTINHGNLSEE	
Pantothenate kinase	PF14_0354	766	MGNTLGIECSFNYVHVTT	Medium confidence
Cytochrome c oxidase copper chaperone	PF10_0252	67	MGMSLNKPINNTNEANKG	
Small ubiquitin related modifier	PFE0285c	100	MGDDDSAVNNNGSSPVNN	Low confidence
ADP ribosylation factor 1	PF10_0203	181	MGLYVSRLFNRLFQKKDV	Experimental proof (Leber *et al.*, 2009)
Conserved *Plasmodium* protein	PF14_0684	574	MGVYFSEAKVYIYDDIKG	Medium confidence

Protein name	Accession number (PlasmoDB)	Protein length (Amino acid)	Recognition motif	Remarks
Conserved *Plasmodium* protein	PFB0870w	2380	MGNTNRKDISHKEYDKSF	Low confidence
Protein kinase	PF3D7_0823000	1332	MGNTLYSNIGHSTTELDD	Medium confidence
BSD domain	PFD1095w	136	MGNKHNKKKYELCEIQYE	
Phosphotyrosyl phosphatase activator	PF14_0280	319	MGDVNSLSYKIINDESII	Low confidence
Conserved *Plasmodium* protein	PFC0690c	365	MGTFINNTGNFRNKTLNS	Low confidence
Protein kinase	PF11_0079	1501	MGNTLDSNKPKNFVTYAD	
Phosphatidylinositol-4-phosphate 5-kinase	PF11_0307	1338	MGNKLTCGEIRNDGVRGL	Medium confidence
Conserved *Plasmodium* protein	PFD0185c	734	MGNALNQLIFRPHPPSYS	
Conserved *Plasmodium* membrane protein	PF14_0312	1123	MGNGNSKVVKIFLLIQNE	
Conserved *Plasmodium* protein	PF14_0333	359	MGNITSEQKKKPLMLHEL	

Table 4.5 Myristoylated protein prediction of the whole proteome of *P. falciparum* by the Myristoylator tool. The medium or low confidence provided by the tool is reported in the remarks line. The experimental proof is mentioned in this line as well.

5 Discussion

5.1 AK networks and energy metabolism

In this thesis, the two new putative adenylate kinase isoforms from *P. falciparum* have been investigated through biochemical characterization of their recombinant proteins. *Pf*AKLP1 displays an especially close relation to human AK6, which is a distant member of the AK family (Ren *et al.*, 2005) and an atypical AK with an unusually broad substrate specificities, nuclear localization, and structural features of ATPase/GTPase proteins (Drakou *et al.*, 2011). Using the heterologous expression and purification methods described previously, pure recombinant protein was obtained. However, PfAKLP1 only showed 3 mU/mg activity, which is rather low compared to other AK isoforms in *P. falciparum* (Rahlfs *et al.*, 2009). This is similar to its homolog human AK6, which has less than 1% activity (0.95 U/mg) compared to human AK1 (Ren *et al.*, 2005). Although we tested various NTP and NMP combinations and assay buffers with different pH (from 6 - 9) and even removed the His-tag, the *in vitro* activity of *Pf*AKLP1 remained low. This indicates that *Pf*AKLP1 might exert functions other than AK activity or needs additional cellular factors for full activity. However, except for similarity to the AK superfamily, extensive sequence alignments only showed similarities to hypothetical proteins with yet unknown functions.

Under the conditions tested in this study, an *in vitro* AK activity was not detectable for *Pf*AKLP2, thus suggesting that it might not belong to the AK superfamily. As shown in Figure 4.1, many amino acids involved in substrate binding such as K70 that are essential for activity in other AKs are not conserved in *Pf*AKLP2; this is consistent with the missing AK activity. Besides that, the residues generally required for catalytic activity (Figure 4.1) are missing. Apart from K70, no residue of the P-loop is present. For *Pf*AKLP2, the highest sequence similarity was found with hypothetical proteins from *P. knowlesi* and *P. yoelii* and a putative AK from *P. vivax*. Moreover, *Pf*AKLP2 is partially homologous – from residue 20 to 173 with 50% similarity – to the AK isoform B of *T. brucei* (Figure 4.1) (Reinstein *et al.*, 1990). In fact, Noma also reported there was no AK activity for human AK4 *in vitro* (Noma *et al.*, 2001).

There are two new AK isoforms, AK7 and AK8, which have been characterized from humans recently. Both of them showed AK activity and cytosolic localization (Panayiotou *et al.*, 2011). Notably, human AK7 is larger, containing 723 amino acid residues, and reveals a NAD binding site at its N-terminus plus an AK-active motif, indicating multiple functions of this enzyme in addition to AK activity alone. Following this discovery, we found a hit in the *Plasmodium falciparum* database when using human AK7 as a blast sequence on NCBI. The hit protein (PFC0260w) has 1114 amino acids and shows ATP and AMP binding sites. This may expand AK members in *P. faciparum* and demonstrate the existence of a larger AK group compared to other isoforms. When employing human AK8 for searching, no homologous protein was found in *P. falciparum*.

Analyzing the subcellular distribution of AK isoenzymes in *Plasmodium* indicates that they are located in different compartments, which allows for an efficient network of energy supply and consumption. In humans, eight AKs with different tissue specificities and kinetic properties have been allocated to specific subcellular compartments (Dzeja *et al.*, 2009; Panayiotou *et al.*, 2011). Human AK6 in the nucleus negatively regulates the number of Cajal bodies, which are nuclear organelles

involved in the maturation of small nuclear ribonucleoproteins, showing that isoforms of AK exert very different functions (Santama *et al.*, 2005). In *P. falciparum*, two adenylate kinases and one GTP:AMP phosphotransferase had been characterized so far (Ulschmid *et al.*, 2004; Rahlfs *et al.*, 2009). Also two more AK-like proteins have been now investigated in our study. *Pf*AK1 was predicted to be targeted to the mitochondria because of its amphipathic helix, while *Pf*GAK was predicted to be localized in the apicoplast due to its N-terminal targeting sequence (Ulschmid *et al.*, 2004). By using AK fused with GFP, we could show three localizations of AK isoforms in *P. falciparum* (Figure 5.1). *Pf*AK1 and *Pf*AKLP2 are localized in the cytosol of *Plasmodium*, while *Pf*GAK and *Pf*AK2 are targeted to the mitochondria and parasitophorous vacuole membrane respectively. *Pf*AKLP1, unlike its homologous human AK6 in the nucleus, is localized in the cytosol of *Plasmodium* as well, implying that a similar function of the proteins is unlikely. These results show that *in silico* predictions of localizations still need to be improved.

Considering its high energy demands and rapid multiplication, *Plasmodium* requires an efficient interconversion system of adenine nucleotides. *Pf*AK1 and *Pf*AKLP1 are located in the cytosol, where most of the energy is consumed. The mitochondrial localization of *Pf*GAK, which transfers the high-energy phosphate from GTP to AMP, is consistent with the fact that GTP is produced in the citric acid cycle in the mitochondrion (Tomasselli *et al.*, 1979).

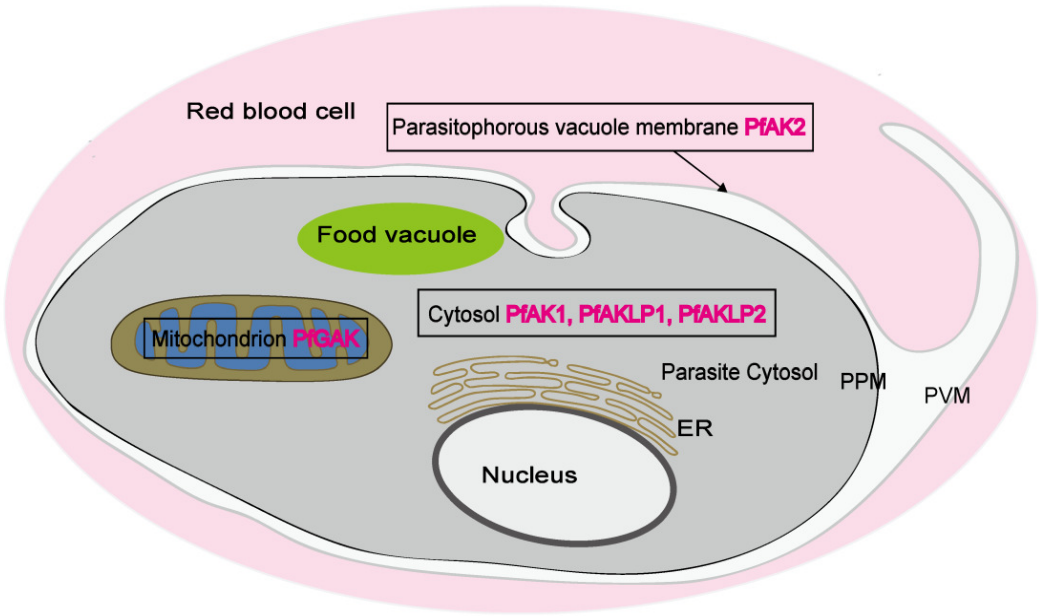

Figure. 5.1 Scheme of the subcellular localization of known adenylate kinases in *P. falciparum*. ER, endoplasmic reticulum; PVM, parasitophorous vacuole membrane; PPM, parasite plasma membrane.

N-myristoylation anchors proteins to a membrane in order to mediate diverse functions such as signal transduction, protein translocation, and cellular regulation (Zha *et al.*, 2000; Ducker *et al.*, 2005). A polybasic stretch of amino acids or one or two palmitoylated cysteine residues next to the myristoyl moiety attached to the protein is necessary for stabilizing the membrane localization (McCabe *et al.*,

1999; Resh, 2004). *Pf*AK2 has an unusual polybasic stretch of amino acids when compared to other AKs in *Plasmodium* (Figure 4.1). The G2A mutation of the N-myristoylation site of *Pf*AK2 demonstrated that N-myristoylation is required in order to bind *Pf*AK2 to the PVM, since the loss of the N-myristoylated glycine alone changes the localization of the protein. Parasite proteins exported into the host erythrocyte must stay in an unfolded state, and an important role for molecular chaperones has been suggested in this context (Gehde *et al.*, 2009). These chaperones are supposed to have a considerable demand for adenine nucleotides. Considering the important role of the parasitophorous vacuole membrane for protein transport from the parasite to the host cell compartment, we propose that *Pf*AK2 plays a vital role for the energy supply of protein transport. Alternatively, Kanaani discovered that parasites supply ATP to their host cells by means of an adenylate translocator and adenylate kinase. They also suggested the important role of adenylate kinase in this metabolic pathway. Thus, *Pf*AK2 may play a role in the ATP transport as well.

Surprisingly, no adenylate kinase isoform that prefers ATP as the substrate is localized in the mitochondria if we compare this to the mitochondrial intermembrane localization of AK2 in other organisms (Walker *et al.*, 1982). Since in other species most ATP is produced by the oxidative phosphorylation and electron transport chains, it is reasonable to have an AK isoform in the mitochondrial intermembrane. Therefore, there may still be new AK isoforms as we mentioned above that have not yet been identified although the whole genome of *P. facliparum* has been mapped since 2002 (Gardner *et al.*, 2002).

ATP produced in the mitochondrial pathway can be utilized in the high-energy phosphotransfer network shown in Figure 5.2 in other organisms. Such a network for facilitated high-energy phosphoryl transfer between ATP-consuming and ATP-generating sites relies on the chains of sequential rapid equilibrating reactions catalyzed by CK and AK (Zeleznikar *et al.*, 1995; Dzeja *et al.*, 2003). It has been shown that intracellular high-energy phosphoryl transfer networks can be compensated by AK and glycolytic enzymes in creatine kinase-deficient muscles (de Groof *et al.*, 2001; Dzeja *et al.*, 2004), demonstrating interplay between different shuttles of phosphoryl transfer. However, a homology search using the creatine kinase sequence revealed that apparently no such enzyme exists in *P. falciparum*. Thus, it is only possible to use ATP generated in the mitochondrion by the glycolytic enzymes such as hexokinase without a fast equilibrium network as in other organisms, considering the probable cytosolic localization of 3-phosphoglycerate kinase. This may demonstrate that mitochondria may not play a vital role in ATP production in *P. falciparum*.

As of 2010, it has been shown that *P. falciparum* may have a unique metabolic pathway in the mitochondria. As mentioned in 1.2.4 and Figure 1.12, *P. falciparum* has been shown to have a novel tricarboxylic acid cycle (Olszewski *et al.*, 2010). Olszewski and co-authors have found that the TCA cycle in the mitochondria of *P. falciparum* was a branched structure rather than a cyclic. In this pathway, several steps of reactions go in the reverse direction compared to the standard one. Therefore, the TCA cycle in *P. falciparum* mainly functions in production of succinyl-CoA for heme biosynthesis and citrate synthesis rather than efficiently supplying ATP (Olszewski *et al.*, 2010). Therefore it is rational that only *Pf*GAK is localized in the mitochondria because GTP can be generated in this branched TCA cycle. The observation that no adenylate kinase isoform is localized in the mitochondria may further prove that the TCA cycle is not the main source of ATP production in

P. falciparum. In spite of this situation, ATP synthase in the mitochondrion of *P. falciparum* assembles as a large dimeric complex like in other eukaryotic organisms and seems to be essential for parasite survival (Balabaskaran Nina *et al.*, 2011). Interestingly, the direct biochemical results showed that the mitochondria play a functional role in ATP synthesis and Ca^{2+} transport in the malaria parasite *Plasmodium berghei* (Uyemura *et al.*, 2000).

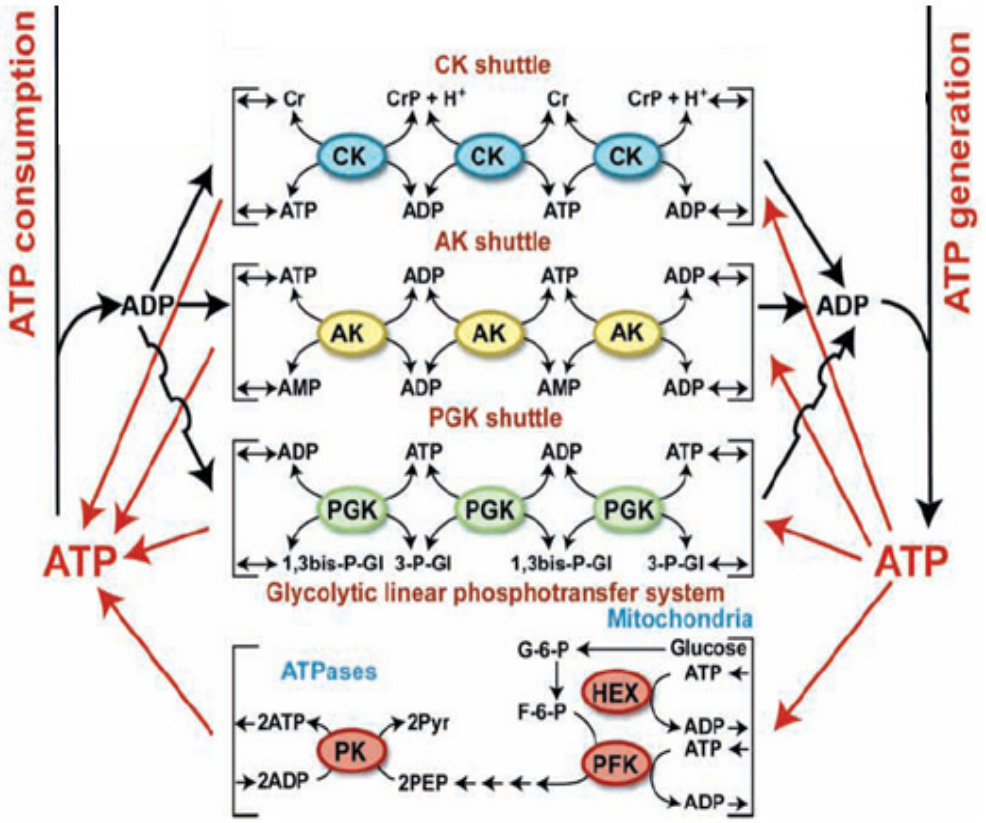

Figure 5.2 Integrated communications between cellular sites of ATP utilization and ATP generation. Adapted from (Dzeja *et al.*, 2003). CK, creatine kinase; AK, adenylate kinase; PGK, 3-phosphoglycerate kinase; HEX, hexokinase; PK, pyruvate kinase; PFK, phosphofructokinase; Gl, glucose; PEP, phosphoenol pyruvate; Pyr, pyruvate.

5.2 N-myristoyltransferase structure analysis for the potency of an antimalarial drug target

An overexpression and purification method for producing pure and homogeneous *Pf*NMT has been established in this report. In a previous study, the difficulty of obtaining *Pf*NMT has been described and the following inhibitor screening and crystallization study\ies have been limited (Bowyer *et al.*, 2007). By utilizing a synthetic codon-optimized *Pf*NMT gene, the overall yield was 0.4 mg/l culture compared to a previous 12 µg/l culture (Bowyer *et al.*, 2007). In our study, initial overexpression of *Pf*NMT in *E. coli* cells resulted in partial insoluble proteins in cell pellets. When introducing a pair of chaperones in the overexpression system, the solubility of *Pf*NMT improved since the chaperones

could assist proteins for proper folding. Meanwhile, the purity of *Pf*NMT was enhanced with the Protino® Ni-TED column rather than Ni-NTA resin. The pure protein was obtained after an additional gel filtration purification step. The overall yield of *Pf*NMT in this method is typically 1 mg/ liter culture. This provides the opportunity for high-throughput screening of inhibitors against *Pf*NMT and crystal screening of *Pf*NMT.

As of today, the structure of NMT from several species including *Leishmania major*, *Saccharomyces cerevisiae*, *Candida albicans*, and *Homo sapiens* has been revealed in order to explain the substrate binding and catalytic mechanism (Bhatnagar *et al.*, 1998; Weston *et al.*, 1998; Sogabe *et al.*, 2002; Frearson *et al.*, 2010), facilitating the elucidation of inhibitor behavior and rational drug design. Therefore, obtaining the details of the binding sites from the crystal structure will provide a chance for selective inhibition against this enzyme. During my thesis I tried several hundred conditions for the crystal screening including those that were already known for the other NMT crystals. Especially, the crystallization conditions of *P. vivax* NMT which shares more than 80% identity with NMT from *P. falciparum* have been tried. The lack of N-terminal 26 amino aicds in *P. vivax* NMT used for crystallization might be the reason for such difference (Goncalves *et al.*, 2012). In fact, most NMt structures have no N-terminal sequence since removal of this region has no significant effect on enzymatic activity (Rudnick *et al.*, 1992). However, it is also possible that this region has influence on the whole structure of NMTs. Therefore, they may require different conditions for crystallization. In fact, it was demonstrated that Asp^{22} and Asp^{23} in *S. cerevisiae* NMT are involved in the binding of the peptide substrate based on the structure of full-length *S. cerevisiae* NMT, although the region may not participate in catalysis (Rudnick *et al.*, 1992; Wu *et al.*, 2007).

In order to demonstrate the peptide binding feature in a *Pf*NMT model, we superposed this structure onto the ternary complex of *Sc*NMT with NHM and the octapeptides GLYASKLA (PDB code 1IIC) (Wu *et al.*, 2007). The residues that are predicted to surround this peptide in *Pf*NMT are Y95, V96, E97, D98, D100, V102, F103, F105, Y107, H213, F226, Y315, L317, S319, F334, E383, G384, D385, G386, L388, L409, and L410. Among all these residues, there are four amino acid differences between *Pf*NMT and *Hs*NMT type I including V102 (M), F334 (Y), E383 (I), and L410 (Q), which may provide the selectivity between both for novel inhibitors.

The high-resolution structure of *Hs*NMT type I in complex with myristoyl-CoA and inhibitor has been resolved by the Structural Genomics Consortium (SGC) and can be obtained from PDB (code 3IWE, unpublished). This structure and the predicted structure of *Pf*NMT can be superimposed, and the image can be displayed as shown in Figure 5.3. From this comparison, we could discover four regions with slight differences between humans and *P. falciparum*. Two regions labeled with red ovals seem to be on the remote surface and may not contribute to substrate binding and catalysis, while the other two marked with purple ovals reveal the possible domains that may participate in the peptide binding site. One of them (the purple oval in the middle of Figure 5.3) is the L410, which plays an important role in peptide binding and catalysis of the reaction (Farazi *et al.*, 2001). The other region also seems to be involved in substrate binding, since the His313 in this region of *Hs*NMT may interact with the peptide substrate derived from the comparison of *Hs*NMT with *Sc*NMT, containing the bound octapeptide GLYASKLA according to Brannigan's finding (Brannigan *et al.*, 2010). The corresponding C228 in *Pf*NMT as shown in multiple sequence alignments in the results section as

well as the close N230 and R232 are clearly different from the residues in this region. The differences in both regions may form the basis of selective inhibition for further selective inhibitor screening.

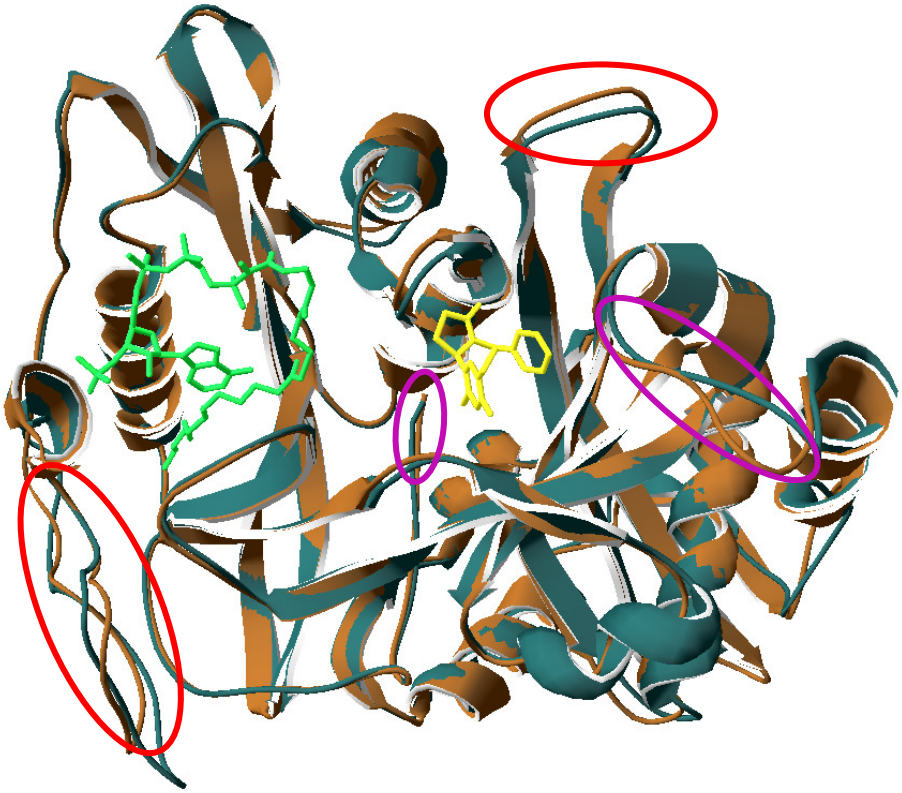

Figure 5.3 Comparison of human NMT type I (brown) (amino acids 115 to 496) and a model of *Pf*NMT (teal) (amino acids 27 to 410). Myristoyl-CoA (green) and inhibitor against human NMT1 (yellow). Slight differences are labeled in ovals (red and purple). Image created by PDB Viewer 4.0.4.

Since evidence of NMT as a druggable target in fungi has been shown, there has been increasing interest in identifying the potency of inhibiting this enzyme against protozoan infectious disease (Lodge *et al.*, 1994; Ebiike *et al.*, 2002; Ohtsuka *et al.*, 2003; Price *et al.*, 2003; Yamazaki *et al.*, 2005). The exciting finding of a nanomolar range inhibitor against *T. brucei* and a cure for trypanosomiasis in mice indicates that targeting NMT could be a promising strategy against protozoan parasites (Frearson *et al.*, 2010). Superposing the structure of *Lm*NMT with inhibitor and the peptide onto the model of *Pf*NMT, two amino acids (E383 and L410) at the C-terminus of *Pf*NMT probably responsible for peptide substrate binding are different from the ones in human NMT. Since the selective inhibition is more related to the peptide binding, this may imply the possibility of selective inhibition of *Pf*NMT as a drug target.

Even though NMT is a highly conserved protein, and the structures of the enzyme from several organisms have been resolved, it is still worth crystallizing this protein from *P. falciparum* in order to show the details of the binding motif. The complexity of inhibition patterns was demonstrated by showing that a subtle change in chain flexibility can cause a significant change in inhibitor selectivity. The study of high-throughput screening of inhibitors against *P. vivax* NMT illustrates that a significant increase in inhibition selectivity can be achieved by removing a group from compound 1 which does not display much selectivity of *P. vivax* and human NMT (Goncalves *et al.*, 2012).

Furthermore, Bell and co-authors discovered two novel series of inhibitors with adequate selectivity for *P. falciparum* NMT over other NMTs, although it seems a challenging task due to the observation of strong overlap between the structure-activity relationships for *P. falciparum* NMT and both human NMTs (Bell *et al.*, 2012). Since the inhibitor studies against NMT focused on the peptide binding site of the enzyme, it is also a good idea to co-crystallize the *Pf*NMT with *Pf*AK2, one of its natural substrate proteins. The structure of such a complex will elucidate the binding relation between NMT and its intact substrate protein, which may greatly enhance our understanding of peptide binding patterns. As a result, it would be helpful for novel inhibitor discovery. Thus, continuous efforts should be undertaken to finally solve the structure of this enzyme and/or its complex.

5.3 Myristoylation in *P. falciparum*

In this work for the first time, we demonstrate that myristoylation in *P. falciparum* can be visualized by using a new metabolic method. Bio-orthogonal chemical reporters have been developed to study protein post-translational modification (van Kasteren *et al.*, 2007). The general principle of this method is to attach the azido or alkynyl group to the substrate, which can be utilized in the metabolic pathway without significantly affecting its bioactivity in the cells. Since the study of fatty acylation in mammalian cells has been successfully established, we therefore explored the capabilities of this method for myristoylation in *P. falciparum*. Considering the unique life cycle of malaria parasite and the feature of parasitized red blood cells, the substrate of azido-myristic acid was fed twice during the metabolic labeling process. The time to initially add this substrate was chosen at the point just before the erythrocyte ruptures with mature schizonts so as to increase the substrate uptake by *P. falciparum*. Additionally, dose-dependent labeling of myristoylated proteins was studied in order to determine the optimal substrate concentration for the labeling step. Not surprisingly, 50 μM was the best concentration for labeling proteins, which is two times more than the substrate concentration for labeling mammalian cells (Wilson *et al.*, 2011). This lower uptake efficiency probably results from various membrane barriers between the parasites and the substrate. The following streptavidin-HRP blot could provide an easy and sensitive method for detecting successful labeling. In our experiment, we also use the anti-biotin antibody for detection. However, the signals were hard to detect, indicating the low proportion of myristoylated proteins within the whole proteome of parasites.

Theoretically, the labeled proteins can be further enriched through a pull-down assay and identified via mass spectrometry. Although this has been illustrated in human cells with cleavable and non-cleavable tags such as biotin (Martin *et al.*, 2009; Wilson *et al.*, 2011), it is likely that the cleavable tag will yield a better recovery and lower the false positives resulting from non-specific binding. In my study, several conditions including various elution buffers, pH, and avidin beads have been tested for eluting the bound proteins. However, such efforts still failed to selectively recover the labeled proteins. This may be ascribed to the low amount of myristoylated proteins and strong affinity between labeled proteins and the affinity material. Therefore cleavable biotin may be the best option for solving this problem. In fact, a second-generation cleavable tag (Figure 5.4) has been synthesized in order to be applied in this label method and has exhibited satisfying compatibility for protein identification (Yang *et al.*, 2010). Because this method is brand new and rapidly developing, such

cleavable tags are not yet commercially available. Only recently could the azido-biotin with bound disulfide be purchased. Therefore, it may eventually provide a new chance for continuing the pull-down assay and identifying the target proteins via mass spectrometry.

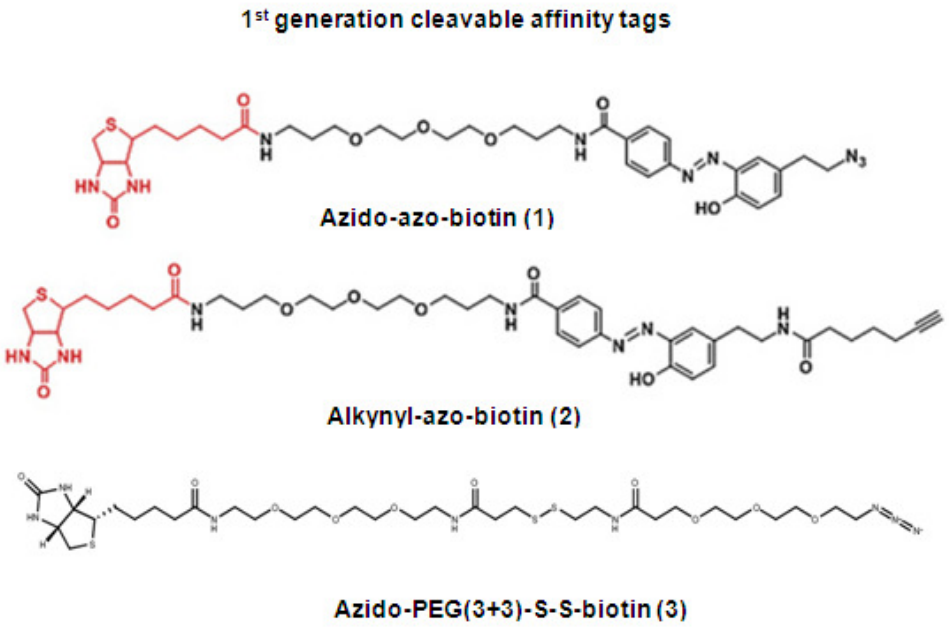

Figure 5.4 Biotin tags for the chemical reporter method. Cleavable azo-biotin tag with the azido group (1) or alkynyl group (2). Cleavable azido-biotin with disulfide bound (3). Adapted from Yang *et al.*, 2010, and a product manual from Jena Bioscience.

Comparing the target lists using two individual tools for myristoylation prediction based on the amino acid sequence, it is likely that the MYR Predictor has more stringent standards than the Myristoylator. The myristoylation proteome in *P. falciparum* comprises phosphatase, serine/threonine protein kinase, Golgi reassembly stacking protein, calcium-dependent protein kinase, ARF, erythrocyte membrane protein family members, and others. Thus it explains the vital function of NMT in parasite survival, showing it to be a promising drug target from another aspect. Even though the conserved motif that can be myristoylated has been well studied, inventing a universal program for myristoylation prediction still might be a challenging task. This may result from slight, progressive variation in different species.

Recently, the apoptosis in *P. falciparum* is a debate topic and is becoming an attractive strategy to combat malaria. As described in the introduction section, myristoylation could be a vital component during apoptosis and this chemical reporter method has shown its potency to label and identify the apoptic plays which have the internal myristoylated motif (Martin *et al.*, 2008). This can also be employed to study post-translational myristoylation during the apoptosis once the apoptosis-like signs can be properly induced in the malaria parasite.

In summary, this method relying on the chemical reporter is becoming a powerful tool to study myristoylation in the malaria parasite. As a consequence, it will contribute to understanding the

biological role played by myristoylation, the significance of NMT inhibition, and possibly even apoptosis in the parasite.

6 References

Agnandji ST, Lell B, *et al.* (**2011**). First results of phase 3 trial of RTS, S/AS01 malaria vaccine in African children. *N Engl J Med* **365**: 1863-1875.

Amor JC, Harrison DH, *et al.* (**1994**). Structure of the human ADP-ribosylation factor 1 complexed with GDP. *Nature* **372**: 704-708.

Anderson TJ, Nair S, *et al.* (**2010**). High heritability of malaria parasite clearance rate indicates a genetic basis for artemisinin resistance in western Cambodia. *J Infect Dis* **201**: 1326-1330.

Arora K and Brooks CL, 3rd (**2007**). Large-scale allosteric conformational transitions of adenylate kinase appear to involve a population-shift mechanism. *Proc Natl Acad Sci U S A* **104**: 18496-18501.

Ashley MV and Stefan HK (**2012**). Malaria vaccine development: persistent challenges. *Curr Opin Immunol* **24**: 324-331.

Bagrodia S, Taylor SJ, *et al.* (**1993**). Myristylation is required for Tyr-527 dephosphorylation and activation of pp60c-src in mitosis. *Mol Cell Biol* **13**: 1464-1470.

Balabaskaran NP, Morrisey JM, *et al.* (**2011**). ATP synthase complex of *Plasmodium falciparum*: dimeric assembly in mitochondrial membranes and resistance to genetic disruption. *J Biol Chem* **286**: 41312-41322.

Barzu O and Michelson S (**1983**). Simple and fast purification of *Escherichia coli* adenylate kinase. *FEBS Lett* **153**: 280-284.

Bell AS, Mills JE, *et al.* (**2012**). Selective Inhibitors of Protozoan Protein N-myristoyltransferases as Starting Points for Tropical Disease Medicinal Chemistry Programs. *PLoS Negl Trop Dis* **6**.

Bergeron R, Russell RR, *et al.* (**1999**). Effect of AMPK activation on muscle glucose metabolism in conscious rats. *Am J Physiol Endocrinol Metab* **276**: E938-E944.

Bhaskara V, Dupre A, *et al.* (**2007**). Rad50 adenylate kinase activity regulates DNA tethering by Mre11/Rad50 complexes. *Mol Cell* **25**: 647-661.

Bhatnagar RS, Futterer K, *et al.* (**1998**). Structure of N-myristoyltransferase with bound myristoylCoA and peptide substrate analogs. *Nat Struct Biol* **5**: 1091-1097.

Bologna G, Yvon C, *et al.* (**2004**). N-Terminal myristoylation predictions by ensembles of neural networks. *Proteomics* **4**: 1626-1632.

Botta D and Jacobson MK (**2008**). Identification of a regulatory segment of poly(ADP-ribose) glycohydrolase. *Biochemistry* **49**: 7674-7682.

Bouvier LA, Miranda MR, *et al.* (**2006**). An expanded adenylate kinase gene family in the protozoan parasite *Trypanosoma cruzi*. *Biochim Biophys Acta* **1760**: 913-921.

Bowyer PW, Gunaratne RS, *et al.* (**2007**). Molecules incorporating a benzothiazole core scaffold inhibit the N-myristoyltransferase of *Plasmodium falciparum*. *Biochem J* **408**: 173-180.

Bowyer PW, Tate EW, *et al.* (**2008**). N-myristoyltransferase: a prospective drug target for protozoan parasites. *ChemMedChem* **3**: 402-408.

Bradford MM (**1976**). A rapid and sensitive method for the quantitation of microgram quantities of protein utilizing the principle of protein-dye binding. *Anal Biochem* **72**: 248-254.

Brannigan JA, Smith BA, *et al.* (**2010**). N-myristoyltransferase from *Leishmania donovani*: structural and functional characterisation of a potential drug target for visceral leishmaniasis. *J Mol Biol* **396**: 985-999.

Brito I (**2001**). Eradicating malaria: high hopes or a tangible goal? *Health Policy at Harvard* **2**: 61-66.

Cao W, Haig-Ladewig L, *et al.* (**2006**). Adenylate kinases 1 and 2 are part of the accessory structures

in the mouse sperm flagellum. *Biol Reprod* **75**: 492-500.

Carrasco AJ, Dzeja PP, *et al.* (**2001**). Adenylate kinase phosphotransfer communicates cellular energetic signals to ATP-sensitive potassium channels. *Proc Natl Acad Sci U S A* **98**: 7623-7628.

Carter R and Mendis KN (**2002**). Evolutionary and historical aspects of the burden of malaria. *Clin Microbiol Rev* **15**: 564-594.

Charron G, Zhang MM, *et al.* (**2009**). Robust fluorescent detection of protein fatty-acylation with chemical reporters. *J Am Chem Soc* **131**: 4967-4975.

Chiu CS, Su S, *et al.* (**1967**). Adenylate kinase from baker's yeast. I. Purification and intracellular location. *Biochim Biophys Acta* **132**: 361-369.

Collavin L, Lazarevic D, *et al.* (**1999**). wt p53 dependent expression of a membrane-associated isoform of adenylate kinase. *Oncogene* **18**: 5879-5888.

Collins WE (**2012**). *Plasmodium knowlesi*: a malaria parasite of monkeys and humans. *Annu Rev Entomol* **57**: 107-121.

Colowick SP and Kalckar HM (**1943**). Role of myokinase in transphosphorylations. I. Enzymatic phosphorylation of hexoses by adenyl pyrophosphate. *J. Biol. Chem* **148**: 117-126.

Cordeddu V, Di Schiavi E, *et al.* (**2009**). Mutation of SHOC2 promotes aberrant protein N-myristoylation and causes Noonan-like syndrome with loose anagen hair. *Nat Genet* **41**: 1022-1026.

Crabb BS, Rug M, *et al.* (**2004**). Transfection of the human malaria parasite *Plasmodium falciparum*. *Methods Mol Biol* **270**: 263-276.

Crosnier C, Bustamante LY, *et al.* (**2011**). Basigin is a receptor essential for erythrocyte invasion by *Plasmodium falciparum*. *Nature* **480**: 534-U158.

Cross FR, Garber EA, *et al.* (**1984**). A short sequence in the p60src N terminus is required for p60src myristylation and membrane association and for cell transformation. *Mol Cell Biol* **4**: 1834-1842.

Crowell DN and Huizinga DH (**2009**). Protein isoprenylation: the fat of the matter. *Trends Plant Sci* **14**: 163-170.

de Groof AJ, Oerlemans FT, *et al.* (**2001**). Changes in glycolytic network and mitochondrial design in creatine kinase-deficient muscles. *Muscle Nerve* **24**: 1188-1196.

Devadas B, Freeman SK, *et al.* (**1998**). Novel biologically active nonpeptidic inhibitors of myristoylCoA:protein N-myristoyltransferase. *J Med Chem* **41**: 996-1000.

Dinglasan RR and Jacobs-Lorena M (**2008**). Flipping the paradigm on malaria transmission-blocking vaccines. *Trends Parasitol* **24**: 364-370.

Dondorp AM, Nosten F, *et al.* (**2009**). Artemisinin resistance in *Plasmodium falciparum* malaria. *N Engl J Med* **361**: 455-467.

Dondorp AM, Yeung S, *et al.* (**2010**). Artemisinin resistance: current status and scenarios for containment. *Nat Rev Microbiol* **8**: 272-280.

Drakou CE, Malekkou A, *et al.* (**2011**). hCINAP is an atypical mammalian nuclear adenylate kinase with an ATPase motif: Structural and functional studies. *Proteins Struct Funct Bioinformat* **80**: 206-220.

Ducker CE, Upson JJ, *et al.* (**2005**). Two N-myristoyltransferase isozymes play unique roles in protein myristoylation, proliferation, and apoptosis. *Mol Cancer Res* **3**: 463-476.

Duronio RJ, Rudnick DA, *et al.* (**1991**). Analyzing the substrate specificity of *Saccharomyces*

cerevisiae myristoyl-CoA:protein N-myristoyltransferase by co-expressing it with mammalian G protein alpha subunits in *Escherichia coli*. *J Biol Chem* **266**: 10498-10504.

Dyck JRB and Lopaschuk GD (**2006**). AMPK alterations in cardiac physiology and pathology: enemy or ally? *J Physiol (London)* **574**: 95-112.

Dzeja P, Chung S, *et al.* (**2007a**). Integration of adenylate kinase and glycolytic and clycogenolytic circuits in cellular energetics. Molecular System Bioenergetics. Energy for Life. V. Saks. Weinheim, Germany, Wiley –**VCH:** 265-301.

Dzeja P, Kalvenas A, *et al.* (**1985**). The effect of adenylate kinase activity on the rate and efficiency of energy transport from mitochondria to hexokinase. *Biochem Int* **10**: 259-265.

Dzeja P and Terzic A (**2009**). Adenylate kinase and AMP signaling networks: Metabolic monitoring, signal communication and body energy sensing. *Int J Mol Sci* **10**: 1729-1772.

Dzeja PP, Bast P, *et al.* (**2007b**). Defective metabolic signaling in adenylate kinase AK1 gene knock-out hearts compromises post-ischemic coronary reflow. *J Biol Chem* **282**: 31366-31372.

Dzeja PP, Pucar D, *et al.* (**2002**). Captured cellular adenylate kinase-catalyzed phosphotransfer using ^{18}O-assisted ^{31}P NMR. *MAGMA* **14**: 180-181.

Dzeja PP, Redfield MM, *et al.* (**2000**). Failing energetics in failing hearts. *Curr Cardiol Rep* **2**: 212-217.

Dzeja PP and Terzic A (**2003**). Phosphotransfer networks and cellular energetics. *J Exp Biol* **206**: 2039-2047.

Dzeja PP, Terzic A, *et al.* (**2004**). Phosphotransfer dynamics in skeletal muscle from creatine kinase gene-deleted mice. *Mol Cell Biochem* **256-257**: 13-27.

Dzeja PP, Vitkevicius KT, *et al.* (**1999**). Adenylate kinase-catalyzed phosphotransfer in the myocardium : increased contribution in heart failure. *Circ Res* **84**: 1137-1143.

Dzeja PP, Zeleznikar RJ, *et al.* (**1996**). Suppression of creatine kinase-catalyzed phosphotransfer results in increased phosphoryl transfer by adenylate kinase in intact skeletal muscle. *J Biol Chem* **271**: 12847-12851.

Ebiike H, Masubuchi M, *et al.* (**2002**). Design and synthesis of novel benzofurans as a new class of antifungal agents targeting fungal N-myristoyltransferase. Part 2. *Bioorg Med Chem Lett* **12**: 607-610.

Farazi TA, Waksman G, *et al.* (**2001**). The biology and enzymology of protein N-myristoylation. *J Biol Chem* **276**: 39501-39504.

Farazi TA, Waksman G, *et al.* (**2001**). Structures of *Saccharomyces cerevisiae* N-myristoyltransferase with bound myristoylCoA and peptide provide insights about substrate recognition and catalysis. *Biochemistry* **40**: 6335-6343.

Feachem RG, Phillips AA, *et al.* (**2010**). Shrinking the malaria map: progress and prospects. *Lancet* **376**: 1566-1578.

Fitch CD (**2004**). Ferriprotoporphyrin IX, phospholipids, and the antimalarial actions of quinoline drugs. *Life Sci* **74**: 1957-1972.

Ford WC (**2006**). Glycolysis and sperm motility: does a spoonful of sugar help the flagellum go round? *Hum Reprod Update* **12**: 269-274.

Frearson JA, Brand S, *et al.* (**2010**). N-myristoyltransferase inhibitors as new leads to treat sleeping sickness. *Nature* **464**: 728-732.

Frottin F, Martinez A, *et al.* (**2006**). The proteomics of N-terminal methionine cleavage. *Mol Cell*

Proteomics **5**: 2336-2349.

Furuishi K, Matsuoka H*, et al.* (**1997**). Blockage of N-myristoylation of HIV-1 gag induces the production of impotent progeny virus. *Biochem Biophys Res Commun* **237**: 504-511.

Gardner MJ, Hall N*, et al.* (**2002**). Genome sequence of the human malaria parasite *Plasmodium falciparum*. *Nature* **419**: 498-511.

Gehde N, Hinrichs C*, et al.* (**2009**). Protein unfolding is an essential requirement for transport across the parasitophorous vacuolar membrane of Plasmodium falciparum. *Mol Microbiol* **71**: 613-628.

Gerstein M, Schulz G*, et al.* (**1993**). Domain closure in adenylate kinase. Joints on either side of two helices close like neighboring fingers. *J Mol Biol* **229**: 494-501.

Giang DG and Cravatt BF (**1998**). A second mammalian N-myristoyltransferase. *J Biol Chem* **273**: 6595-6598.

Ginger ML, Ngazoa ES*, et al.* (**2005**). Intracellular positioning of isoforms explains an unusually large adenylate kinase gene family in the parasite *Trypanosoma brucei*. *J Biol Chem* **280**: 11781-11789.

Ginsburg H (**2010**). Metabolism: Malaria parasite stands out. *Nature* **466**: 702-703.

Giroux V, Iovanna J*, et al.* (**2006**). Probing the human kinome for kinases involved in pancreatic cancer cell survival and gemcitabine resistance. *Faseb J* **20**: 1982-1991.

Glover CJ, Hartman KD*, et al.* (**1997**). Human N-myristoyltransferase amino-terminal domain involved in targeting the enzyme to the ribosomal subcellular fraction. *J Biol Chem* **272**: 28680-28689.

Goncalves V, Brannigan JA*, et al.* (**2012**). Discovery of *Plasmodium vivax* N-myristoyltransferase inhibitors: screening, synthesis, and structural characterization of their binding mode. *J Med Chem* **55**: 3578-3582.

Goodman AL, Blagborough AM*, et al.* (**2011**). A viral vectored prime-boost immunization regime targeting the malaria Pfs25 antigen induces transmission-blocking activity. *PLoS One* **6**: e29428.

Gunaratne RS, Sajid M*, et al.* (**2000**). Characterization of N-myristoyltransferase from *Plasmodium falciparum*. *Biochem J* **348 Pt 2**: 459-463.

Hancock CR, Janssen E*, et al.* (**2005**). Skeletal muscle contractile performance and ADP accumulation in adenylate kinase-deficient mice. *Am J Physiol Cell Physiol* **288**: C1287-1297.

Hancock CR, Janssen E*, et al.* (**2006**). Contraction-mediated phosphorylation of AMPK is lower in skeletal muscle of adenylate kinase-deficient mice. *J Appl Physiol* **100**: 406-413.

Hang HC, Geutjes EJ*, et al.* (**2007**). Chemical probes for the rapid detection of Fatty-acylated proteins in Mammalian cells. *J Am Chem Soc* **129**: 2744-2745.

Hantschel O, Nagar B*, et al.* (**2003**). A myristoyl/phosphotyrosine switch regulates c-Abl. *Cell* **112**: 845-857.

Hardie DG (**2008**). AMPK: a key regulator of energy balance in the single cell and the whole organism. *Int J Obes (Lond)* **32 Suppl 4**: S7-12.

Hardie DG, Ross FA*, et al.* (**2012**). AMPK: a nutrient and energy sensor that maintains energy homeostasis. *Nat Rev Mol Cell Biol* **13**: 251-262.

Hay SI, Guerra CA*, et al.* (**2004**). The global distribution and population at risk of malaria: past, present, and future. *Lancet Infect Dis* **4**: 327-336.

Hertz-Fowler C, Ersfeld K, *et al.* (**2001**). CAP5.5, a life-cycle-regulated, cytoskeleton-associated protein is a member of a novel family of calpain-related proteins in *Trypanosoma brucei*. *Mol Biochem Parasitol* **116**: 25-34.

Hu CJ, Iyer S, *et al.* (**2006**). Differential regulation of the transcriptional activities of hypoxia-inducible factor 1 alpha (HIF-1alpha) and HIF-2alpha in stem cells. *Mol Cell Biol* **26**: 3514-3526.

Janssen E, Dzeja PP, *et al.* (**2000**). Adenylate kinase 1 gene deletion disrupts muscle energetic economy despite metabolic rearrangement. *Embo J* **19**: 6371-6381.

Janssen E, Kuiper J, *et al.* (**2004**). Two structurally distinct and spatially compartmentalized adenylate kinases are expressed from the AK1 gene in mouse brain. *Mol Cell Biochem* **256-257**: 59-72.

Kalckar HM (**1944**). Adenylpyrophosphatase and myokinase. *J Biol Chem* **153**: 355-367.

Kanaani J and Ginsburg H (**1989**). Metabolic Interconnection between the Human Malarial Parasite *Plasmodium-Falciparum* and Its Host Erythrocyte - Regulation of Atp Levels by Means of an Adenylate Translocator and Adenylate Kinase. *J Biol Chem* **264**: 3194-3199.

Kawai M and Uchimiya H (**1995**). Biochemical properties of rice adenylate kinase and subcellular location in plant cells. *Plant Mol Biol* **27**: 943-951.

Kehr S, Sturm N, *et al.* (**2010**). Compartmentation of redox metabolism in malaria parasites. *PloS Pathog* **6**: e1001242.

Kishore NS, Wood DC, *et al.* (**1993**). Comparison of the Acyl Chain Specificities of Human Myristoyl-Coa Synthetase and Human Myristoyl-Coa-Protein N-Myristoyltransferase. *J Biol Chem* **268**: 4889-4902.

Klier H, Magdolen V, *et al.* (**1996**). Cytoplasmic and mitochondrial forms of yeast adenylate kinase 2 are N-acetylated. *Biochim Biophys Acta* **1280**: 251-256.

Kotel'nikova AV (**2001**). Fiftieth anniversary of the discovery of adenylate kinase. *Biochemistry (Mosc)* **66**: 816-817.

Kuehnel MP, Reiss M, *et al.* (**2009**). Sphingosine-1-phosphate receptors stimulate macrophage plasma-membrane actin assembly via ADP release, ATP synthesis and P2X7R activation. *J Cell Sci* **122**: 505-512.

Lagresle-Peyrou C, Six EM, *et al.* (**2009**). Human adenylate kinase 2 deficiency causes a profound hematopoietic defect associated with sensorineural deafness. *Nat Genet* **41**: 106-111.

Law AW, Lescar J, *et al.* (**2012**). Expression, purification, crystallization and preliminary X-ray analysis of *Plasmodium falciparum* GTP:AMP phosphotransferase. *Acta Crystallogr Sect F Struct Biol Cryst Commun* **68**: 671-674.

Le Bras J and Durand R (**2003**). The mechanisms of resistance to antimalarial drugs in *Plasmodium falciparum*. *Fundam Clin Pharmacol* **17**: 147-153.

Leber W, Skippen A, *et al.* (**2009**). A unique phosphatidylinositol 4-phosphate 5-kinase is activated by ADP-ribosylation factor in *Plasmodium falciparum*. *Int J Parasitol* **39**: 645-653.

Lee Y, Kim JW, *et al.* (**1998**). Cloning and expression of human adenylate kinase 2 isozymes: differential expression of adenylate kinase 1 and 2 in human muscle tissues. *J Biochem* **123**: 47-54.

Linder ME (**2000**). Reversible modification of proteins with thioester-linked fatty acids. Protein Lipidation. F. Tamanoi and D. S. Sigman. San Diego, CA, USA, Academic Press**:** 215-240.

Liu R, Strom AL, *et al.* (**2009**). Enzymatically inactive adenylate kinase 4 interacts with mitochondrial ADP/ATP translocase. *Int J Biochem Cell Biol* **41**: 1371-1380.

Lodge JK, Jackson-Machelski E*, et al.* (**1994**). Targeted gene replacement demonstrates that myristoyl-CoA: protein N-myristoyltransferase is essential for viability of Cryptococcus neoformans. *Proc Natl Acad Sci U S A* **91**: 12008-12012.

Lodge JK, Johnson RL*, et al.* (**1994**). Comparison of myristoyl-CoA:protein N-myristoyltransferases from three pathogenic fungi: *Cryptococcus neoformans*, *Histoplasma capsulatum*, and *Candida albicans*. *J Biol Chem* **269**: 2996-3009.

Luz CM, Konig I*, et al.* (**1990**). Human cytosolic adenylate kinase allelozymes; purification and characterization. *Biochim Biophys Acta* **1038**: 80-84.

Ma J, Rahlfs S*, et al.* (**2012**). Subcellular localization of adenylate kinases in *Plasmodium falciparum*. *FEBS Lett*.

Mann RK and Beachy PA (**2000**). Cholesterol modification of proteins. *Biochim Biophys Acta* **1529**: 188-202.

Martin BR and Cravatt BF (**2009**). Large-scale profiling of protein palmitoylation in mammalian cells. *Nat Meth* **6**: 135-138.

Martin DD, Beauchamp E*, et al.* (**2010**). Post-translational myristoylation: Fat matters in cellular life and death. *Biochimie* **93**: 18-31.

Martin DD, Vilas GL*, et al.* (**2008**). Rapid detection, discovery, and identification of post-translationally myristoylated proteins during apoptosis using a bio-orthogonal azidomyristate analog. *Faseb J* **22**: 797-806.

Matsubara M, Nakatsu T*, et al.* (**2004**). Crystal structure of a myristoylated CAP-23/NAP-22 N-terminal domain complexed with Ca2+/calmodulin. *Embo J* **23**: 712-718.

Maurer-Stroh S, Eisenhaber B*, et al.* (**2002**). N-terminal N-myristoylation of proteins: refinement of the sequence motif and its taxon-specific differences. *J Mol Biol* **317**: 523-540.

Maurer-Stroh S and Eisenhaber F (**2004**). Myristoylation of viral and bacterial proteins. *Trends Microbiol* **12**: 178-185.

Maurer-Stroh S, Gouda M*, et al.* (**2004**). MYRbase: analysis of genome-wide glycine myristoylation enlarges the functional spectrum of eukaryotic myristoylated proteins. *Genome Biol* **5**: R21.

Mazzanti L, Cacciari E*, et al.* (**2003**). Noonan-like syndrome with loose anagen hair: a new syndrome? *Am J Med Genet A* **118A**: 279-286.

McCabe JB and Berthiaume LG (**1999**). Functional roles for fatty acylated amino-terminal domains in subcellular localization. *Mol Biol Cell* **10**: 3771-3786.

McLaughlin S and Aderem A (**1995**). The myristoyl-electrostatic switch: a modulator of reversible protein-membrane interactions. *Trends Biochem Sci* **20**: 272-276.

McRee DE (**1993**). Practical Protein Crystallography. San Diego, Academic Press.(1-23.)

Mendis K, Rietveld A*, et al.* (**2009**). From malaria control to eradication: The WHO perspective. *Trop Med Int Health* **14**: 802-809.

Moskes C, Burghaus PA*, et al.* (**2004**). Export of *Plasmodium falciparum* calcium-dependent protein kinase 1 to the parasitophorous vacuole is dependent on three N-terminal membrane anchor motifs. *Mol Microbiol* **54**: 676-691.

Muller CW and Schulz GE (**1992**). Structure of the Complex between Adenylate Kinase from *Escherichia coli* and the Inhibitor Ap5a Refined at 1.9 a Resolution - a Model for a Catalytic Transition-State. *J Mol Biol* **224**: 159-177.

Munier-Lehmann H, Chenal-Francisque V*, et al.* (**2003**). Relationship between bacterial virulence and nucleotide metabolism: a mutation in the adenylate kinase gene renders *Yersinia pestis*

avirulent. *Biochem J* **373**: 515-522.

Murray CJ, Rosenfeld LC, *et al.* (**2012**). Global malaria mortality between 1980 and 2010: a systematic analysis. *Lancet* **379**: 413-431.

NODA LH (**1973**). Adenylate kinase. The Enzymes. P. D. Boyer. New York, USA, Academic Press. **8:** 279-305.

Noma T (**2005**). Dynamics of nucleotide metabolism as a supporter of life phenomena. *J Med Invest* **52**: 127-136.

Noma T, Fujisawa K, *et al.* (**2001**). Structure and expression of human mitochondrial adenylate kinase targeted to the mitochondrial matrix. *Biochem J* **358**: 225-232.

Nussenzweig RS, Vanderberg J, *et al.* (**1967**). Protective immunity produced by the injection of x-irradiated sporozoites of *Plasmodium berghei*. *Nature* **216**: 160-162.

Nussenzweig V, Good MF, *et al.* (**2011**). Mixed results for a malaria vaccine. *Nat Med* **17**: 1560-1561.

O'Neill HM, Maarbjerg SJ, *et al.* (**2011**). AMP-activated protein kinase (AMPK) beta1beta2 muscle null mice reveal an essential role for AMPK in maintaining mitochondrial content and glucose uptake during exercise. *Proc Natl Acad Sci U S A* **108**: 16092-16097.

Ohtsuka T and Aoki Y (**2003**). N-myristoyltransferase inhibitors as potential antifungal drugs. *Drugs Future* **28**: 143-152.

Olsson U and Wolf-Watz M (**2010**). Overlap between folding and functional energy landscapes for adenylate kinase conformational change. *Nat Commun* **1**: 111.

Olszewski KL, Mather MW, *et al.* (**2010**). Branched tricarboxylic acid metabolism in *Plasmodium falciparum*. *Nature* **466**: 774-778.

Panayiotou C, Solaroli N, *et al.* (**2011**). The characterization of human adenylate kinases 7 and 8 demonstrates differences in kinetic parameters and structural organization among the family of adenylate kinase isoenzymes. *Biochem J* **433**: 527-534.

Pannicke U, Honig M, *et al.* (**2009**). Reticular dysgenesis (aleukocytosis) is caused by mutations in the gene encoding mitochondrial adenylate kinase 2. *Nat Genet* **41**: 101-105.

Patwardhan P and Resh MD (**2010**). Myristoylation and membrane binding regulate c-Src stability and kinase activity. *Mol Cell Biol* **30**: 4094-4107.

Paulick MG and Bertozzi CR (**2008**). The glycosylphosphatidylinositol anchor: a complex membrane-anchoring structure for proteins. *Biochemistry* **47**: 6991-7000.

Paull TT and Gellert M (**1999**). Nbs1 potentiates ATP-driven DNA unwinding and endonuclease cleavage by the Mre11/Rad50 complex. *Genes Dev* **13**: 1276-1288.

Peitsch MC, Wells TN, *et al.* (**1995**). The Swiss-3DImage collection and PDB-Browser on the World-Wide Web. *Trends Biochem Sci* **20**: 82-84.

Peitzsch RM and McLaughlin S (**1993**). Binding of acylated peptides and fatty acids to phospholipid vesicles: pertinence to myristoylated proteins. *Biochemistry* **32**: 10436-10443.

Price HP, Guther MLS, *et al.* (**2010**). Myristoyl-CoA:protein N-myristoyltransferase depletion in trypanosomes causes avirulence and endocytic defects. *Mol Biochem Parasitol* **169**: 55-58.

Price HP, Menon MR, *et al.* (**2003**). Myristoyl-CoA:protein N-myristoyltransferase, an essential enzyme and potential drug target in kinetoplastid parasites. *J Biol Chem* **278**: 7206-7214.

Price HP, Stark M, *et al.* (**2007**). Trypanosoma brucei ARF1 plays a central role in endocytosis and Golgi-lysosome trafficking. *Molecular Biology of the Cell* **18**: 864-873.

Pucar D, Bast P, *et al.* (**2002**). Adenylate kinase AK1 knockout heart: energetics and functional performance under ischemia-reperfusion. *Am J Physiol Heart Circ Physiol* **283**: H776-782.

Pucar D, Janssen E*, et al.* (**2000**). Compromised energetics in the adenylate kinase AK1 gene knockout heart under metabolic stress. *J Biol Chem* **275**: 41424-41429.

Rahlfs S, Koncarevic S*, et al.* (**2009**). Myristoylated adenylate kinase-2 of Plasmodium falciparum forms a heterodimer with myristoyltransferase. *Mol Biochem Parasitol* **163**: 77-84.

Raj DK, Mu J*, et al.* (**2009**). Disruption of a *Plasmodium falciparum* multidrug resistance-associated protein (PfMRP) alters its fitness and transport of antimalarial drugs and glutathione. *J Biol Chem* **284**: 7687-7696.

Rajala RV, Datla RS*, et al.* (**2001**). Phosphorylation of human N-myristoyltransferase by N-myristoylated SRC family tyrosine kinase members. *Biochem Biophys Res Commun* **288**: 233-239.

Reed MB, Saliba KJ*, et al.* (**2000**). Pgh1 modulates sensitivity and resistance to multiple antimalarials in *Plasmodium falciparum*. *Nature* **403**: 906-909.

Rees-Channer RR, Martin SR*, et al.* (**2006**). Dual acylation of the 45 kDa gliding-associated protein (GAP45) in *Plasmodium falciparum* merozoites. *Mol Biochem Parasitol* **149**: 113-116.

Reinstein J, Schlichting I*, et al.* (**1990**). Structurally and catalytically important residues in the phosphate binding loop of adenylate kinase of Escherichia coli. *Biochemistry* **29**: 7451-7459.

Ren H, Wang L*, et al.* (**2005**). The crystal structure of human adenylate kinase 6: An adenylate kinase localized to the cell nucleus. *Proc Natl Acad Sci U S A* **102**: 303-308.

Resh MD (**2004**). Membrane targeting of lipid modified signal transduction proteins. *Subcell Biochem* **37**: 217-232.

Resh MD (**2006**). Trafficking and signaling by fatty-acylated and prenylated proteins. *Nat Chem Biol* **2**: 584-590.

Rhodes G (**1993**). Crystallography Made Crystal Clear. San Diego, Academic Press.(8-10,29-38.)

Ribaut C, Berry A*, et al.* (**2008**). Concentration and purification by magnetic separation of the erythrocytic stages of all human *Plasmodium* species. *Malar J* **7**: 45.

Roberts RJ (**1976**). Restriction endonucleases. *CRC Crit Rev Biochem* **4**: 123-164.

Rocque WJ, McWherter CA*, et al.* (**1993**). A comparative analysis of the kinetic mechanism and peptide substrate specificity of human and *Saccharomyces cerevisiae* myristoyl-CoA:protein N-myristoyltransferase. *J Biol Chem* **268**: 9964-9971.

Roth E, Jr. (**1990**). *Plasmodium falciparum* carbohydrate metabolism: a connection between host cell and parasite. *Blood Cells* **16**: 453-460; discussion 461-456.

Ruan Q, Chen Y*, et al.* (**2002**). Cellular characterization of adenylate kinase and its isoform: two-photon excitation fluorescence imaging and fluorescence correlation spectroscopy. *Biophys J* **83**: 3177-3187.

Rudnick DA, Johnson RL*, et al.* (**1992**). Studies of the catalytic activities and substrate specificities of *Saccharomyces cerevisiae* myristoyl-coenzyme A: protein N-myristoyltransferase deletion mutants and human/yeast Nmt chimeras in Escherichia coli and S. cerevisiae. *J Biol Chem* **267**: 23852-23861.

Rudnick DA, McWherter CA*, et al.* (**1991**). Kinetic and structural evidence for a sequential ordered Bi Bi mechanism of catalysis by *Saccharomyces cerevisiae* myristoyl-CoA:protein N-myristoyltransferase. *J Biol Chem* **266**: 9732-9739.

Russo I, Oksman A*, et al.* (**2009**). Fatty acid acylation regulates trafficking of the unusual *Plasmodium falciparum* calpain to the nucleolus. *Mol Microbiol* **72**: 229-245.

Sa JM, Twu O*, et al.* (**2009**). Geographic patterns of *Plasmodium falciparum* drug resistance

distinguished by differential responses to amodiaquine and chloroquine. *Proc Natl Acad Sci U S A* **106**: 18883-18889.

Sambrook J and Russell DW (**2001**). Molecular Cloning: A Laboratory Manual. New York, Cold Spring Harbor Laboratory Press.

Sanchez CP, Dave A*, et al.* (**2010**). Transporters as mediators of drug resistance in *Plasmodium falciparum*. *Int J Parasitol* **40**: 1109-1118.

Santama N, Ogg SC*, et al.* (**2005**). Characterization of hCINAP, a novel coilin-interacting protein encoded by a transcript from the transcription factor TAFIID32 locus. *J Biol Chem* **280**: 36429-36441.

Sato N, Koyama Y*, et al.* (**1982**). Antigenic structure of adenylate kinase from porcine skeletal muscle. I. Three immunochemically active peptides obtained by cleavage with cyanogen bromide. *J Biochem* **91**: 1749-1757.

Schoff PK, Cheetham J*, et al.* (**1989**). Adenylate kinase activity in ejaculated bovine sperm flagella. *J Biol Chem* **264**: 6086-6091.

Schubbert S, Shannon K*, et al.* (**2007**). Hyperactive Ras in developmental disorders and cancer. *Nat Rev Cancer* **7**: 295-308.

Schultz AM and Oroszlan S (**1983**). In vivo modification of retroviral gag gene-encoded polyproteins by myristic acid. *J Virol* **46**: 355-361.

Schwede T, Kopp J*, et al.* (**2003**). SWISS-MODEL: An automated protein homology-modeling server. *Nucleic Acids Res* **31**: 3381-3385.

Seaton KE and Smith CD (**2008**). N-Myristoyltransferase isozymes exhibit differential specificity for human immunodeficiency virus type 1 Gag and Nef. *J Gen Virol* **89**: 288-296.

Semenza GL (**2000**). HIF-1 and human disease: one highly involved factor. *Genes Dev* **14**: 1983-1991.

Shimomura O, Johnson FH*, et al.* (**1962**). Extraction, purification and properties of aequorin, a bioluminescent protein from the luminous hydromedusan, Aequorea. *J Cell Comp Physiol* **59**: 223-239.

Shoji S, Kurosawa T*, et al.* (**1990**). Human cellular src gene product: identification of the myristoylated pp60c-src and blockage of its myristoyl acylation with N-fatty acyl compounds resulted in the suppression of colony formation. *Biochem Biophys Res Commun* **173**: 894-901.

Sidhu AB, Valderramos SG*, et al.* (**2005**). pfmdr1 mutations contribute to quinine resistance and enhance mefloquine and artemisinin sensitivity in *Plasmodium falciparum*. *Mol Microbiol* **57**: 913-926.

Singh B, Kim Sung L*, et al.* (**2004**). A large focus of naturally acquired *Plasmodium knowlesi* infections in human beings. *Lancet* **363**: 1017-1024.

Sogabe S, Masubuchi M*, et al.* (**2002**). Crystal structures of *Candida albicans* N-myristoyltransferase with two distinct inhibitors. *Chem Biol* **9**: 1119-1128.

Spearman P, Horton R*, et al.* (**1997**). Membrane binding of human immunodeficiency virus type 1 matrix protein in vivo supports a conformational myristyl switch mechanism. *J Virol* **71**: 6582-6592.

Srivastava IK, Rottenberg H*, et al.* (**1997**). Atovaquone, a broad spectrum antiparasitic drug, collapses mitochondrial membrane potential in a malarial parasite. *J Biol Chem* **272**: 3961-3966.

Stanojevic V, Habener JF*, et al.* (**2008**). Cytosolic adenylate kinases regulate K-ATP channel activity

in human beta-cells. *Biochem Biophys Res Commun* **368**: 614-619.

Struck NS, de Souza Dias S*, et al.* (**2005**). Re-defining the Golgi complex in *Plasmodium falciparum* using the novel Golgi marker PfGRASP. *J Cell Sci* **118**: 5603-5613.

Summy JM and Gallick GE (**2003**). Src family kinases in tumor progression and metastasis. *Cancer Metastasis Rev* **22**: 337-358.

Swinnen JV, Beckers A*, et al.* (**2005**). Mimicry of a cellular low energy status blocks tumor cell anabolism and suppresses the malignant phenotype. *Cancer Res* **65**: 2441-2448.

Tanabe T, Yamada M*, et al.* (**1993**). Tissue-specific and developmentally regulated expression of the genes encoding adenylate kinase isozymes. *J Biochem* **113**: 200-207.

Tomasselli AG, Schirmer RH*, et al.* (**1979**). Mitochondrial GTP-AMP phosphotransferase. 1. Purification and properties. *Eur J Biochem* **93**: 257-262.

Tonkin CJ, van Dooren GG*, et al.* (**2004**). Localization of organellar proteins in *Plasmodium falciparum* using a novel set of transfection vectors and a new immunofluorescence fixation method. *Mol Biochem Parasitol* **137**: 13-21.

Towbin H, Staehelin T*, et al.* (**1979**). Electrophoretic transfer of proteins from polyacrylamide gels to nitrocellulose sheets: procedure and some applications. *Proc Natl Acad Sci U S A* **76**: 4350-4354.

Towler DA, Eubanks SR*, et al.* (**1987**). Amino-terminal processing of proteins by N-myristoylation. Substrate specificity of N-myristoyl transferase. *J Biol Chem* **262**: 1030-1036.

Trager W and Jensen JB (**1976**). Human malaria parasites in continuous culture. *Science* **193**: 673-675.

Trape JF (**2001**). The public health impact of chloroquine resistance in Africa. *Am J Trop Med Hyg* **64**: 12-17.

Tsai MD and Yan HG (**1991**). Mechanism of adenylate kinase: site-directed mutagenesis versus X-ray and NMR. *Biochemistry* **30**: 6806-6818.

Tsien RY (**1998**). The green fluorescent protein. *Annu Rev Biochem* **67**: 509-544.

Tsutsumi R, Fukata Y*, et al.* (**2008**). Discovery of protein-palmitoylating enzymes. *Pflugers Arch* **456**: 1199-1206.

Ulschmid JK, Rahlfs S*, et al.* (**2004**). Adenylate kinase and GTP:AMP phosphotransferase of the malarial parasite Plasmodium falciparum. Central players in cellular energy metabolism. *Mol Biochem Parasitol* **136**: 211-220.

Utsumi T, Nakano K*, et al.* (**2004**). Vertical-scanning mutagenesis of amino acids in a model N-myristoylation motif reveals the major amino-terminal sequence requirements for protein N-myristoylation. *Eur J Biochem* **271**: 863-874.

Uyemura SA, Luo S*, et al.* (**2000**). Oxidative phosphorylation, Ca(2+) transport, and fatty acid-induced uncoupling in malaria parasites mitochondria. *J Biol Chem* **275**: 9709-9715.

van Horssen R, Janssen E*, et al.* (**2009**). Modulation of cell motility by spatial repositioning of enzymatic ATP/ADP exchange capacity. *J Biol Chem* **284**: 1620-1627.

van Kasteren SI, Kramer HB*, et al.* (**2007**). Expanding the diversity of chemical protein modification allows post-translational mimicry. *Nature* **446**: 1105-1109.

Walker EJ and Dow JW (**1982**). Location and properties of two isoenzymes of cardiac adenylate kinase. *Biochem J* **203**: 361-369.

Wegmann G, Zanolla E*, et al.* (**1992**). In situ compartmentation of creatine kinase in intact sarcomeric muscle: the acto-myosin overlap zone as a molecular sieve. *J Muscle Res Cell Motil* **13**:

420-435.

Weinburg RA, Mcwherter CA, *et al.* (**1995**). Genetic-Studies Reveal That Myristoylcoa-Protein N-Myristoyltransferase Is an Essential Enzyme in *Candida albicans*. *Mol Microbiol* **16**: 241-250.

Weiss JN, Yang L, *et al.* (**2006**). Systems biology approaches to metabolic and cardiovascular disorders: network perspectives of cardiovascular metabolism. *J Lipid Res* **47**: 2355-2366.

Weston SA, Camble R, *et al.* (**1998**). Crystal structure of the anti-fungal target N-myristoyl transferase. *Nat Struct Biol* **5**: 213-221.

Whitford PC, Gosavi S, *et al.* (**2008**). Conformational transitions in adenylate kinase. Allosteric communication reduces misligation. *J Biol Chem* **283**: 2042-2048.

Whitford PC, Miyashita O, *et al.* (**2007**). Conformational transitions of adenylate kinase: switching by cracking. *J Mol Biol* **366**: 1661-1671.

WHO (**1999**). Making a difference. The World Health Report 1999. *Health Millions* **25**: 3-5.

WHO (**2010**). Global Report on Antimalarial Drug Efficacy and Drug Resistance 2000-2010. Geneva, Switzerland.

WHO (**2011**). World Malaria Report 2011. Geneva, Switzerland, WHO Press**:** 259.

Wilcox C, Hu JS, *et al.* (**1987**). Acylation of proteins with myristic acid occurs cotranslationally. *Science* **238**: 1275-1278.

Willcox ML and Bodeker G (**2004**). Traditional herbal medicines for malaria. *Bmj* **329**: 1156-1159.

Wilson JP, Raghavan AS, *et al.* (**2011**). Proteomic analysis of fatty-acylated proteins in mammalian cells with chemical reporters reveals S-acylation of histone H3 variants. *Mol Cell Proteomics* **10**: M110 001198.

Wright MH, Heal WP, *et al.* (**2009**). Protein myristoylation in health and disease. *J Chem Biol* **3**: 19-35.

Wu J, Tao Y, *et al.* (**2007**). Crystal structures of *Saccharomyces cerevisiae* N-myristoyltransferase with bound myristoyl-CoA and inhibitors reveal the functional roles of the N-terminal region. *J Biol Chem* **282**: 22185-22194.

Wyllie AH (**1997**). Apoptosis: an overview. *Br Med Bull* **53**: 451-465.

Yamazaki K, Kaneko Y, *et al.* (**2005**). Synthesis of potent and selective inhibitors of *Candida albicans* N-myristoyltransferase based on the benzothiazole structure. *Bioorg Med Chem* **13**: 2509-2522.

Yan H and Tsai MD (**1999**). Nucleoside monophosphate kinases: structure, mechanism, and substrate specificity. *Adv Enzymol Relat Areas Mol Biol* **73**: 103-134, x.

Yang SH, Shrivastav A, *et al.* (**2005**). N-myristoyltransferase 1 is essential in early mouse development. *J Biol Chem* **280**: 18990-18995.

Yang YY, Grammel M, *et al.* (**2010**). Comparative analysis of cleavable azobenzene-based affinity tags for bioorthogonal chemical proteomics. *Chem Biol* **17**: 1212-1222.

Yoneda T, Sato M, *et al.* (**1998**). Identification of a novel adenylate kinase system in the brain: cloning of the fourth adenylate kinase. *Brain Res Mol Brain Res* **62**: 187-195.

Young LH, Li J, *et al.* (**2005**). AMP-Activated protein kinase: A key stress signaling pathway in the heart. *Trends Cardiovasc Med* **15**: 110-118.

Zeleznikar RJ, Dzeja PP, *et al.* (**1995**). Adenylate kinase-catalyzed phosphoryl transfer couples ATP utilization with its generation by glycolysis in intact muscle. *J Biol Chem* **270**: 7311-7319.

Zeleznikar RJ, Heyman RA, *et al.* (**1990**). Evidence for compartmentalized adenylate kinase catalysis

serving a high energy phosphoryl transfer function in rat skeletal muscle. *J Biol Chem* **265**: 300-311.

Zha J, Weiler S*, et al.* (**2000**). Posttranslational N-myristoylation of BID as a molecular switch for targeting mitochondria and apoptosis. *Science* **290**: 1761-1765.

Zheng J, Knighton DR*, et al.* (**1993**). Crystal structures of the myristylated catalytic subunit of cAMP-dependent protein kinase reveal open and closed conformations. *Protein Sci* **2**: 1559-1573.

Websites

CDC: http://www.cdc.gov/MALARIA/

WHO: http://www.who.int/mediacentre/news/releases/2005/pr_concert/en/index.html

PlasmoDB: http://plasmodb.org/plasmo/

SWISS-MODEL: http://swissmodel.expasy.org/

Myristoylator: http://web.expasy.org/myristoylator/

The MYR Predictor: http://mendel.imp.ac.at/myristate/SUPLpredictor.htm